VOLUMETRIC MASS FLOW SENSOR FOR CPAP

By

Sarkis Juvelekian

BS in Mechanical Engineering, University of Pittsburgh, 2000

Submitted to the Graduate Faculty of

Mechanical Engineering in partial fulfillment

of the requirements for the degree of

Master's degree

University of Pittsburgh

2002

UNIVERSITY OF PITTSBURGH

SCHOOL OF ENGINEERING

This thesis was presented

By

Sarkis Juvelekian

It was defended on

August 6, 2002

And approved by

Marlin H.Mickle, PhD,
Electrical Engineering

William W.Clark, Associate Professor,
Mechanical Engineering

Thesis Advisor, Michael R.Lovell, Associate
Professor, Mechanical Engineering

ABSTRACT

VOLUMETRIC MASS FLOW SENSOR FOR CPAP

Sarkis S.Juvelekian, MS

University of Pittsburgh, 2002

The current project involves the design and performance evaluation of different flow sensor technologies. The goal of this project is to quantify the performance of existing flow sensor technology and improve the sensitivity and repeatability of flow sensors used in CPAP and BiPAP devices. In this thesis, different theories of flow measurement are investigated and discussed. A standard testing procedure for flow sensors is then established for determining their overall performance. Using this procedure, tests were conducted on four different mass flow sensors that could potentially be used in a CPAP device. Based on the results of these tests, a comparison is made between each of the flow sensors studied. Finally, the relevance of the experimental results and procedure are ascertained with respect to final product performance and cost.

ACKNOWLEDGMENTS

One and a half years have passed since I joined the graduate school of Mechanical Engineering at the University of Pittsburgh, it seems like yesterday, and time flew by. My Masters' experience was a very pleasant one, and that was due to the help and encouragement of my advisor Dr. Michael R.Lovell, who consistently restored my confidence. The members of my committee, Dr. William W.Clark and Dr. Marlin H.Mickle, who were always there for me whenever I needed their professional opinion or help.

The unconditional love and support I received from my families in the United States, and back home in Lebanon was crucial. I am grateful to my parents who believed in me and encouraged me all the way, especially my brother Georges whose help, support and inspiration were behind what I have achieved. I would finally like to dedicate my Thesis to my father, whose mentoring helped me be the engineer I am today, thank you Dad.

TABLE OF CONTENTS

LIST OF TABLES

LIST OF FIGURES

1.0 INTRODUCTION

1.1 Background To Current Work

1.1.1 Introduction To Sleep Apnea

Sleep apnea is a very prevalent syndrome. It is estimated to affect 2 to 9 percent of the U.S. population (1-3). The American Thoracic Society defines an apnea as "a cessation of airflow through the nose and mouth for ten seconds", and is divided into three categories: obstructive, central, and mixed. Apnea is considered obstructive if continued respiratory effort occurs with upper airway obstruction. Central apnea defines no respiratory effort while mixed apnea is characterized when components of both the central and obstructive efforts exist (4). Apneas are usually associated with either an arousal from sleep or a fall in oxyhemoglobin saturation (4-6). Hypopnea is defined as reduction in airflow associated with an arousal from sleep and a fall in saturation. The sleep apnea syndrome is defined as "recurrent apneas or hypopneas that are associated with clinical impairment as manifest by increased sleepiness or altered cardiopulmonary function (ATS ref). The number of episodes of apnea and hypopnea per hour of sleep are recorded as a single apnea-hypopnea index, or respiratory disturbance index.

Patients with sleep apnea have an increased risk of diurnal and pulmonary hypertension, nocturnal dysrhythmias, ventricular failure, myocardial infarction, and stroke (7). Also, the relation between sleep apnea and diurnal hypertension is independent of obesity, age, and sex (8).

Most patients with sleep apnea suffer from daytime sleepiness. Loud snoring, fatigue, or both are also common symptoms among these patients. Patient characteristics include male sex, obesity, age of over 40 years, habitual snoring, nocturnal gasping or choking, and a history of hypertension (9, 10).

One of the most important therapeutic advances for apnea occurred with the introduction of continuous positive airway pressure (CPAP). Well-documented evidence exists for the immediate clinical effectiveness of CPAP for patients with obstructive apnea. The signs and symptoms associated with obstructive sleep apnea are reduced as proved by improved cognition and psychological function (11), improved daytime awareness (12-15), reductions in carbon

dioxide retention (16), and reduction in heart rate and blood pressure (17). Long-term treatment with CPAP is associated with decreased **hematocrit** (18, 19), and improved **ventricular ejection fraction (20).** CPAP has also been used to eliminate snoring associated with obstructive sleep apnea (21, 22). In one study, both the snoring and the associated apneas were eliminated (21). In a second study, CPAP effectively restored normal breathing and eliminated nighttime arousals (22).

Much less is known about the effectiveness of CPAP on periodic breathing and associated central apneas. CPAP causes a variable reduction in the number of apneas (23-25). Studies suggest that there is either an immediate direct reduction in apnea frequency or possibly an indirect time-dependent reduction in apnea that results from improved cardiac function (26). In one study involving CPAP in central apnea, a 3-month follow-up with patients revealed improved sleep, less restlessness, and subjective alleviation of fatigue and hyper somnolence (25). It also led to improved left ventricular function and decreased symptoms of heart failure. Other studies failed to show any benefit (27).

1.1.2 Mechanism Of Upper Airway Dysfunction

Upper airway dysfunction and the specific sites of narrowing or closure are influenced by the underlying muscle tone, upper-airway muscle synchrony, and the stage of sleep (28). These events occur mostly during REM sleep. Upper-airway size is determined by soft-tissue and skeletal factors that are also the major determinants of upper-airway potency during sleep (29). Increased adipose tissue in the neck, mainly in obese patients, may also predispose the airway to narrowing. Genetically determined craniofacial features or abnormalities of ventilatory control may account for the pattern of apnea common to families. If the soft palate is continuously exposed to snoring and high pressure, it can be lengthened due to stretching and thickening (30). These changes in the soft palate due to apnea may therefore be a consequence of breathing against increased upper-airway resistance. An increased body-mass index (BMI), hypertension, and an increased neck circumference are often characteristic of patients.

Alcohol selectively reduces upper-airway muscle tone and increases the frequency of abnormal breathing during sleep. It also prolongs apnea by delaying arousal. In obese patients, weight loss can significantly decrease the severity of apnea (31).

Sleep studies are performed to confirm the presence of upper-airway closure during sleep and to assess the patient's level of risk of apnea.

1.1.3 Treatment Of Sleep Apnea Syndrome

Several treatment modalities are used in the management of sleep apnea. They include CPAP, pharmacologic agents, and surgery.

CPAP

Continuous positive airway pressure delivered through a mask is the preferred initial treatment for obstructive sleep apnea. Continuous pressure is applied to the upper airway with a nasal mask, nasal prongs, or a mask that covers both the nose and mouth (32-34). Patients treated with continuous pressure delivered nasally have repeatedly demonstrated improvement in neuropsychiatric function and a lessening of daytime sleepiness (35,36). Nocturnal desaturation, ventilatory-related arousals, nocturnal dysrhythmias, pulmonary hypertension, and right-sided heart failure have also been effectively treated. The treatment may also improve control of hypertension (37). Studies also suggest that patients treated with positive airway pressure have improved survival.

Pharmacologic agents

The use of medications in the treatment of sleep apnea has not been successful. Several medications are used with varying success in mild cases, but are of little help in more severe cases. They include thephylline, progestational agents, opiate antagonists and nicotine, thyroxine, acetazolamide, serotonergic-active agents, and antihypertensive agents (38).

Theophylline has been used for years to stimulate ventilatory drive. It is most helpful in patients who have periodic breathing and central apneas during sleep (39). However, it has not been useful in diminishing the severity or symptoms of obstructive sleep apnea, and usually disturbs sleep further. In a study comparing theophylline dosage with CPAP given for one night, the theophylline decreased total sleep time, while the CPAP dramatically decreased apneas, increased deep sleep, and decreased sleep transitions.

Progestational agents have not been found to be helpful with sleep apnea conditions. In one report, the administration of a progestational agent produced no response (40).

Opiate antagonists and nicotine have been demonstrated to improve oxygenation with sleep apnea patients, but they also cause significant sleep disruption. They are very short acting, making them impractical for routine use (41-44).

Thyroid replacement led to resolution of sleep apnea in some, but not all, trials (45-47). It is unpredictable whether thyroid replacement can reverse sleep apnea in hypothyroid patients.

Acetazolamide has different effects in different populations. In one study using acetazolamide, a minimal improvement was noticed in the frequency of apneas, but no improvement in symptoms (48). Patients must also use acetazolamide carefully, since excessive stimulation of the ventilatory drive may worsen obstructive sleep apnea.

Serotonin reuptake inhibitors have also been used in the treatment of obstructive sleep apnea. However, their effectiveness is variable. In one study, patients were treated for six months, with no changes in sleepiness, memory, or mood (49). The use of serotonin reuptake inhibitors should therefore not be recommended for routine use.

Antihypertensive agents may work in obstructive sleep apnea by influencing the input to ventilatory control centers. However, no consistent effects have been reported. In a controlled trial, cilazapril, an angiotensin converting enzyme inhibitor, had no effect on the ventilatory pattern during sleep (50).

Surgical Treatment

The most commonly performed procedure is uvulopalatopharyngoplasty, which is effective in less than 50 percent of patients, and is not recommended for the treatment of sleep apnea. Maxillofacial surgery is another common option. This procedure enhances upper-airway patency during sleep in patients with obstruction (51,52). These operations are not consistently successful, even though individual patients have had satisfying results.

Tracheotomy, in a sub-group of patients that cannot tolerate CPAP, can dramatically improve the symptoms of obstructive sleep apnea.

1.1.4 Available CPAP Systems

Several commercial CPAP systems are available. These systems include features such as a mask that is connected to the positive pressure device, a device to generate positive airway pressure, filters, humidifiers, and standard maintenance requirements.

The masks consist of a hard plastic outer shell with a soft inner flap seal of vinyl or silicone. The vinyl masks, however, usually harden after prolonged contact due to facial oils.

Delivery Systems

Originally, compressors were used to generate airflow to deliver CPAP. However, the compressors were noisy, bulky, and needed high flow rates to maintain adequate pressures. Currently, blowers are used to deliver the pressures. These blowers have significant advantages over the compressors. The sizes of the blowers can be reduced, the sound can be insulated, and they can compensate for variations in mask pressure (53). To maintain a constant pressure, the blowers reduce flow during expiration as the pressure rises and increase flow during inspiration as the pressure falls.

Some discomfort can occur with higher levels of CPAP just before sleep onset. Therefore, some manufacturers have developed a "pressure ramping" feature that allows a slow buildup of pressure after sleep onset.

BIPAP (bi-level positive airway pressure) is a modification of the CPAP delivery method. This method allows for independent adjustment of the airway pressures (54). During expiration, BIPAP pressure can be significantly lowered.

Use of CPAP

The level of nasal airway pressure is first adjusted to a level that restores ventilation and continuous sleep. Various body positions, REM, and non-REM sleeps are studied to determine optimal CPAP pressure. REM or rapid eye movement is the first stage of sleep. Supplemental oxygen or assisted mechanical ventilation can also be administered, if needed. Patients must be involved in clinical outpatient follow-ups to determine the response of treatment and the level of compliance. A repeat evaluation is necessary for patients who do not respond to initial treatment.

Effects of CPAP

CPAP is a safe form of therapy with relatively few major complications. As the nasal airway pressure is raised to an optimal level, all abnormalities in the respiratory parameters, including nighttime arousals, are eliminated, and normal sleep is obtained (55). CPAP also has an immediate and dramatic effect in patients with neurocognitive dysfunction and daytime sleepiness (56, 57, and 15). Long-term benefits include improved cardiopulmonary function (58-61). Potential advantages of CPAP compared with surgery include the avoidance of complications of general anesthesia and the preservation of lymphoid tissue.

1.1.5 Summary

CPAP is effective in the treatment of patients with clinically important obstructive sleep apnea. It is a safe, effective form of therapy with rare complications. Most patients are compliant with CPAP, with higher levels of compliance associated with relief of sleepiness, fatigue, and restoration of alertness.

1.2 Overview Of Thesis

The main focus of this thesis is to evaluate different mass flow sensor technology for use in a commercial CPAP unit. The outline for the reaming portion of the thesis will be as follows. The second chapter will cover the theory behind several flow measurement techniques including a hot wire anemometer, a constant resistance circuit and a constant voltage circuit. The third chapter will focus on the experimental procedure used in this work and will include the experimental setup, the operating conditions, and a standard testing protocol. The results are discussed in Chapter four, with particular emphasis being placed on comparing and analyzing the differences in results between each sensor. Chapter five is the conclusion where a table is presented which shows the advantages and disadvantages of each sensor and justification is made for selected an optimum sensor type in CPAP devices.

2.0 FLOW MEASUREMENT THEORY

2.1 General Measurement

2.1.1 Pressure Measurement Theory

There are currently many parameters that are measured in fluids. These parameters include pressure, velocity, discharge, shock waves, density gradients, turbulence, and viscosity. The measurement of these parameters may be taken using various methods such as direct, indirect, gravimetric, volumetric, electronic, electromagnetic, and optical techniques. Direct measurements for discharge involve the determination of the volume or weight of fluid that passes through a section during a given time interval. Indirect methods of discharge measurement require the determination of head, difference in pressure, or velocity at several points in a cross section. With these measurements, the discharge can then be computed. The two most precise methods of flow measurement are the gravimetric or volumetric methods. In these methods, the weight or volume is determined by weight scales or by calibrated tanks for a time interval that is measured by a stopwatch. The weight or volume is then used to determine the flow

Pressure measurement

Pressure measurements are required in numerous devices to determine the velocity of a fluid stream or its rate of flow. The ***energy equation*** gives this relationship between velocity and pressure:

$$\rho \frac{dV}{dt} = \rho g - \nabla p \qquad \text{(Equation 1)}$$

Various methods are used in measuring pressure. Figure 1, shows a "*Piezometer*" opening, which is one method of determining static pressure. When the flow is laminar or parallel, the pressure variation is hydrostatic normal to the streamlines. If the pressure at the wall is measured, the pressure at any other point in the cross section is known, since it is equal to the pressure at the wall. For this method of measurement to be effective, the *piezometer* should be normal to the surface of the pipe in question, and it's opening should be small. The length should be at least twice its diameter. The *piezometer* is extremely sensitive, however, and a slight misalignment or roughness at the opening may cause errors in measurement. Therefore, several *piezometer*

openings connected together into what is called a "*piezometer ring"* can give a more accurate reading. The above drawbacks are enough to rule out the use of this method for high production manufacturing purposes, not to mention that this method does not give the direction of the flow.

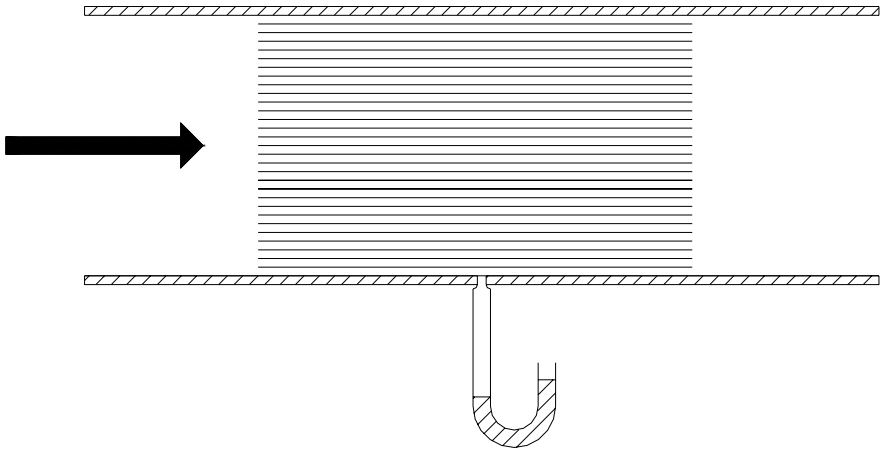

Figure 1: Piezometer opening for measurement of static pressure

For rough surfaces, the static tube shown in figure 2 can be used to measure the pressure. It consists of a tube that is directed upstream with the end closed. It has radial holes in the cylindrical portion downstream from the nose. The flow is presumed to be moving by the openings as if it were undisturbed. The static tube must first be calibrated as it may read too high or too low, and some disturbances may occur due to both the nose and the right-angled leg that are normal to the flow. If the tube does not read true static pressure, the discrepancy Δh normally varies as the square of the velocity of flow by the tube.

$$\Delta h = C * \frac{v^2}{2g} \qquad \text{(Equation 2)}$$

The value of "C" in the above equation is determined by towing the tube in still fluid where the pressure and velocity are known. Those tubes are relatively insensitive to the Reynolds number

and to Mach numbers below unity. Their alignment with the flow is not critical. An error of a few percent is to be expected for a yaw misalignment of 15 degrees.

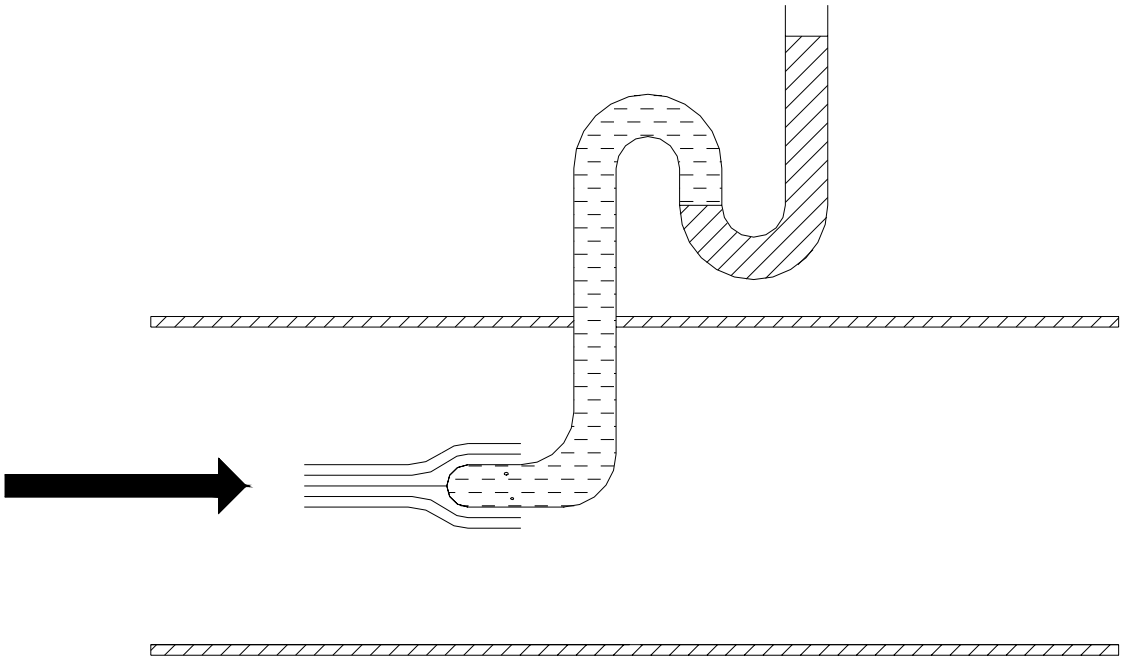

Figure 2: Static tube

Electric transducers can also be used to sense the pressure changes by electronically measuring the displacement of a diaphragm or elbows. A schematic diagram of one arrangement is shown in figure 3. As the diaphragm is distended by a difference in pressure between the gas inside and outside the pressure chamber, the core of a differential transformer moves between the coils. The electric output of this transformer depends upon the position of the core, which is determined by the pressure difference at the two ports. Thus, the transducer gives an electric change for a pressure change. Different elastic characteristics for the diaphragm can cover a wide variety of pressure ranges. *The electric strain gage*, a piece of fine wire bonded to the piece that will be distorted, can also detect the distortion of elastic elements. As the member changes shape, it deforms and thereby stretches the fine wire and alters its electric resistivity. The change in the resistance can be measured with a Wheatstone-bridge circuit, similar to the one used with the constant-voltage hot-wire anemometer, shown in figure 5.

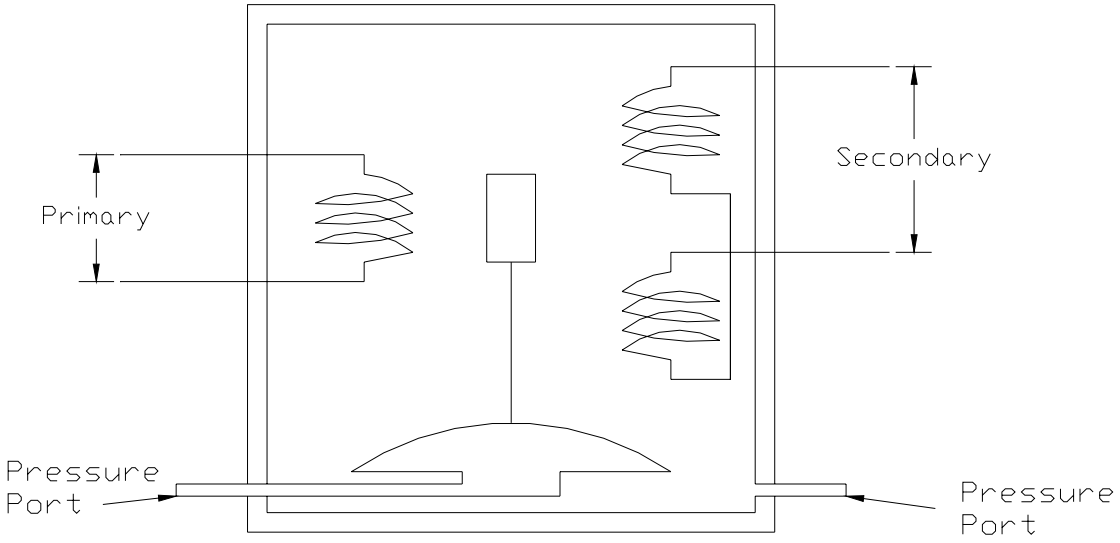

Figure 3: Schematic diagram of pressure transducer using differential transformer

2.1.2 The Hot Wire Anemometer

Gas velocities can be successfully measured using a *hot-wire anemometer*. In the anemometer an electric current is used to heat a short length of fine platinum wire. The resistance to the flow of electricity through the wire is a function of its temperature. The flow of the gas around the hot wire cools the wire and thus changes its resistance. By holding either the current through the wire or the voltage across the wire constant using a precision circuit, the change in voltage or amperes respectively become a function of the speed of gas flow. This circuit may be calibrated by putting the hot wire in a gas stream of known velocity. The hot-wire anemometer has a very quick response to the change in the velocity of the gas, and is the most practical means for measuring the rapid fluctuation caused by turbulence at a certain point.

Two methods exist for measuring the speed of the flow using the hot-wire anemometer. The methods are the constant resistance circuit and the constant voltage method.

2.1.3 The Constant Resistance Circuit

In the constant-resistance circuit (figure 4), the circuit is first adjusted so that the galvanometer reads zero. The temperature of the wire is held constant and hence its resistance remains constant. For a change in fluid flow over the wire, the variable resistance B is adjusted to bring the galvanometer reading back to zero, and the voltmeter reading changes. By calibration in a stream of known velocity, the voltmeter reading is directly proportional to fluid velocity.

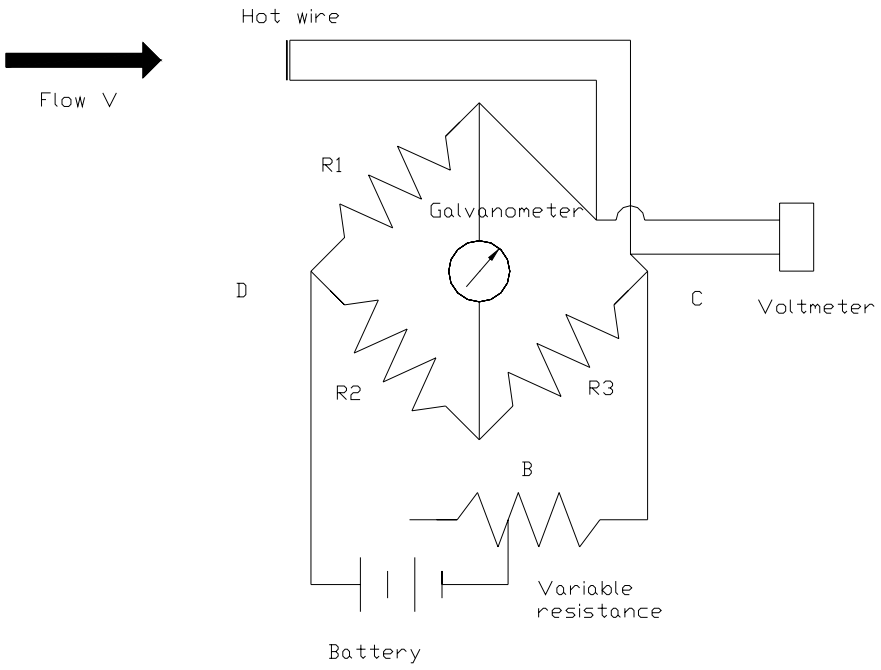

Figure 4: Constant resistance hot-wire anemometer

2.1.4 The Constant Voltage Method

In the constant-voltage method (figure 5) the variable resistance B is first adjusted so that the galvanometer reads zero when the hot wire is exposed to fluid at rest. Flow over the wire then cools the wire and varies its resistance, causing a change in galvanometer reading. Calibration in a stream of known velocity relates the gas velocity to galvanometer reading.

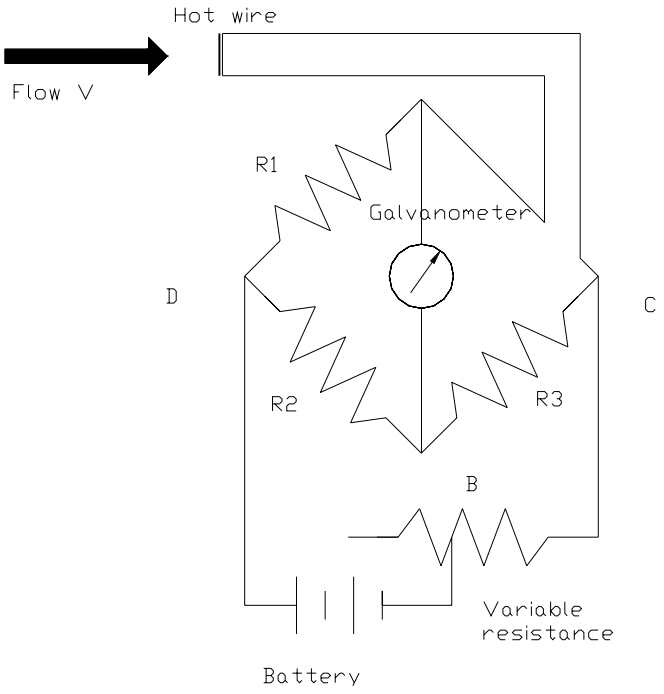

Figure 5: Constant voltage hot-wire anemometer

2.2 Other Existing Flow Measurement Research

2.2.1 A New Class Of Thermal Flow Sensor Using ΔT=0 As A Control Signal

Flow sensors based on thermal principles are widely used. With these sensors, heat is generated in the structure, and the fluid flow dependent temperature distribution is recorded. The sensor system is a classical stimulus-response measurement system (Fig6). Thermal sensors are divided into different classes, based on (62):

The driving mode for constant power or constant temperature. Single probe, directional insensitive, or multi-probe, directional sensitive.

The constant power-driving mode also referred to as Constant Power Anemometry or CPA, has its advantages and disadvantages. The advantage is its simple electronic implementation. The disadvantage is that the temperature dependence of the fluid properties and the sensor sensitivity must be taken into consideration. This disadvantage can be overcome by the constant temperature-driving mode, where the power needed to keep a heater at a constant temperature is a measure of the flow velocity (62).

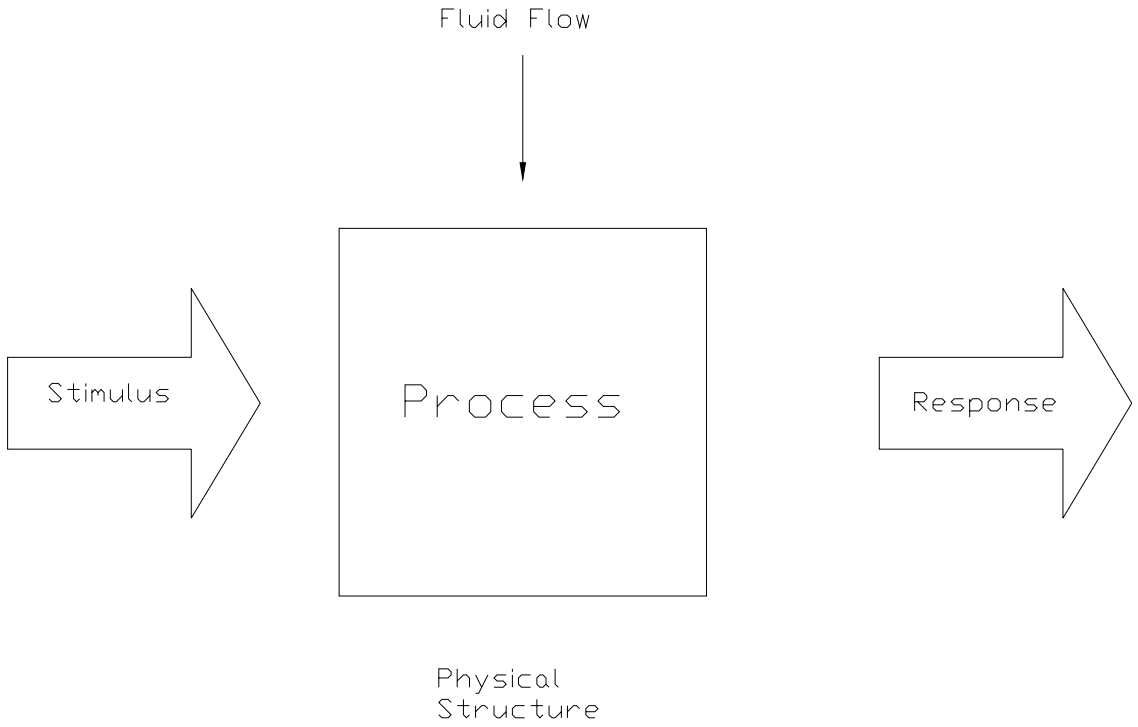

Figure 6: General structure of a thermal flow sensor

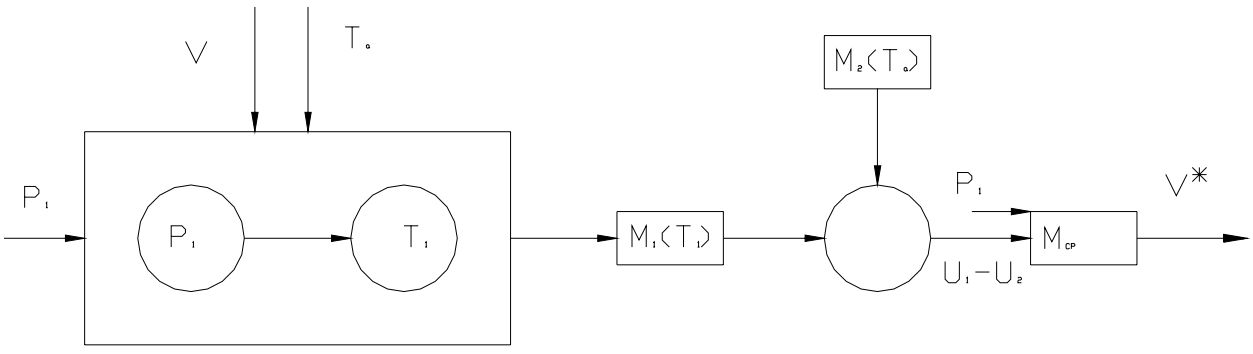

Figure 7: System structure of "constant power anemometry" thermal flow sensor with single probe

In the single probe CPA (figure 7), a fixed amount of heat is dissipated in a resistor in the flow and the temperature of that resistor is a measure of the flow. With increasing flow velocity, the temperature of the sensor will decrease. We can describe the temperature of the sensor using King's law (63):

$$T_1 = \frac{P_1}{G_0 + K_0 * v^{0.5}} + T_a \qquad \text{(Equation 3)}$$

Where T_a = ambient temp, G_0= the zero flow conductance, and K_o = the flow sensitivity.

To measure the unknown flow velocity, v, with power P_1, two sensors are needed to measure both T_1 and T_a (fig 2). The sensor systems output signal, v* can be derived using the flow sensor model M_{cp}. For a small signal analysis,

$$dv^* = m_{cp} * d(U_1 - U_2) \qquad \text{(Equation 4)}$$

Or with m_1 (T_1) = dU_1/dT_1 and $m_2(T_a) = dU_2/dT_a$,

$$dv^* = m_{cp} * (m_1 dT_1 - m_2 dT_a) \qquad \text{(Equation 5)}$$

dv* is a function of dT_a unless m_1 and m_2 are equal for all temperatures.

Multi-probe CPA

By implementing a differential temperature measurement, (figure 8), direct measurements of the ambient temperature can be omitted (64-67). Then,

$$dv^* = m_{DT} * d(U_2 - U_1) \qquad \text{(Equation 6)}$$

Although T_a is no longer used as a reference, its influence on v* still exists. When $T1=T_2$, $m_1$does not equal m_2.

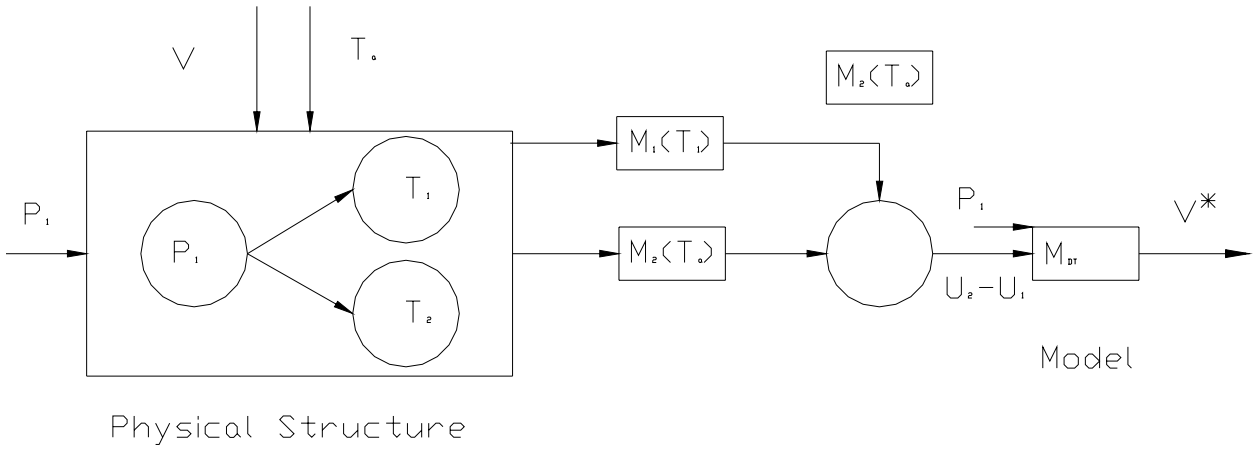

Figure 8: System structure of "constant power anemometry" differential temperature measurement thermal flow sensor

Constant Temperature Anemometry (CTA)

Single probe CTA

In CTA, the absolute temperature of the sensor in the physical structure (fig 9) is kept at a constant value above the ambient temperature, Ta. Therefore, this type of sensor must consist of a control loop (68). The process can be summarized as:

$$P_1 = (G_0 + K_0 \cdot v^{0.5}) \cdot (T_1 - T_a) \qquad \text{(Equation 7)}$$

Then v can be calculated from the required power.

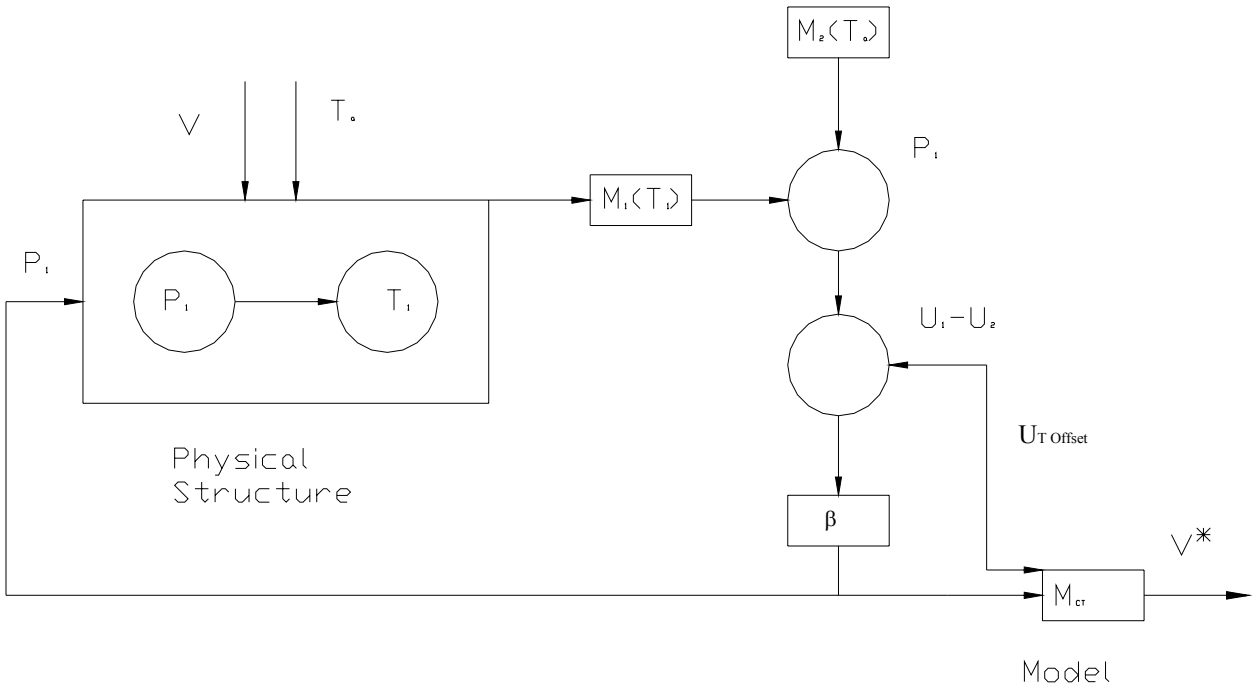

Figure 9: System structure of "constant temperature anemometry" thermal flow sensor

Temperature Balance Anemometry (TBA)

Multiprobe TBA

In multiprobe TBA, the temperature difference between the upstream and downstream sensors is kept at zero. The ratio between the upstream and downstream heating power is then a measure for the fluid flow. The sensor consists of two heater-sensor pairs, which are located at the same position along the length of the tube. Their temperatures are determined by the heat transport in the sensor. The system output v* no longer depends on the sensitivities $m_1 = m_2$.

2.2.2 A Novel Flow Sensor With High Time Resolution Based On Differential Pressure Principle

Many different methods exist to measure low flow rates. The differential pressure principle is one of these methods. The pressure drop is measured with two piezoelectric (69) or capacitive (70) pressure sensors. These sensors are located at the inlet and outlet of the micro channel. This principle gives a linear relationship between flow rate and pressure difference.

There are also disadvantages to this method, however. Two pressure sensors are needed, to measure the differential pressure, and there is an influence of temperature on the sensor signal.

Principle of the sensor

The sensor directly measures the pressure drop at the orifice of the sensor. Three types of flow sensors with different orifice sizes have been recognized (Table 1).

Table 1: Realized Sensors

Sensor Type	Orifice back d[μm]	Orifice front d_f[μm]	Cone angle Γ [°]
1 psi	28	44	24
5 psi	68	80	19
30 psi	160	169	14

Theory

An orifice in the middle of the diaphragm leads to a decrease of mechanical stress for a given pressure difference. If the orifice is too large, the sensor's sensitivity significantly decreases. Also, if the ratio between the diameter of the orifice and the thickness of the membrane is small, then the flow can be described by the Hagen-Poiselle equation:

$$Q = \frac{A^2}{8\pi \cdot \eta \cdot l} \cdot \Delta p_f \qquad \text{(Equation 8)}$$

If the ratio is large, then Torricelli's law gives the flow:

$$Q = \mu A \sqrt{\frac{2\Delta p_a}{\rho}} \qquad \text{(Equation 9)}$$

The flow number, μ, is determined by the constriction of the flow in the orifice.

Gas bubbles

Bubbles can be a disturbance to the sensor signal. For small orifices, these bubbles caused a blocking effect. The threshold pressure must be overcome between the positions shown in (fig 10a and 10b). This threshold pressure is given as:

$$\Delta p_b = \frac{2\sigma_{wa}}{r} \qquad \text{(Equation 10)}$$

The bending radius is given by:

$$r = \frac{d}{2\sin(90^\circ + \Gamma - \Theta)} \qquad \text{(Equation 11)}$$

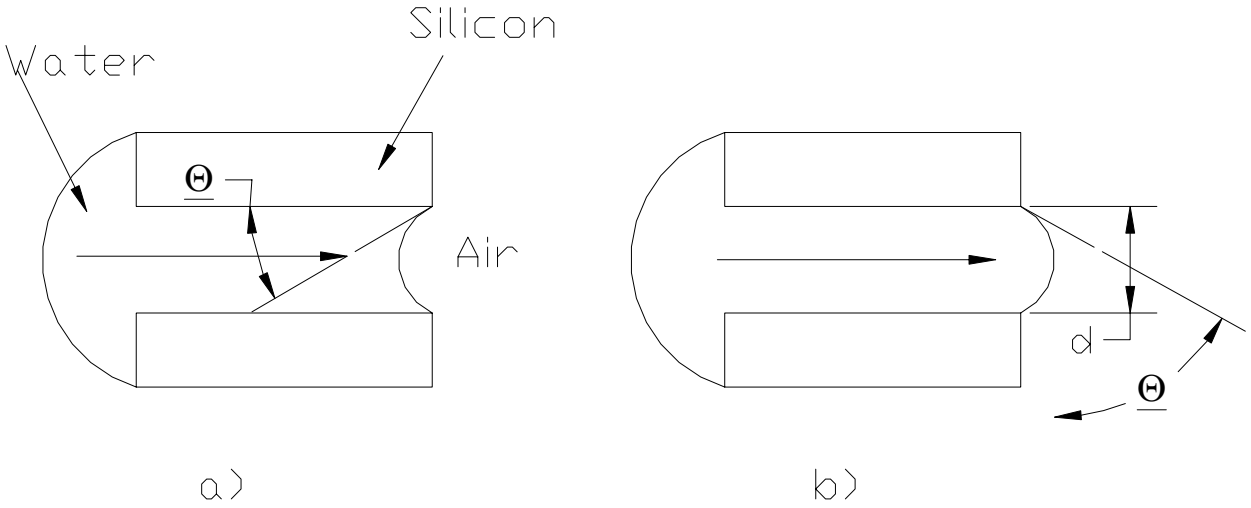

Figure 10: Pressure barrier during the priming procedure

Where the contact angle is found in reference (71).

The threshold pressure necessary to transport a gas bubble into the orifice (fig 11a, 11b) is also given by equations 10 and 11.

Table 2 shows a comparison of measurement and theory for the gas bubbles.

Table 2: Measured and calculated threshold pressure for different orifices

	d[µm]	Δp_b [hPa] Measured	Δp_b [hPa] Theory
Priming	68	22	24
	28	47	44
Gas bubble	68	40	43
	28	102	104

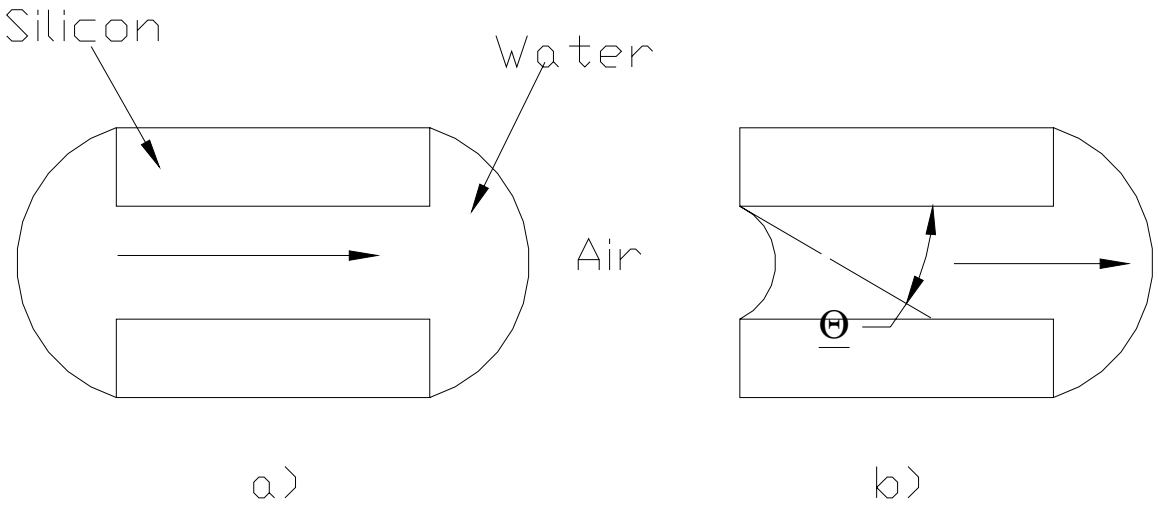

Figure 11: Pressure barrier for a gas bubble

2.2.3 Thermal Flow Sensor For Liquids And Gases

Two principles are important in the consideration of sensing mechanisms: differential pressure detection and thermal flow measurement. Thermal flow sensors are thermally isolated structures carrying heaters and thermometers, and are superior for low volume liquid flow and for gas flow (72, 73). Microsystems technology is offering favorable features in the manufacturing of these systems, including very good thermal isolation from the microstructure to

their support, a small size, which gives the sensor a small time constant, and small geometrical dimensions, which allow sensor application of interactions that can not be used in larger devices (micro calorimeter, time of flight.)

Two technologies are applied in the manufacturing of thermally isolated structures. Silicon bridges and cantilevers operate as hot wire probes with wires made by lithography and etching. Membranes or bridges made from insulating materials are made by LPCVD (74), PECVD (75), or silicon carbide (76). These methods give a small thermal conductivity and a small thickness. For example, nitride membranes with a 200nm thickness can handle a pressure of more than 1 bar (77, 78, 79). An advantage of the membrane solution is the freedom of design, since several heaters and thermometers can be integrated on one membrane.

Four strategies can be applied in measuring the flow with a thermal device. Heat loss, thermo transfer principle, micro thermo transfer principle, and thermal time of flight (TOF).

In the heat loss (thermal anemometer method) (figure 12), when a heated membrane is exposed to a moving fluid, the wall heat transfer rises with rising flow. The velocity is then calculated from the power needed to heat the membrane or from the temperature reached with a given current.

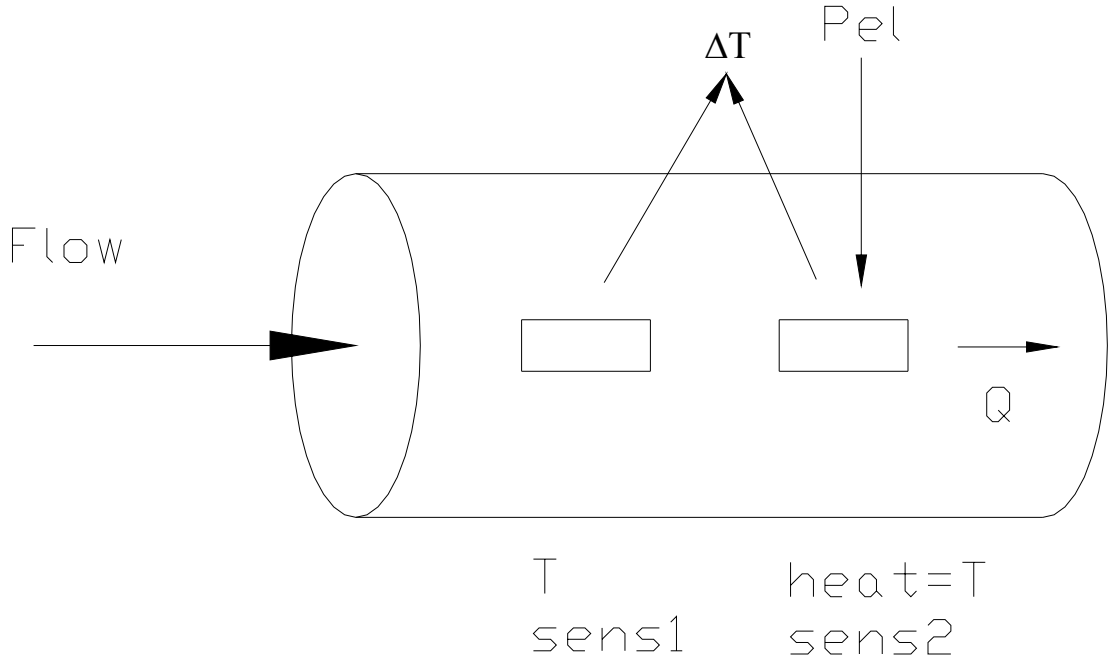

Figure 12: Heat loss measurement

In the thermo transfer principle, the fluid is heated, and the energy needed to heat the fluid is used to calculate the mass flow (figure 13).

The micro transfer principle, like in thermo transfer measurement, heats the fluid and the temperature rise of the fluid is measured. In this method, the heater and thermometer are small and close to each other with respect to the fluid channel (fig 14). This method needs only small heating energy and is very sensitive.

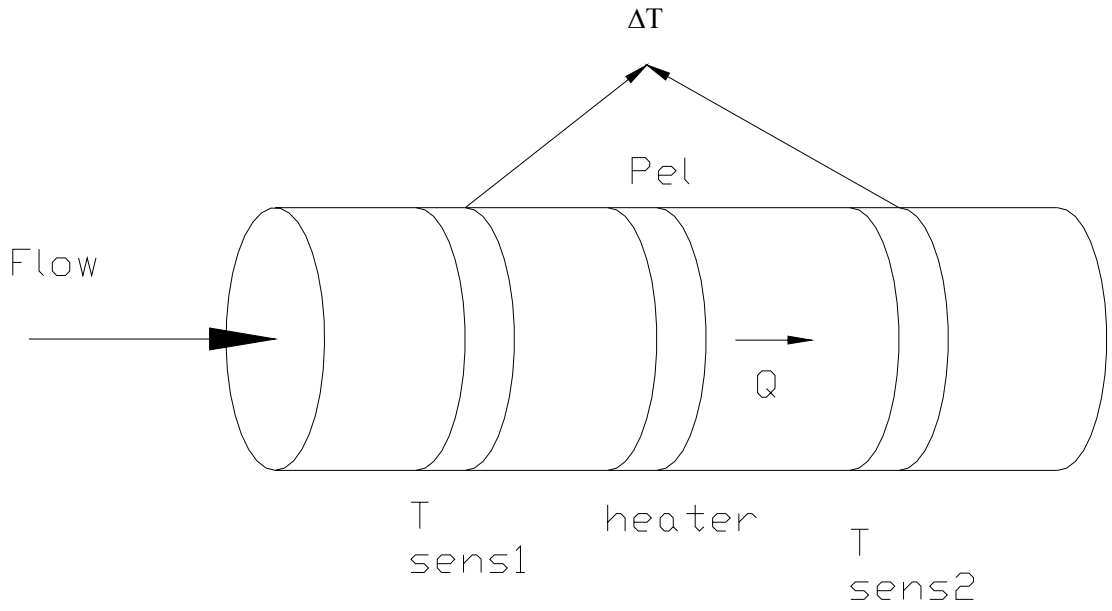

Figure 13: Thermo transfer measurement

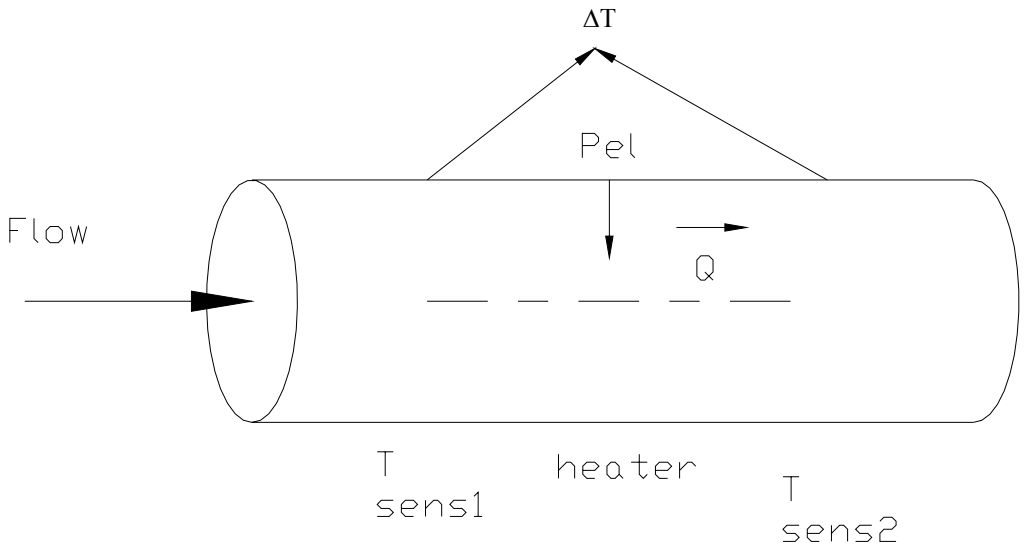

Figure 14: Micro thermo transfer measurement

In the thermal-time-of-flight method, the heater gives a small heat impulse on the fluid (fig 15). The thermometer measures the time when the pulse arrives.

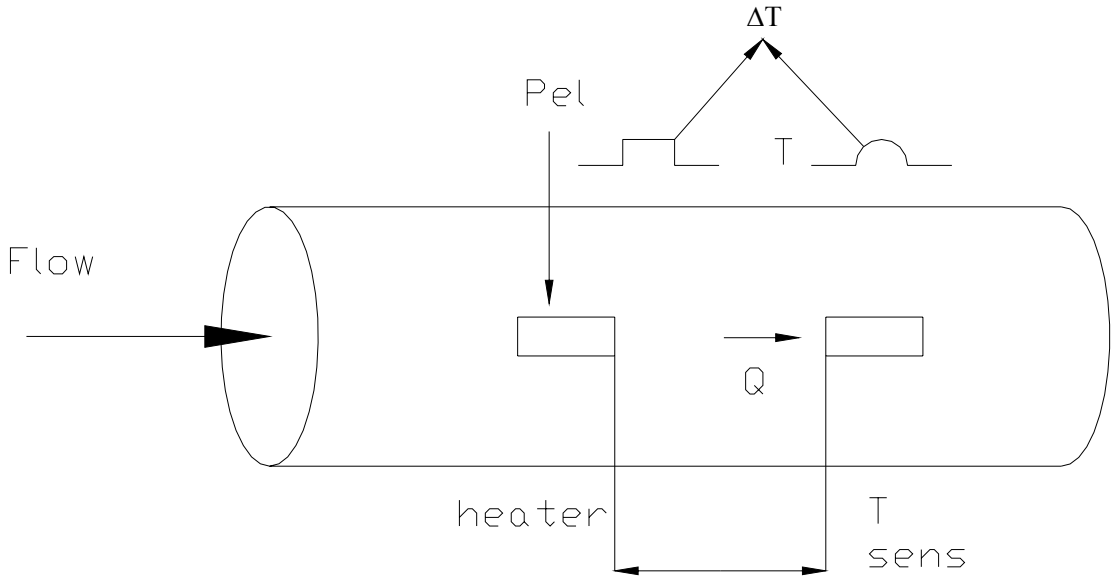

Figure 15: Thermal time-of-flight

A numerical model can be developed, describing the propagation of the heat pulse. The pulse movement is a superposition of the diffusion of the pulse into the fluid, and transport of the heated fluid by the flow.

Consequences of these results also exist, however. The silicon membranes can only be applied for heat loss measurements, and the heater and thermometer must be close to each other to prevent distortion of the pulse. Also, a micro-thermo transfer device has sensitivity at low flow velocities, and in using the time of flight measurement, the heat pulse will be distorted.

For measurement in liquids, the flow channel has dimensions of .4mm x. 6mm. An electronic power supply for the heater uses a constant power mode. The heater is continuously activated with a power of 5 mW, and the differential pressure is measured. Measurement is sensitive at small flow velocities.

2.2.4 A High Speed Mass Flow Sensor With Heated Silicon Carbide Bridges

In most micro-machined thermal mass flow sensors; the transfer of heat detects a flow of air as the air is passed over the surface of the device. Response times have been obtained of the order of a few milliseconds (80, 81, 82). The consequence for the short response times is the limited mechanical and thermal stability of the silicon devices. Micro machined thermal mass flow sensors have a significantly enhanced mechanical and thermal stability.

To obtain higher stability, β-SiC films are used on silicon to fabricate the heater and sensing elements. Figure 11 shows the temperature dependence of the electrical conductivity of different β-SiC films (83). Highly conductive films are for forming heater elements while semi-insulating films form sensitive temperature sensing elements. The conductivity of these films is not influenced by contamination effects, due to the high density of defects that are formed at the surface due to the mismatch between Si and SiC of about 20% (83). Another material property of thermal mass flow sensors is the thermal conductivity of the heated SiC bridges. Measured thermal conductivities are shown in (Fig 16) (84).

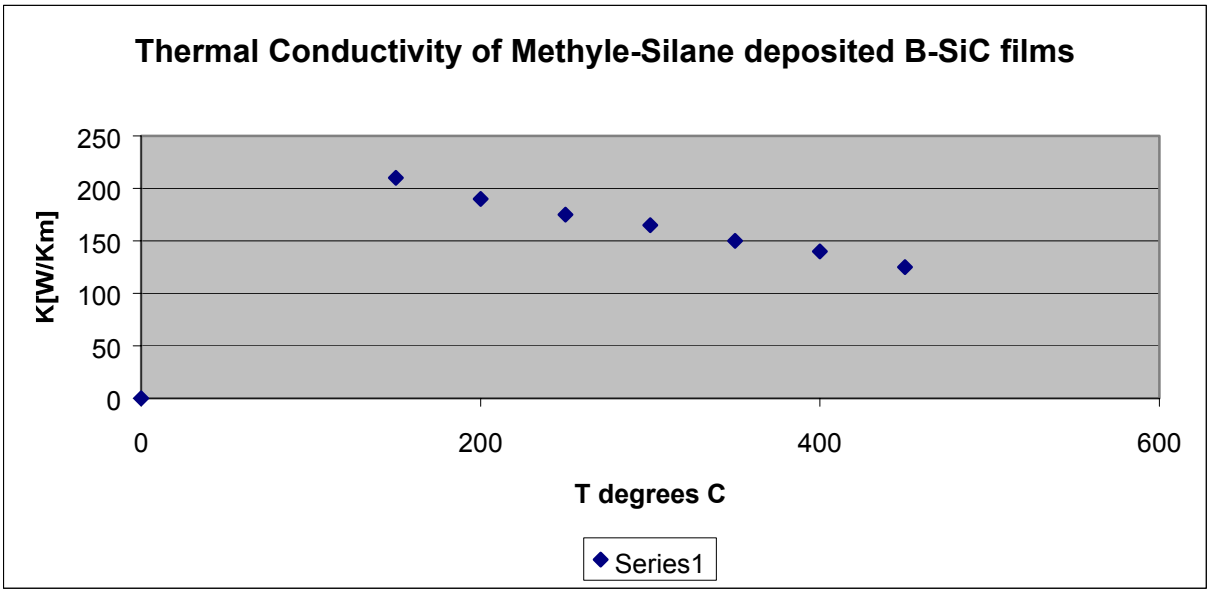

Figure 16: Thermal conductivity of Methyle-Silane deposited B-SiC films

The SiC thin films have a high level of thermal conductivity. These high conductivities lead to small thermal response times of the micro bridges; however, they also result in poor thermal isolation of the bridges from their supporting substrates, resulting in a high level of power consumption.

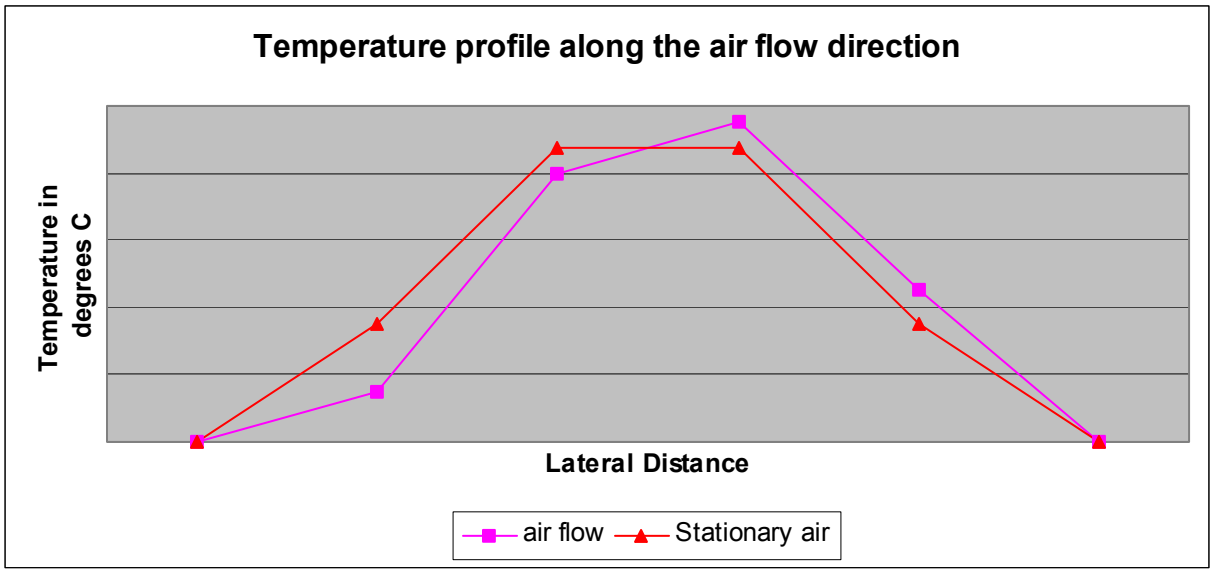

Figure 17: Temperature profile along the flow direction

Figure 17 shows the temperature profile across the SiC heaters in the direction of the flow channel.

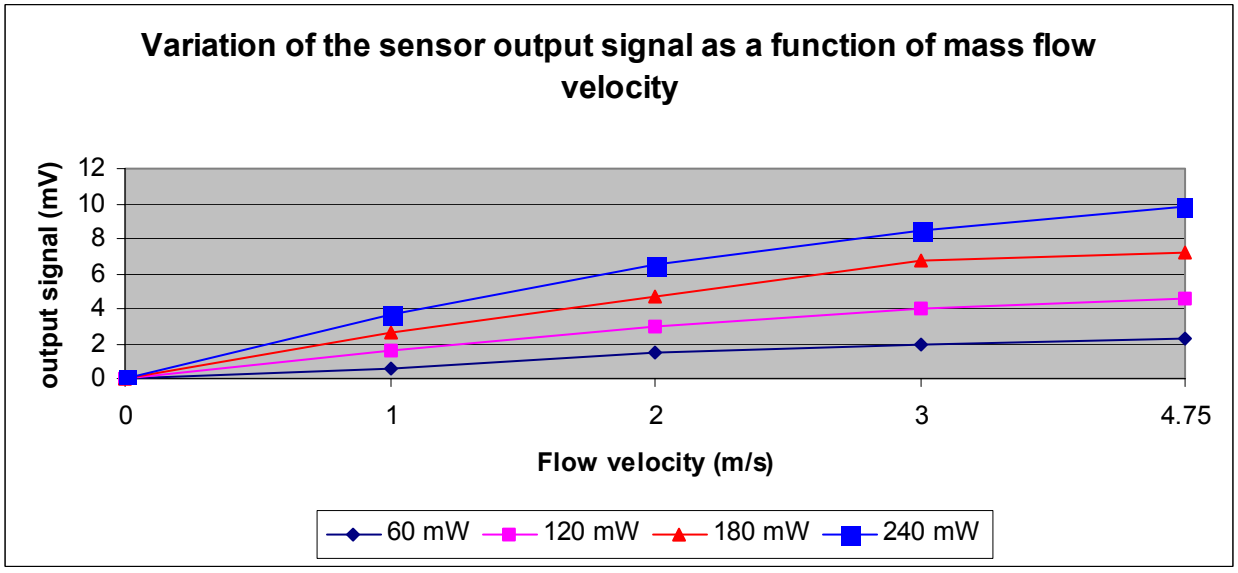

Figure 18: Variation of the sensor output signal as a function of mass flow velocity

Figure 18 shows the variation of the sensor output signal as a function of mass flow velocity. It shows that the output signal increases with the heating power input into the SiC bridges.

Sensors with longer and narrower bridges give a larger output signal due to reduced heat conduction. The response is limited by the thermal time constant of the SiC bridges, given by:

$$\tau = l^2 \rho C_p / \lambda \qquad \text{(Equation 12)}$$

Where L = length of SiC bridge.

Equation 12 reveals that extremely small thermal response times are obtainable by shortening the SiC bridges. However, this would also increase the power consumption.

Many factors distinguish SiC bridge devices from devices using standard silicon micro machining. Due to the high doping and large defect density in the SiC material (83) the resistors showed little drift, and performed better than devices with Pt heater elements. In tests, the SiC devices could be exposed to compressed air without damaging the bridges. Shows the thermal stability of the SiC bridges. Since SiC has a high melting point, the bridges can be operated under white glow for several hours before breakages occur.

2.2.5 Three Dimensional Silicon Triple-Hot-Wire Anemometer Based On Polyimide Joints

The Design and operation of the miniaturized hot wire probe is shown in figure 19. This type of flow sensor is based on the anemometer principle. The thermal anemometer measures fluid velocity by sensing changes in heat transfer. The sensor can be operated with either the total power dissipation or the heated wire temperature kept at a constant value. Constant power dissipation allows the temperature of the heated hot-wire to decrease with increased velocity of flow. For spatial resolution, the hot wire must have a length to diameter ratio of at least 100. Silicon nitride around the hot wires prevents oxidation, making it possible to use at high temperatures.

Time constants of 120 and 330 μs were measured for the cooling and the heating of the hot wire. The response time of the sensor can be improved by operating at constant temperature (85). Heating the whole chip in a controlled climate chamber at zero flow performed measurements of the resistance temperature dependency of the hot wire. The range of operation of this flow sensor is limited between 0 and 60 LPM. No hysteresis effects were measurable during cycling of the temperature. The glue used for mounting the silicon chip to the circuit board limited the maximum substrate temperature to 150 degrees C.

The hot-wire resistance is a function of supplied power. Possible temperature variations over the wire mean that only an average temperature can be obtained and that the maximum

temperature is higher. A measurement set up was used to demonstrate the flow sensitivity of the hot wire.

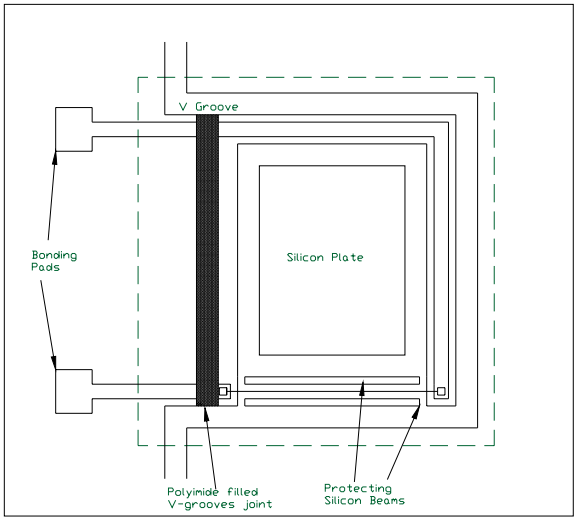

Figure 19: Miniaturized hot wire probe

2.2.6 Nano-Fluid Handling By Micro-Flow-Sensor Based On Drag Force Measurements

Micro fluidic components such as pumps, valves, and flow channels have been miniaturized, integrated and assembled, forming single intelligent components (86), and complex integrated chemical analysis systems (87, 88).

In all of the micro fluidic systems, measurement of small flows must be precise for the controlled handling of fluids. Approaches such as mass flow (89), ion pulse generation (90), differential pressure and hot wire anemometry (91) have been presented. The best systems can measure flow rates at 0.1 µl per minute with response times of 1 millisecond.

With laminar flow and a small Reynolds's number, the force due to the pressure difference in the fluid is negligible compared to the force induced by the shear in the liquid due to viscosity. The drag force parallel to the flow direction is given by Navier-Stokes:

$$F_D = C \cdot L \cdot v \cdot \eta \qquad \text{(Equation 13)}$$

Where,

C: Constant depending on the form of the obstacle

L: dimension of the obstacle

V: speed of the fluid

η : absolute viscosity of the fluid

To obtain the flow velocity profile inside the channel, the pressure drop is given by (92)

$$\Delta P = \rho \xi a (v_0^2 / 2) \qquad \text{(Equation 14)}$$

Where,

ρ: Density

ζ a : Geometrical factor

v_0 : average fluid velocity

The flow velocity profile in an equivalent cylindrical channel as a function of its radius is (93):

$$V(r) = \Delta P\{(d_h / 2)^2 - r^2\} / 4\eta I \qquad \text{(Equation 15)}$$

Where I is the channel length.

For the cantilever beam, assuming that the mass is negligible, a

Force exerted on its end will induce a moment M where the piezo-resistors are diffused.

Then, the stress at the surface is given by (94):

$$\mathrm{O} = 6 * F_D * L_b / W * T^2 \qquad \text{(Equation 16)}$$

Where,

T: Thickness of the suspension

W: Active width of the suspension

L_b: Length of the thicker beam

The stress is measured with a Wheatstone bridge diffused into the surface of the suspensions.

$$\Delta U / U = \Delta R / R = K * \Delta \mathrm{O} \qquad \text{(Equation 17)}$$

Where,

K: gauge factor

U: bridge voltage

The fluid passes through the chip displacing the obstacle suspended by silicon beams. The force is a linear function of the fluid's velocity in laminar flow, and a quadratic function of the velocity in turbulent flow.

Experimental results

The measurement of the drag force is obtained by measuring the output voltage of a Wheatstone bridge diffused into the support beams. When applying a DC voltage to the bridge, output sensitivity of 20μV/V per μl/min was obtained. Figure 20 shows sensor output vs. flow-rate curve after amplification by 500.

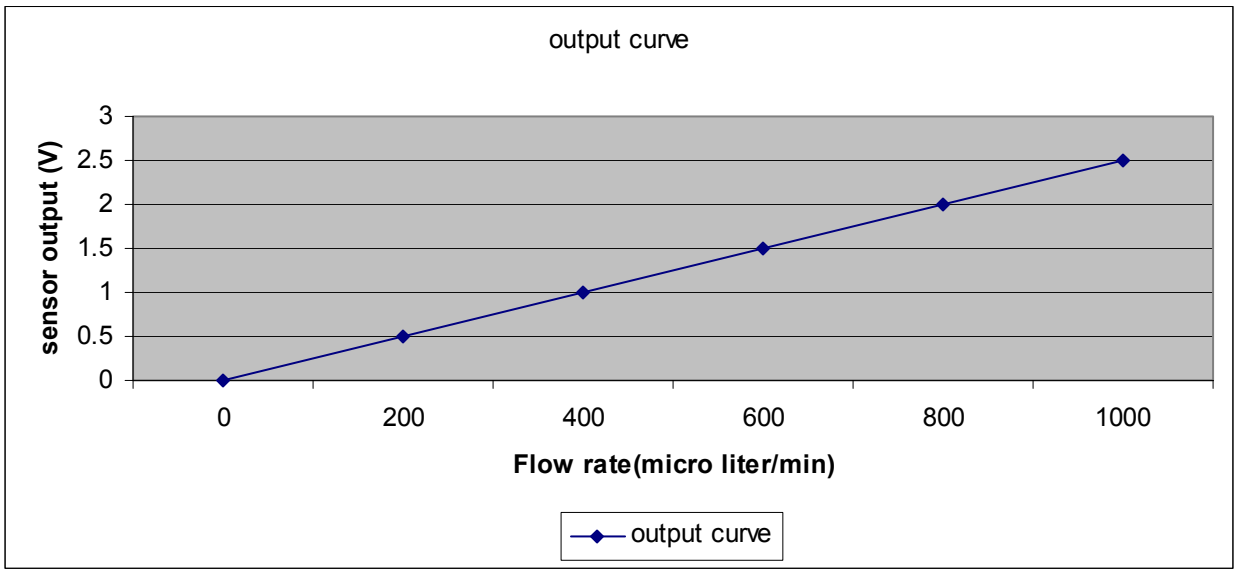

Figure 20: output voltage versus flow rate

3.0 EXPERIMENTAL PROCEDURE

3.1 Description

In this section an experimental procedure is described for the testing of CPAP flow sensors. The experiments were specially designed to quantify new and cheaper flow sensors for use in the manufacturing of CPAP devices. CPAP stands for continuous positive airway pressure. The CPAP machine is an FDA approved medical device and a doctor's prescription is required for its use. The CPAP consists of a blower, power supply, and a printed circuit board. The printed circuit board monitors and controls the blower pressure output by using pressure and flow sensor feedback. The primary scope of the present investigation is to optimize the flow sensor of the CPAP unit.

People with sleep apnea primarily use the machine. Sleep apnea is a condition in which a patient temporarily ceases to breathe during sleep and is awakened. The arousals occur when the patient "snorts" to open a closed airway or high levels of CO_2 trigger a response in the brain to awaken the patient. The CPAP machine treats this condition by stinting the airway open with positive pressure. The patients usually are diagnosed through an overnight sleep study at a hospital. A person with sleep apnea will often be extremely tired and lethargic during the day. Some studies show sleepiness to be as dangerous as alcohol in work related and automobile accidents.

Purpose.

In the experiments several sensors were tested. These sensors have different designs, sensitivity and performance. The experiments differ for each design but a standard procedure was maintained in order to have comparable data. In the experiments, sensors were tested at different temperatures and different days in order to simulate a real life situation. The following sensors shown in figure 21a, 21b, 21c, and 21d were tested using the general setup shown in figure 22:

a. Honeywell AWM2100V
b. Honeywell AWM92100V
c. Silicon Micro Structure Pressure Sensor
d. Thalis Greek Sensor

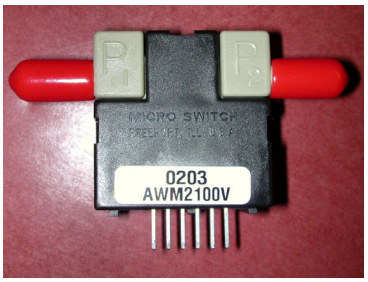

a. Honeywell AWM2100V

b. Honeywell AWM92100V

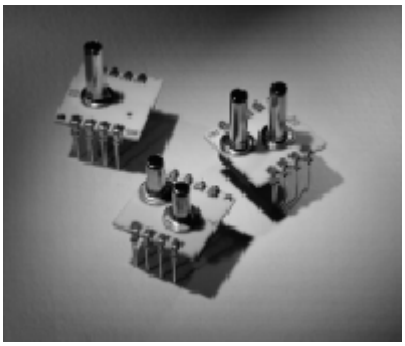

c. Silicon Micro-Structure pressure sensor

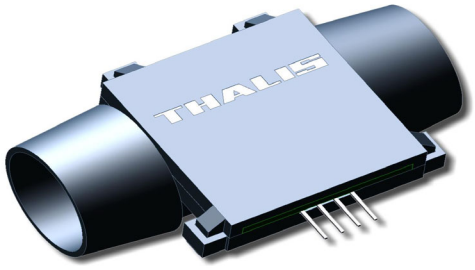

d. Thalis Greek flow sensor

Figure 21: Types of sensors tested

3.2 Development Of Standard Testing Protocol

One of the primary focuses of the current research was to establish a standard testing procedure for analyzing mass flow sensors. As will be described in this section, a protocol was created that can be utilized to compare the performance of mass flow measurement devices. Different flow sensors are known to have different properties. In order to determine which flow sensor has the best performance for a certain application, a standard test should be established that eliminates the variables. When considering flow sensors performance, there are two variables that have the most substantial influence: Temperature and pressure. This is due to the fact that as temperature and pressure change, the density of the fluid passing through a sensor will vary. Since sensors typically use Nano-technology (i.e. they work as a bypass that is very narrow compared to the to the main flow in the tube), a change in fluid density will substantially

change the output of the sensor. To differentiate between sensors, a standard procedure that eliminated the variable of temperature was specially designed and constructed. This procedure, which is schematically shown in Figure 22, is outlined below:

1- Set a blower to a specific pressure and keep the pressure constant at all times when conducting the experiment.
2- Use enough tubing between the blower and the sensor to make sure the flow is laminar before it hits the sensor.
3- Most sensors are connected to the tubing in parallel and require a certain piece specifically designed to compensate for the pressure drop across the tube in question; make sure this piece is always oriented in the same direction as shown in figure 25. A change in orientation might show some deviation in the graph of the output as seen in figures 26 and 27.
4- Use enough tubing after the sensor and before the valve to eliminate the effect of backpressure.
5- Use a calibrated TSI flow sensor to link its reading, the flow output, to the voltage output reading of the voltmeter.
6- Make sure the TSI flow sensor, the voltmeter, and the power supply have been recently calibrated.
7- Test all sensors in an environmental chamber at different temperatures, in our case 0, 20, and 40°C.
8- Make sure all the equipment used and all the sensors subject to testing are kept in the environmental chamber at all times. Wait at least half an hour after the chamber reaches the targeted temperature and then start the testing of the sensors.
9- Every time you open the chamber, repeat procedure 8.
10- It is recommended to have one person test all the sensors.
11- For best results, at least 10 sensors from each production date should be tested; a total of three different production dates should be enough.

To conduct a test one must check that all the tubes are sealed and the environmental room is at the right temperature. After the blower and the sensor circuit board are on, the flow rate can be read on the TSI flow sensor and the voltage output of the sensor can be read on the voltmeter.

These two reading are used to generate all the charts to compare the output of different sensors as shown in chapter 4.

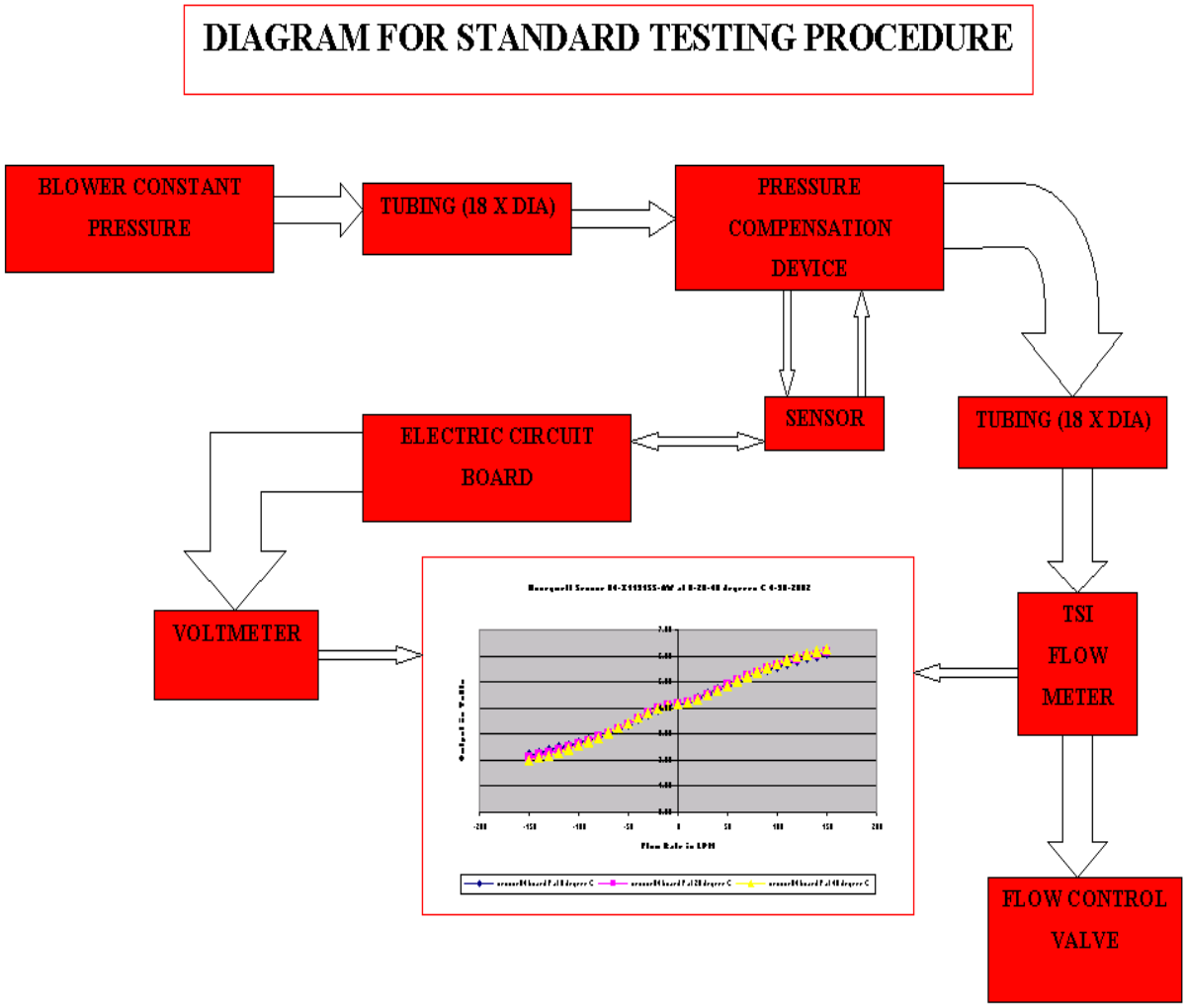

Figure 22: Diagram for Standard Testing Procedure

3.3 Equipment Setup

a- B&k-Precision model 1660 triple output DC powers supply

b- Thermal Mass Flow Sensor TSI Model 4040

c- FLUKE 87 True RMS MULTIMETER

d- Blower- CPAP machine set to 20-cmH20 constant flows

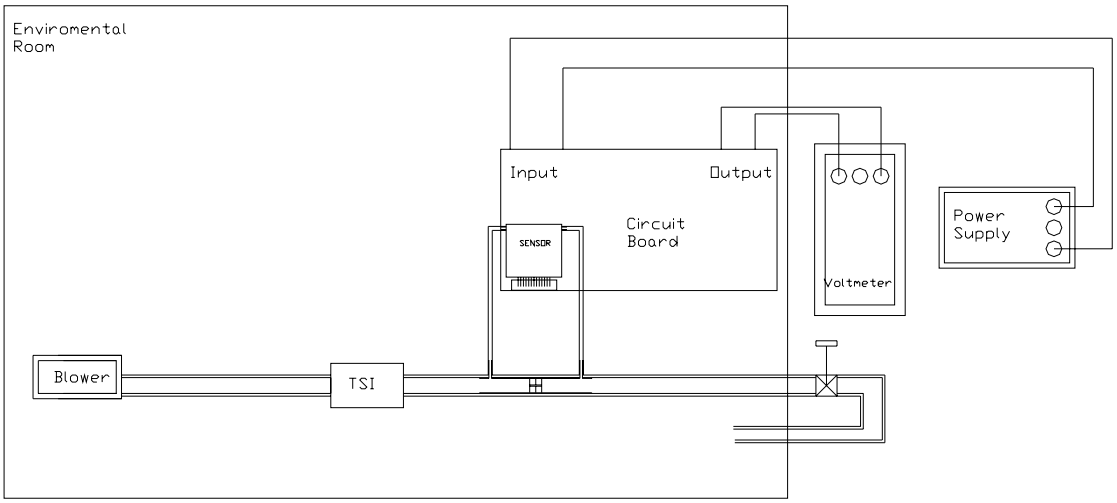

Figure 23: General setup

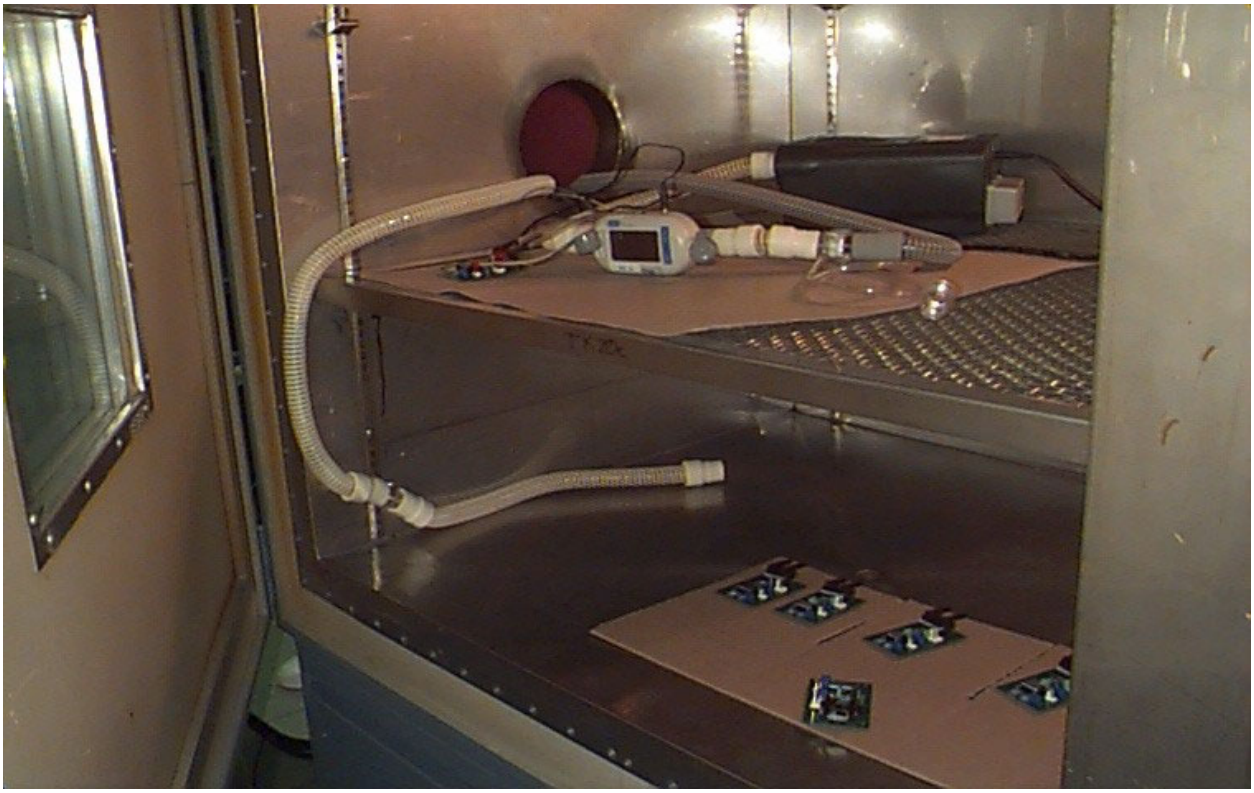

Figure 24: Blower, TSI flow meter, sensors and circuit boards inside the environmental chamber

The test experiments took place in an environmental chamber with temperature and humidity control. The flow sensors were tested at temperatures of 0˚C, 20˚C and 40˚C, at a humidity of 65%. In order to keep all of the comparative sensors at the precise test temperature and humidity conditions, all sensors were placed inside the chamber during testing (see figure 23). When testing of a specific sensor was completed, the room was opened for a short period of time (approximately 30 seconds) in order to replace the sensor. Before the testing of the new sensor began, 30 minutes elapsed to allow the room to stabilize to the original test conditions. The equipment needed for the flow control (control Valve), the data collection (Fluke 87 Voltmeter) and the powering of the sensor and circuit board (Power supply) were kept outside the chamber as shown in Figure 24.

Figure 25: Power supply, control valve and voltmeter

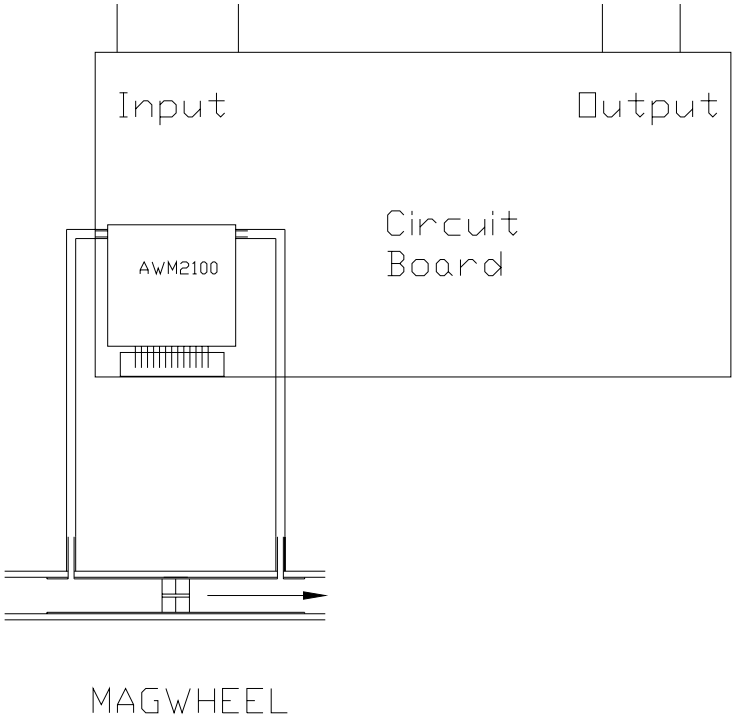

Figure 26: Magwheel Direction

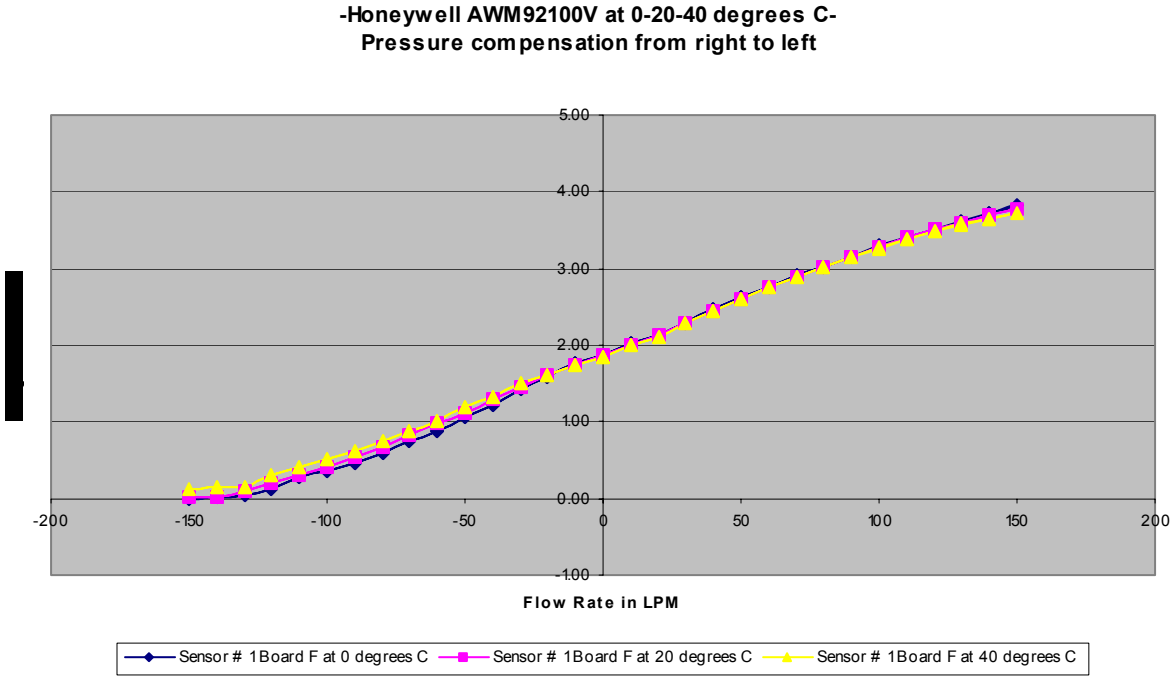

Figure 27: output when Pressure compensation equipment oriented from right to left

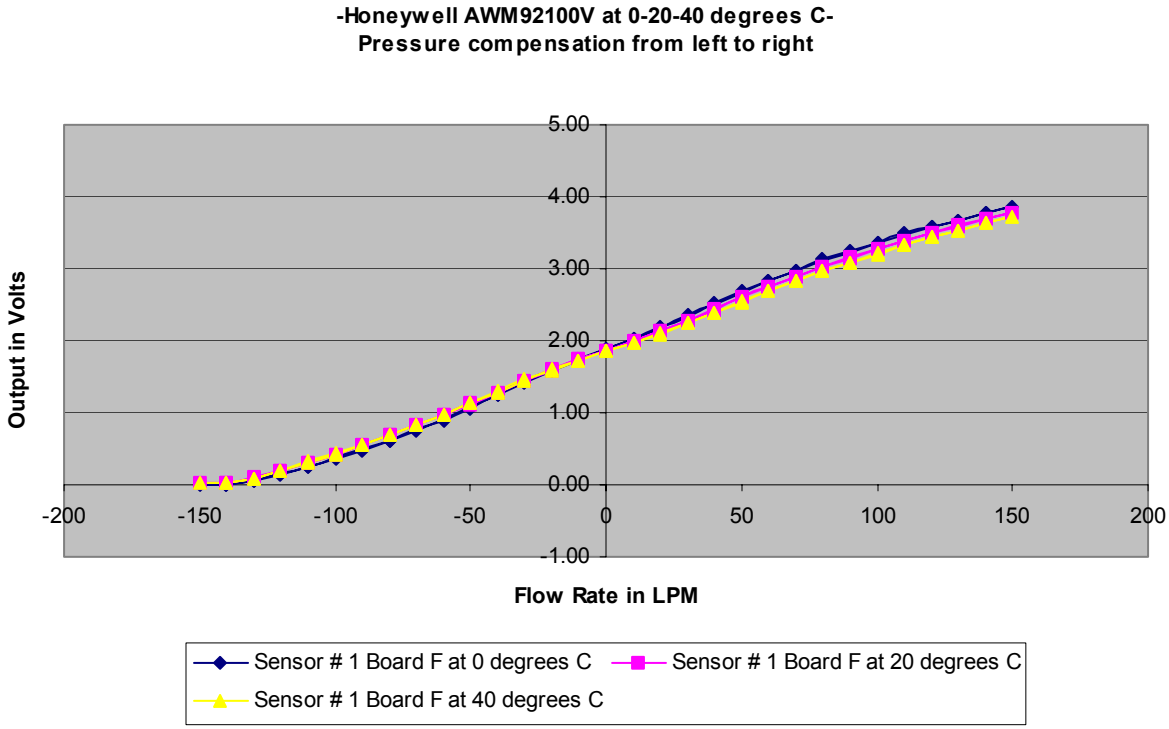

Figure 28: output when Pressure compensation equipment oriented from left to right

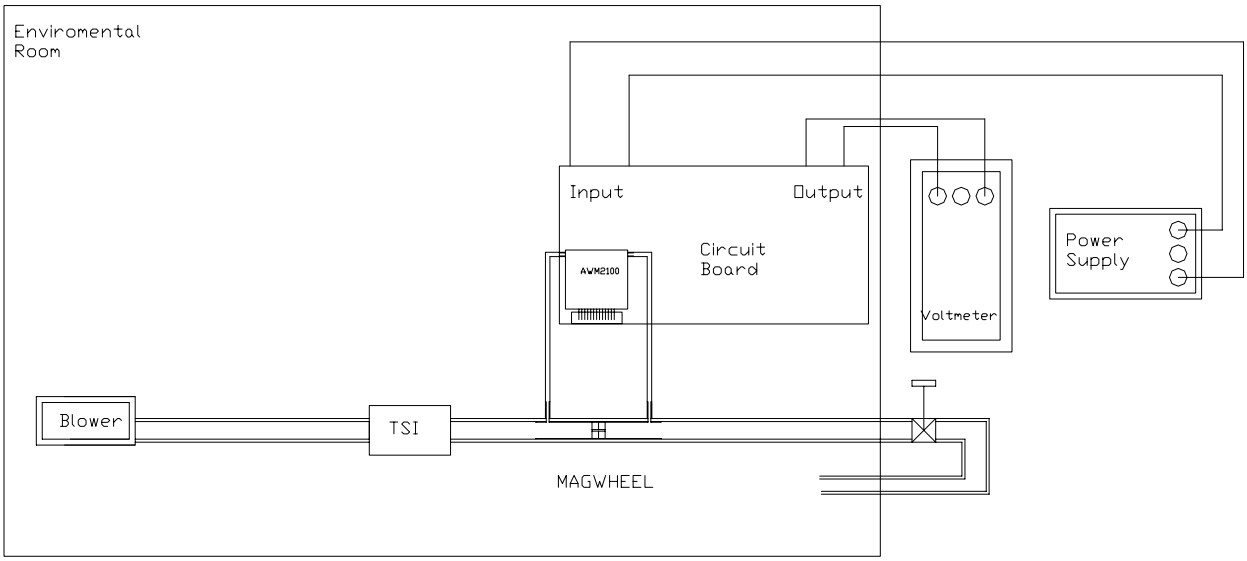

Figure 29: Test setup for Honeywell sensor AWM2100V

To test the Honeywell AWM series flow sensors and the Silicon Micro-Structure pressure sensor a printed circuit board was designed. The board was powered with a constant DC voltage from a regulated BK PRECISION triple output DC power supply model 1660. Each sensor was mounted onto this circuit board. The board was then adjusted and the flow sensor zero point and span (or maximum) measurements were found. The sensitivity of the flow sensors with respect to the flow velocity read on the TSI flow sensor, was interpreted into a voltage output from the circuit board, and read using a FLUKE 87 true RMS multimeter.

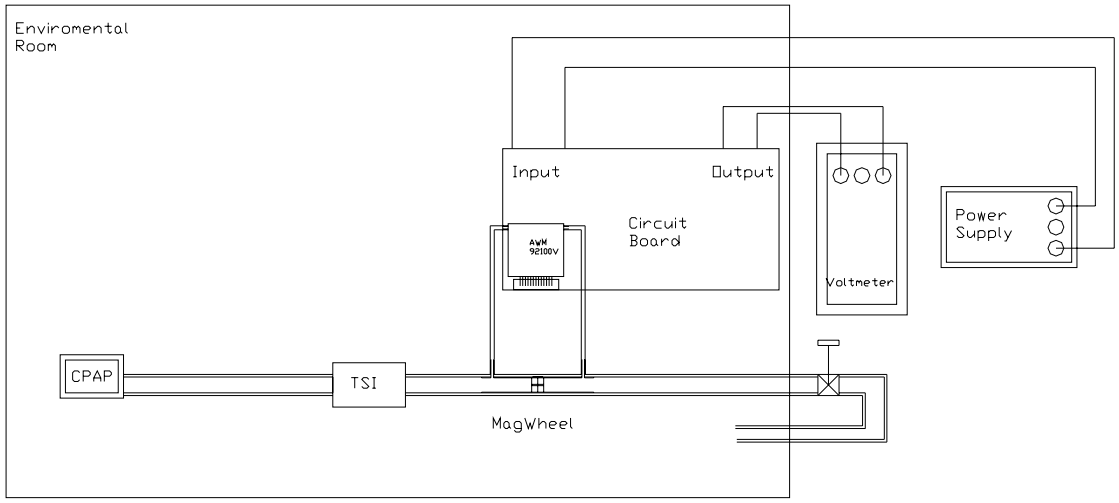

Figure 30: Test setup for Honeywell sensor AWM92100V

The procedure was completed using one Honeywell AWM2100V, since the data for this sensor was available and it was only a matter of verifying it using our test setup. Eighteen different Honeywell AWM92100V sensors were then tested using the same procedure. The output voltage was recorded for each increment of flow ranging from 0 to 150 Liters per minute, then from 150 back to 0. Each sensor was then tested from 0 to –150 Liters per minute and –150 back to zero. In a few sensors, the testing was done in increments of 1 Liter per minute between 0 and +/- 10 Liters per minute, and in increments of 10 Liters per minute for all other flow rates. For the increments ranging from 0 to +/- 5 Liters per minute, the valve was manually adjusted due to its low sensitivity at these levels. In all the remaining experiments, increments of

10 Liters per minute from (zero to 150-150 to zero-zero to –150 and –150 to zero) liters per minutes were used.

An identical testing procedure was used for a Silicon Microstructure pressure sensor. This sensor was also mounted on the existing circuit board that was used for the Honeywell AWM2100V. The board was powered with a constant DC voltage of + 25 volts DC from a regulated BK PRECISION triple output DC power supply model 1660. The sensors were mounted onto this circuit board, which regulates the input and gives +15 volts to excite the pressure sensor. The board was then adjusted for the zero point and span (or maximum) measurements. The data of the output of the flow sensor read using a FLUKE 87 true RMS multimeter versus the airflow velocity read on the TSI flow sensor were then plotted in Excel. The test setup is shown in figure 28.

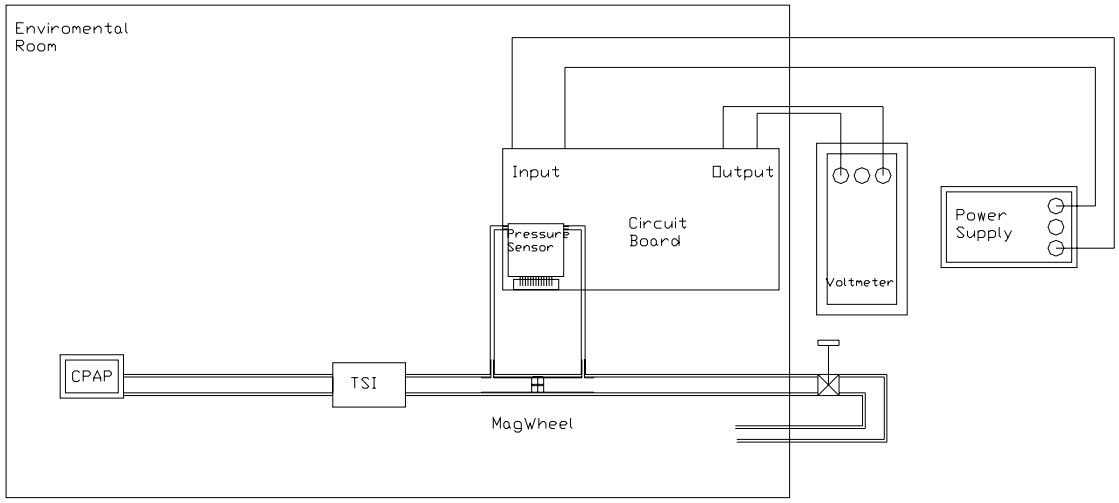

Figure 31: Test setup for Silicon Micro-Structure pressure sensor

An identical procedure was conducted for the Greek sensor, but the setup for this sensor was slightly different. The Magwheel was not included because the Greek sensor contains its own type of design that compensated for the pressure drop through the pipe. The Greek sensor didn't need a circuit board either. The electronics needed were imprinted on the Silicon chip

using C-MOS technology. The sensor was mounted on the same silicon ship inside the pipe, which eliminates the use of parallel tubing as shown in Appendix C. The same regulated BK PRECISION triple output DC power supply model 1660 powered the sensor. A constant bipolar DC voltage of +16 and –16 Volts excited the sensor and powered the accompanying electronics. The test setup included a CPAP machine set to 20-cmH_20 constant flows. Air was transferred through patient tubing to the TSI flow meter. The tubing was 22mm ID plastic tubing. The TSI flow meter measured airflow in standard liters per minute (SLPM). After the TSI flow meter, the air entered the inline Greek sensor, which included a design to compensate for the pressure drop. The output of the sensor is directly read for every flow rate reading on the FLUKE 87 true RMS multimeter. The flow rate and the output voltage data was collected and plotted in an Excel chart. After the Greek sensor, the airflow goes through tubing to an in-line hand valve that controls airflow. The length of the hose between the blower and the flow meter is at least 18 times its diameter to accommodate the test standards. The test setup is shown in figure29.

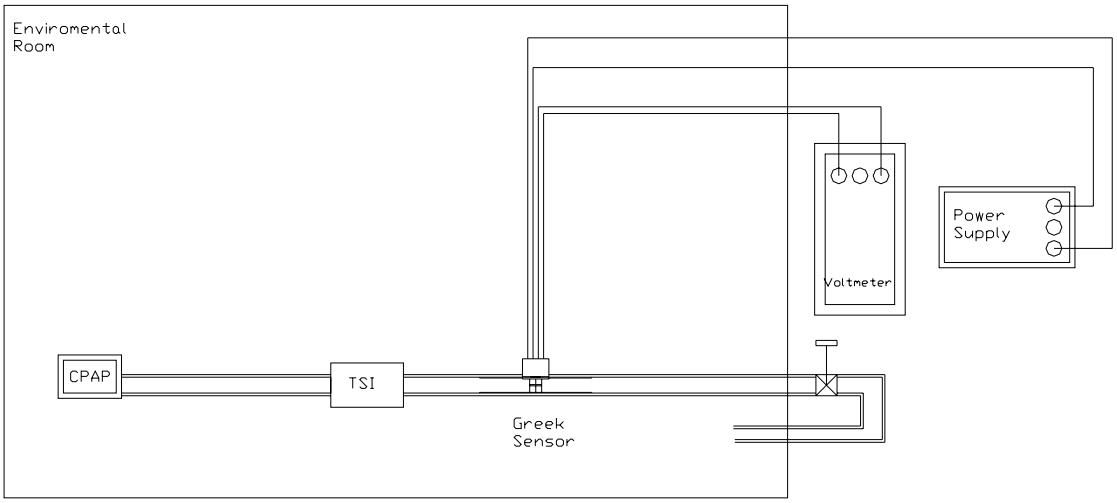

Figure 32: Test setup for Thalis Greek sensor

The data collection tables for all sensors, showing the output voltage at different flow velocities for varying temperatures (0, 20 and 40ºC), are given in Appendix B. The plots showing the voltage output versus the airflow velocity will be discussed in section 5.

Testing was completed between 0 and +/- 150 Liters per minute to show the hysteresis of each sensor. The results show the repeatability of each sensor and whether the flow is increasing or decreasing. Also, the testing of the sensors was repeated on different days to show how each sensor behaves at different conditions.

3.4 Measuring The Noise Level Of A Flow Sensor

Experiments were also conducted to help quantify the electrical noise output of a flow sensor and its instrumentation when there is both no flow and a fixed flow passing through the resistive element of the flow sensor. The noise level at zero flow quantifies the clarity of the electronic circuitry without any mechanical turbulence. The mechanical noise or turbulence as it affects the electrical signal is subsequently measured in the constant flow test.

Procedure:

Before testing, the sensor was properly energized and all tubing was securely hooked between the sensor and the resistive element. Using an oscilloscope that is set to measure AC voltage, the output voltage of the sensor and the instrumentation (amplifier and offset controller) of the flow electronics were examined. Both the conditions of no flow passing through the flow element and a 100 LPM of air is passing through the flow element were examined. The peak-to-peak voltage and the frequency of the output signal for each sensor tested were recorded.

The procedure was repeated for various resistive elements (with approximately equivalent resistance) if necessary.

Results:

Sensor: Honeywell, AWM92100V with C-flex evaluation board excited with +12 VDC.

Noise detected with Vision AFM flow element or Magwheel resistor:

At Zero flow:

50 mVpk-pk at 250 kHz

At 100 lpm flow:

No discernable periodic signal (indicating turbulence) with 200mV peak-to-peak amplitude.

Discussion:

Due to its high sensitivity, the new Honeywell flow sensor eliminates noise from the system because the electrical gain is significantly lower. The Magwheel design was tested and

found to produce similar noise levels to the AFM flow element considered here as the gold standard. The "Plascore" and "Hexcel" designs were significantly noisier under testing.

3.5 Sensor Calibration

3.5.1 Multi-Point Calibration

The method of multi-point calibration helps the engineers use cheaper sensors. One advantage of this method is that it removes the requirement for linearity in the sensor's output. There are two methods to utilize multi-points calibration:

Higher order polynomial curve fitting

Interpolation

Using either method improves accuracy as long as the curve is generally smooth.

3.5.2 Auto-Zero

A software auto zero or drift correction method is another technique for improving sensors. As sensors age or as temperature fluctuates, the output of most sensors will drift at the zero or null point. When using in combination with a high gain, this issue becomes very important. For example in a given sensor configuration the gain is set to 1800 V/V and the sensor has drifted ±1mV at its zero.

$$1800 * 1mV = 1.8V \qquad \text{(Equation 18)}$$

The error is 1.8 V in the positive or negative direction. If the maximum acceptable output is 0 to 5V, and if the auto zero is not used, the usable span now becomes:

$$5V - (1.8 * 2) = 1.4V \qquad \text{(Equation 19)}$$

Having 1.4V instead of 5V span is a significant decrease in resolution. The solution for that is to use "auto zero" to keep the usable span at 5V.

Using multi-point calibration combined with auto zero may reduce cost and increase the resolution.

4.0 DISCUSSION

4.1 Background Of Sensors

4.1.1 Background Of Honeywell AWM2100V Flow Sensor

The commercially available sensors consist of single hot wires that are mounted on the end of a long probe. The elements are fully exposed to the air stream and are therefore susceptible to breakage and contamination. The commercially available mass flow sensor consists of a metal tube through which the air is passed, a transformer which resistively heats a segment of the tube, and two thermocouples attached to the tube symmetrically. Airflow through the tube cools the upstream thermocouple and heats the downstream thermocouple. The difference between thermocouple voltages at constant power input is a measure of the mass flow. The AWM2100V sensor consists of a pair of thin film heat sensors (22, 24), a thin film heater (26), and a base supporting the sensors and heater out of contact with the base. The sensors are on opposite sides of the heater. The base is a semiconductor, usually silicon, chosen for its adaptability to precision etching techniques and the ease of manufacturability. The embodiment includes two temperature sensing resistor grids (22, 24), and a heater resistor grid (26). The temperature sensing resistor grids act as the thin film heat sensors and the heater resistor grid acts as the thin film heater. The sensors are made of nickel-iron, with a composition of 80 percent nickel and 20 percent iron. A thin film of dielectric, comprising layers to form thin film members, (see figures 30 and 31) surrounds the grids.

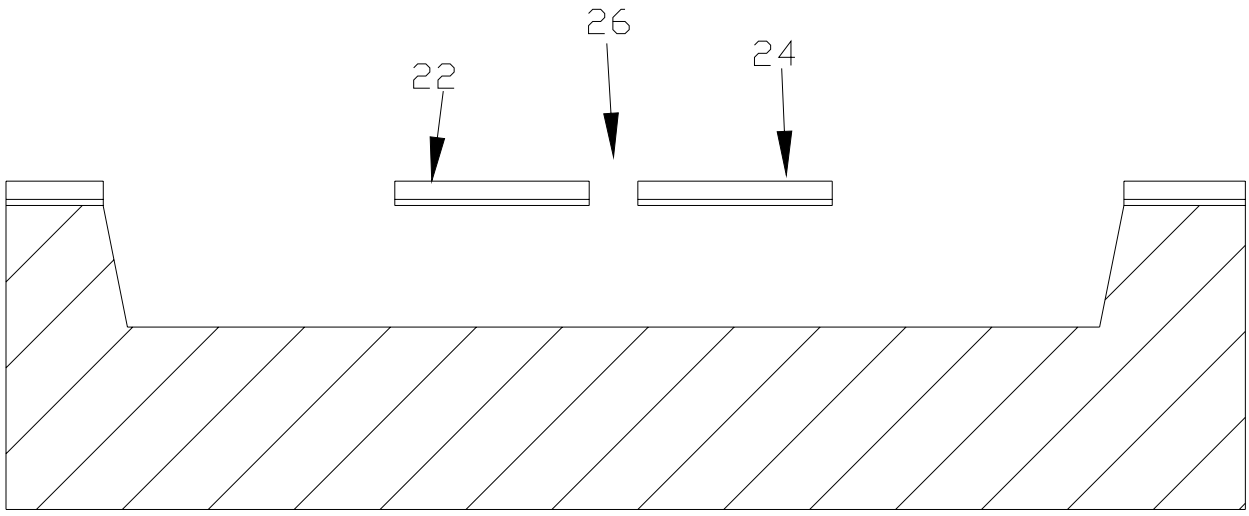

Figure 33: Embodiment of the sensors

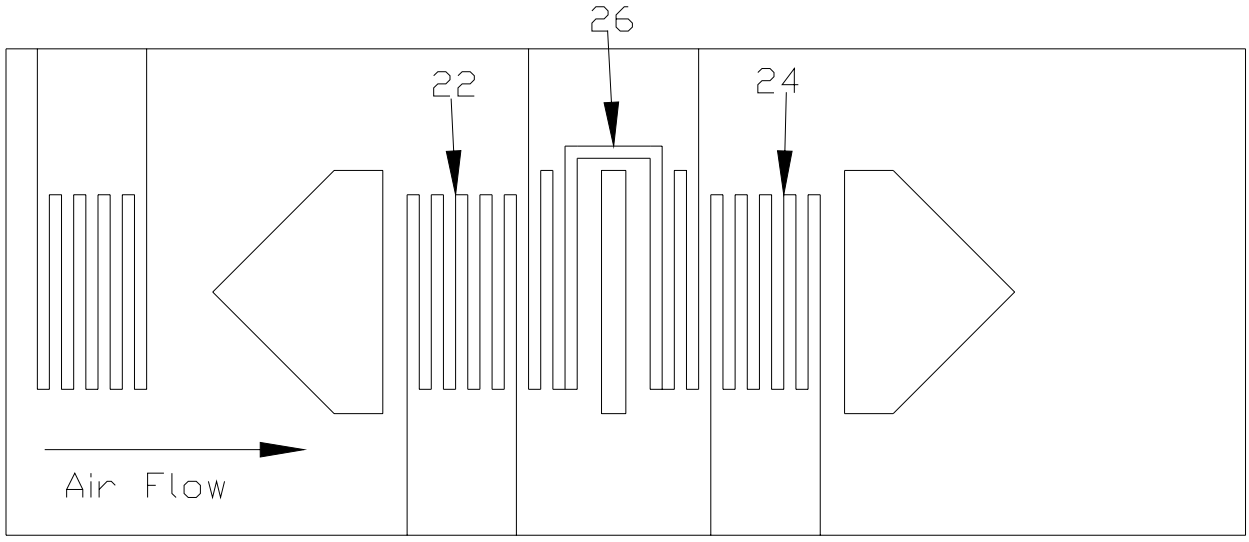

Figure 34: Top view showing the sensors and the heater

The sensor comprises two thin film members as shown if figures30 and 31. These films have a preferred dimension of 150 microns wide and 400 microns long. The embodiment of the sensor uses a defined air space surrounding the thin film elements. These elements have a preferred thickness of 0.08 to 0.12 microns with lines on the order of 5 microns wide. The elements are in a thin silicon nitride film with a total thickness of less than 0.8 microns.

The thin film members connect to the top surface of the semiconductor body at one or more edges. Figure 32 shows that the members are bridged across the depression. Alternatively, figure 33 shows that the members could be cantilevered over the depression.

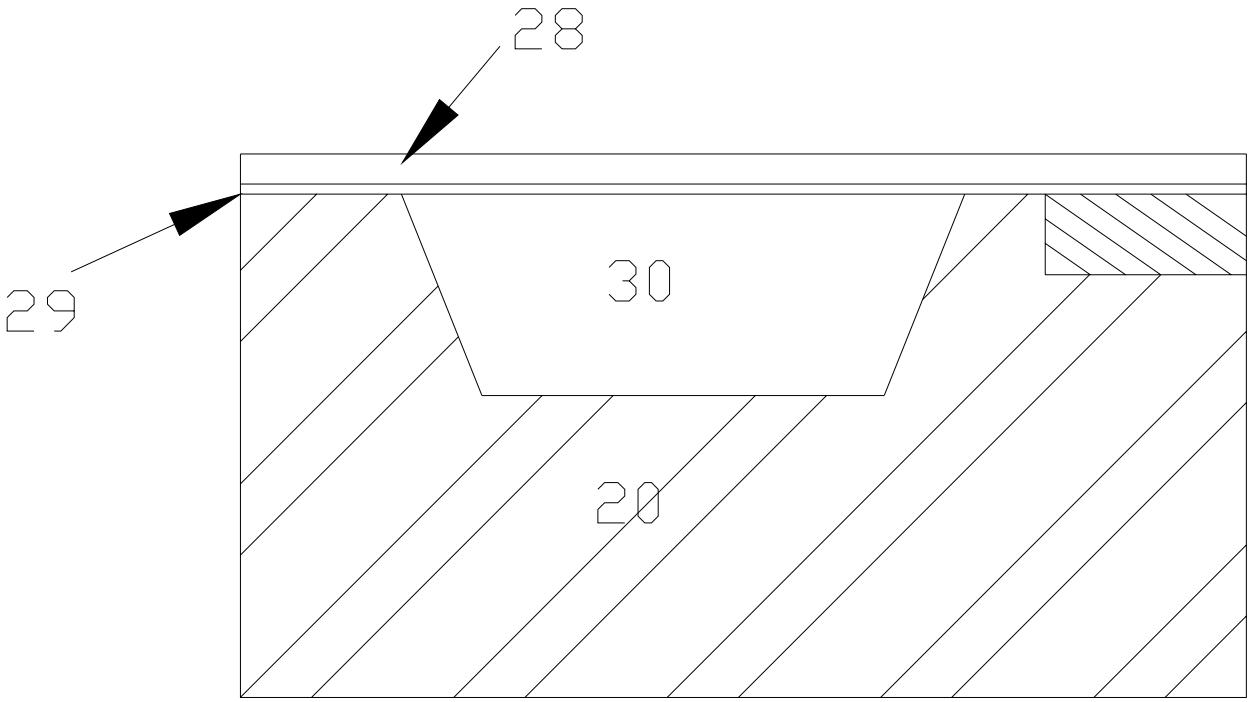

Figure 35: bridged members

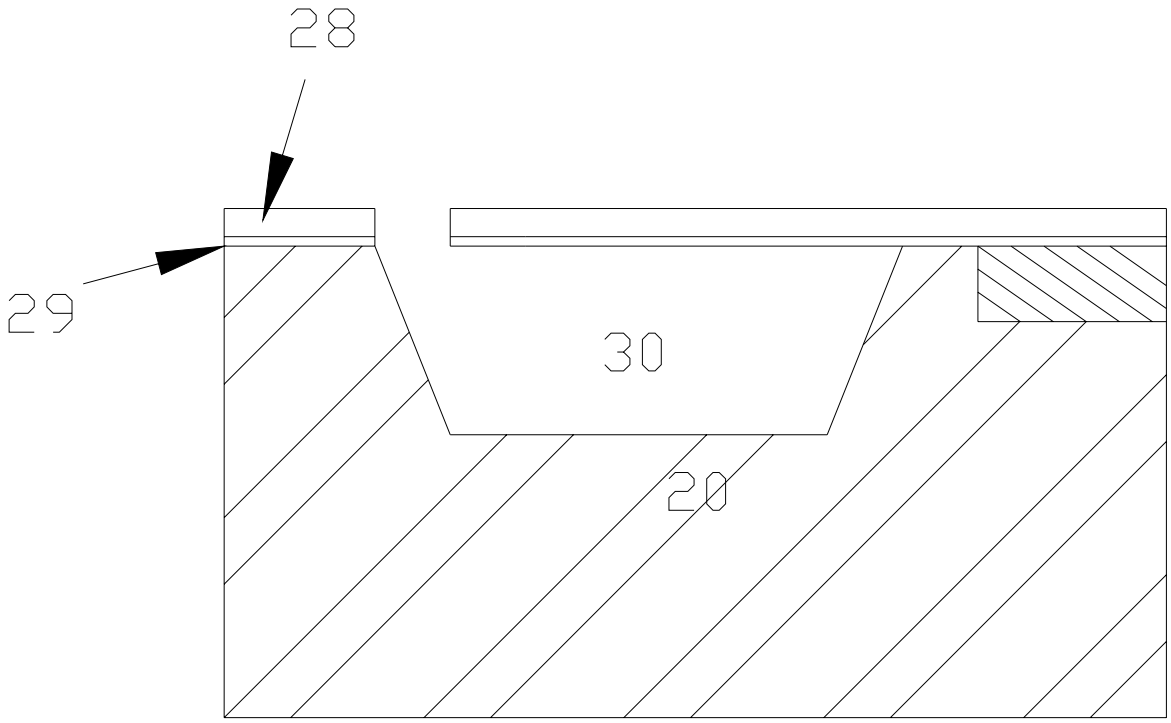

Figure 36: Cantilevered members

Silicon nitride is a highly effective solid thermal insulator; therefore it contributes very little to the loss of heat from the heater. The film also has such a low conductivity property that the resistor grids can be located immediately adjacent to the heating resistor grid and still allow most of the heat to pass through the surrounding air. Therefore, the sensing resistor grids are suspended in the air space near the heater resistor and act a thermal probe to measure the temperature of the air.

The operation of the present sensor in the sensing of airflow can be described using figure 31. The heater resistor grid operates at a temperature difference of 200 degrees Celsius above the temperature of the silicon chip, which changes by only about 0.5 degrees Celsius. The power required to achieve this temperature difference is less than 0.010 Watts. With zero airflow velocity, the thermal conduction heats the sensing resistor grids to about 140 degrees Celsius, or about 70 percent of the temperature elevation of the heater element. With airflow present, however, the upstream resistor sensor will be cooled by the transportation of heat away from the sensor, whereas the downstream sensor will be heated by transportation of heat toward the sensor. A resistance difference will also be present with a corresponding difference in

voltage drop, which is a measure of airflow. The unamplified voltage differences can be as high as 0.1 volts at 1500 feet per minute flow velocity, with a response time of 1millisecond.

In the operation of the device, the heater is operated at constant temperature above ambient temperature, the sensors are operated at constant current, and the changing temperatures of the sensors are sensed in terms of changes in resistance. Circuits are used for accomplishing this and are illustrated in figures 34 and 35. The circuit in figure 34 controls the temperature of the heater, while the circuit in figure 35 provides an output voltage that is proportional to the resistance difference between the heat sensing resistors.

The heater controls circuit shown in figure 34 uses a Wheatstone bridge to maintain the heater at a constant temperature rise above ambient. The circuitry of figure 35 monitors the resistance difference between the downstream and upstream sensors. It includes a constant current source comprising of an amplifier. The current source drives the Wheatstone bridge, and an output voltage is given that is proportional to the resistance difference between the two sensing resistors.

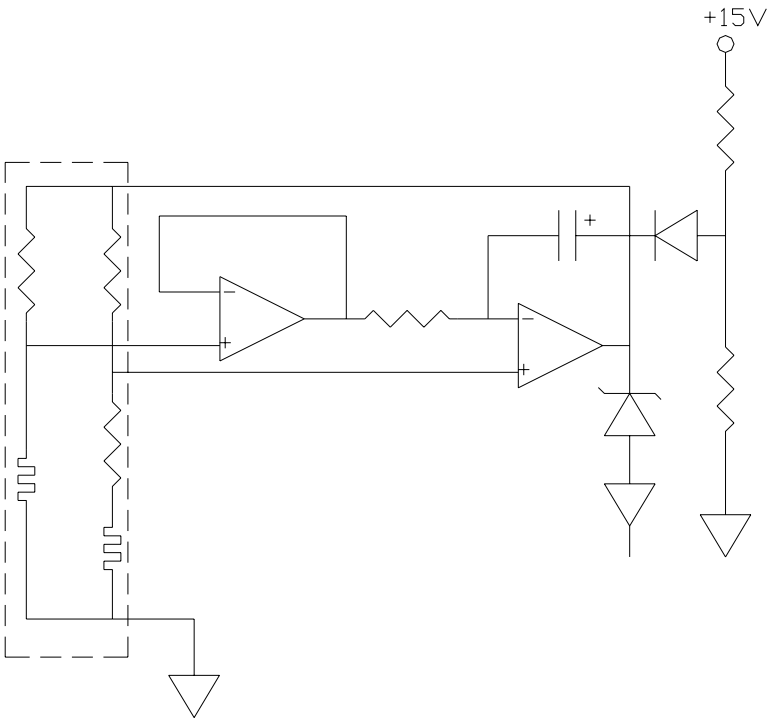

Figure 37: Heater temperature control

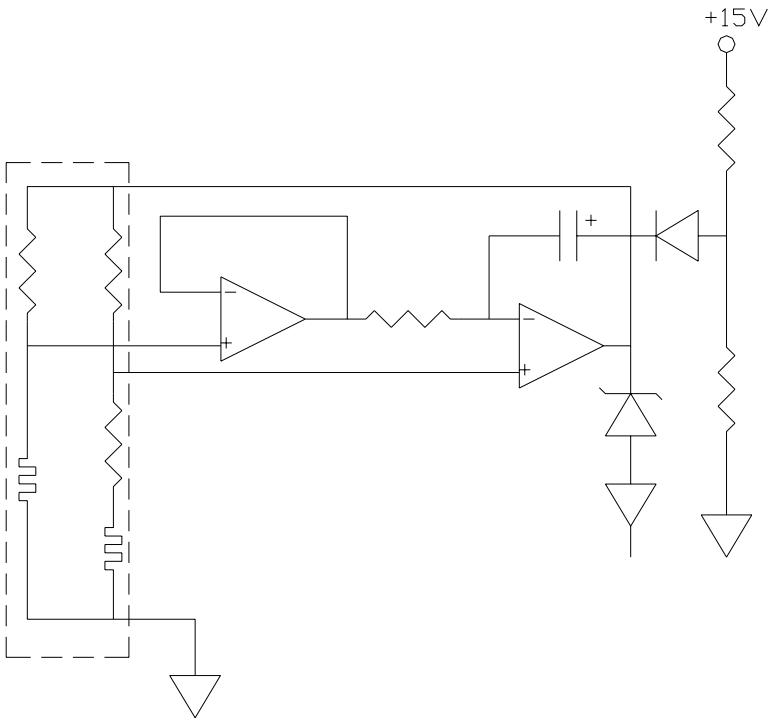

Figure 38: Output voltage

The AWM2100V sensor is capable of obtaining large temperature differences result in a large voltage output with greater accuracy and ease of flow measurement. As shown in figure 36, the large temperature differences are obtained by the combined effect of airflow cooling of upstream sensor and airflow heating of downstream sensor. The large heating and cooling effect is made possible by the thermal insulation of the silicon, and also by the large heating effect of the downstream resistor grid, between sensing resistors for a broad range of flow velocities. The large temperature differences

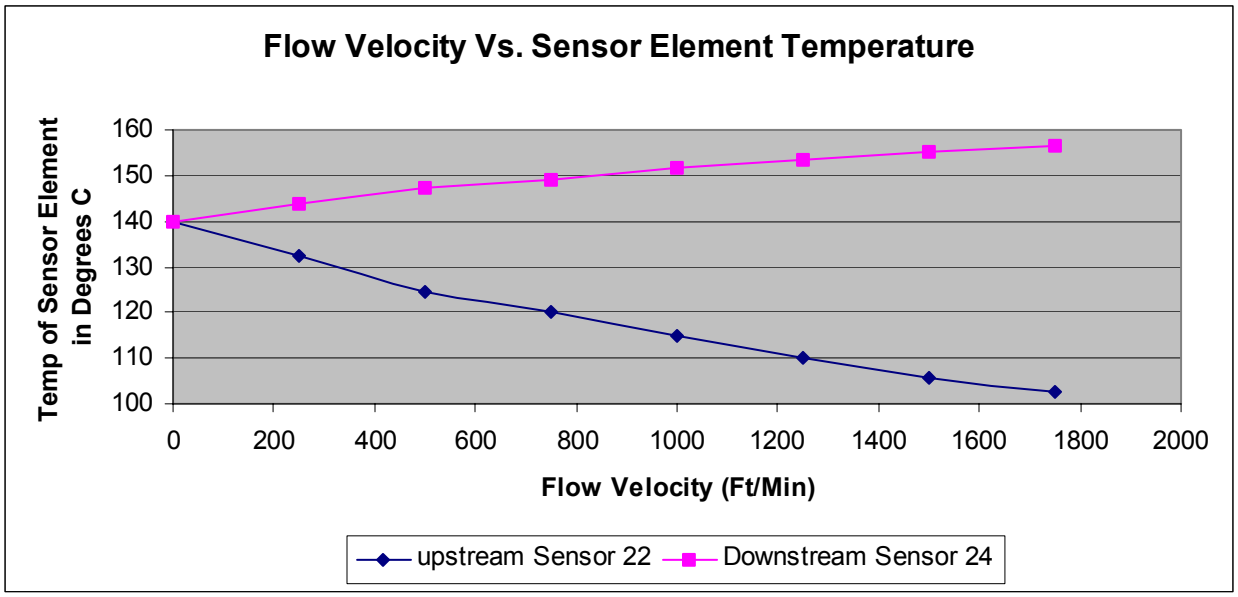

Figure 39: Temperature difference vs. flow velocity

Figure 37 shows the relationship between a zero flow temperature profile, an idealized profile and the optimal spacing for narrow sensor elements. The cooling effect of the airflow lowers the temperature profile by an amount that varies with distance.

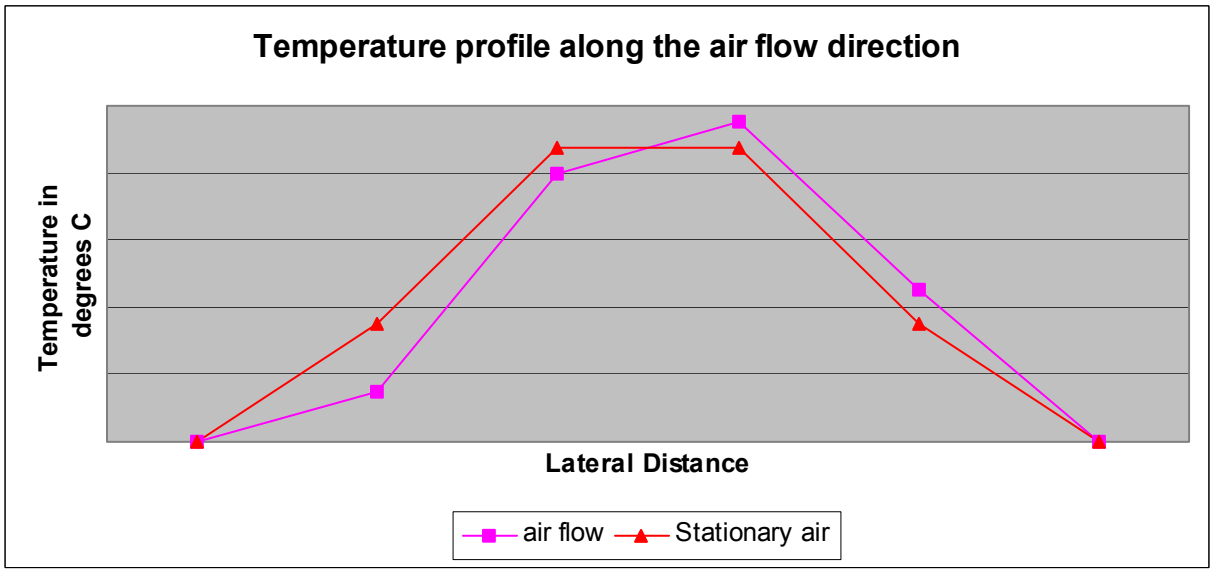

Figure 40: Temperature profile vs. flow

In the model created by Rahnamai et al, the heating and sensing elements are deposited on a lithium tantalite slab, and the elements are in contact with the slab. The slab is at least 60

microns thick. The heater is not effectively surrounded by an air space, and a large part of the conducted heat passes through the slab.

An advantage to the present design is that the defined air space around the sensor and heater elements effectively thermally isolates them from the silicon-supporting chip. Therefore, there is a negligible temperature elevation of 0.5 degrees Celsius. The airflow response of the present model is independent of the contact between the silicon chip and its supporting body. Another advantage of the present model is a more linear dependence of the temperature differential between the sensors over a broad flow range. Therefore, the response time of the change in the airflow velocity versus the change in the sensor temperature difference becomes substantially smaller at higher flow velocities. An airflow velocity response is shown in figure 38.

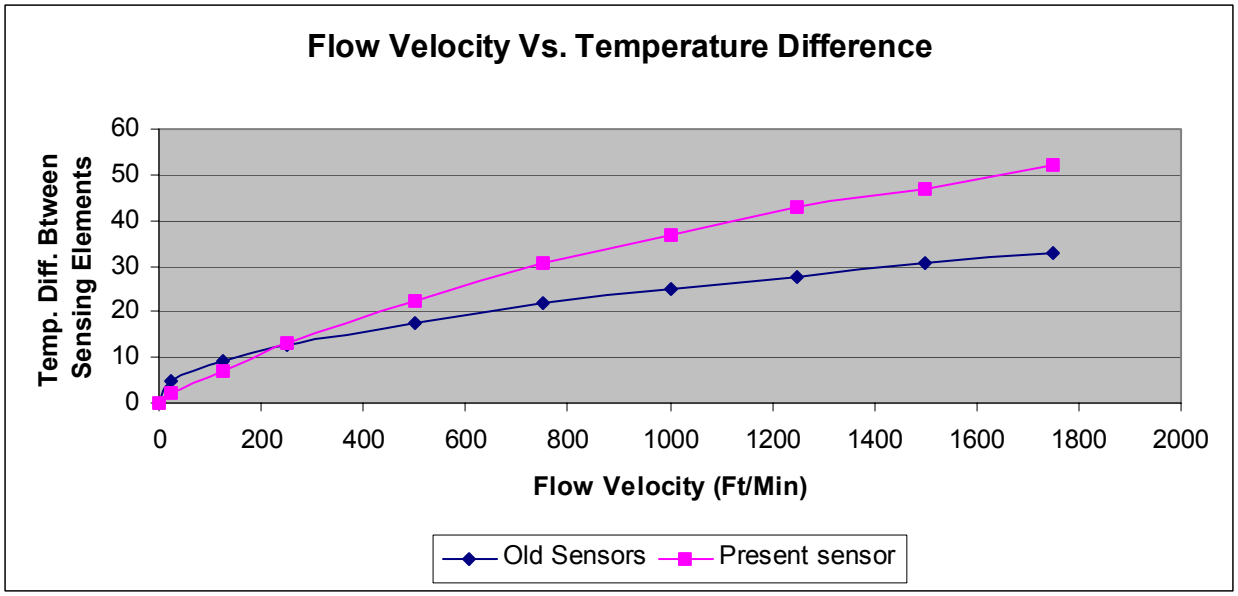

Figure 41: Flow velocity vs. temperature difference

In the present sensor, the resistance of the heater is held constant by the disclosed circuitry. The upstream sensor resistor has an inner edge close to the edge of the heater resistor grid. The zero airflow temperature is closer to that of the ambient air and to the silicon chip than to the temperature of the heater resistor (see figure 38). This large response to airflow velocity with the AWM2100V sensor facilitates applications where it is desirable to reduce flow velocity to achieve longer sensor life and greater freedom from turbulent effects. Also, the thin film sensors

and heater are protected from damage since the high velocity regions are at a substantial distance away from the films.

In order to use this sensor in our CPAP/BiPAP design, the sensor should be compatible with the flow element used. Some calculations must be made in order to find the right flow element design that matches the sensor. A detailed solution for the design parameters is included in Appendix A.

Table 3: AWM2100V SPECIFICATION

AWM2100V	
Rated Flow range	± 200 SCCM
Rated Pressure	N.A
Output Type	± 44.5 mV
Select by typical full scale pressure drop	0.5 cm H_2O or 0.49 mbar
Hysteresis & repeatability	±0.35% reading
Supply voltage range	8 to 15 VDC
Power Consumption	30 mW
Response time	1 msec
Operating temperature range	-25 to + 85 ºC
Null shift Typ.	±0.2 mV
Output shift Typ.	-25 to 25 ºC +2.5% reading +12 to 85 ºC -2.5%reading

4.1.2 Background of Honeywell AWM92100V Flow Sensor

The AWM92100V uses the same technology as the AWM2100V. It is a bi-directional flow sensor with slightly modified specifications. The new sensor requires the same calculation as the old one in order to solve for the ultimate flow element dimensions. The results of these calculations come out to be the same due to the similar geometry of this new sensor.

Table 4: AWM92100V SPECIFICATIONS

AWM92100V	
Rated Flow range	± 150 LPM
Hysteresis & repeatability	± 0.35 % reading
Supply voltage range	8to 12 VDC
Power Consumption	50 mW max.
Pressure drop at 200 SCCM	0.49 Typ.
Response time	1 mS typ.
Common Mode Pressure	25 PSI (1.7 Bar)
Storage temperature	-40 to 90 ºC
Operating temperature range	-25 to 85 ºC
Null shift Typ.	25 to –25 ºC and 25 to 85 ºC ± 0.2 mV[1]
Output shift Typ.	25 to –25 ºC +2.5% reading and (25 to 85 ºC) –2.5% reading[2]

The operation of the AWM92100V sensor is described as follows. The heater resistor grid operates at a temperature difference of 200 degrees Celsius above the temperature of the silicon chip, which changes by only about 0.5 degrees Celsius. With zero airflow velocity, the thermal conduction heats the sensing resistor grids to about 140 degrees Celsius, or about 70 percent of the temperature elevation of the heater element. With airflow present, however, the upstream resistor sensor will be cooled by the transportation of heat away from the sensor, whereas the downstream sensor will be heated by transportation of heat toward the sensor. A resistance difference will also be present with a corresponding difference in voltage drop, which is a measure of airflow. The unamplified voltage differences can be as high as 0.1 volts at 1500 feet per minute flow velocity, with a response time of 1 millisecond.

In the operation of the device, the heater is operated at constant temperature above ambient temperature. The sensors are operated at constant current, and the changing

temperatures of the sensors are sensed in terms of changes in resistance. Circuits are used for accomplishing this as illustrated in figure 39. The circuit in figure 39 controls the temperature of the heater as well as the output voltage that is proportional to the resistance difference between the heat sensing resistors.

The heater control circuit shown uses a Wheatstone bridge to maintain the heater at a constant temperature rise above ambient. The circuitry monitors the resistance difference between the downstream and upstream sensors. It includes a constant current source comprising an amplifier. The current source drives the Wheatstone bridge, and an output voltage is given that is proportional to the resistance difference between the two sensing resistors.

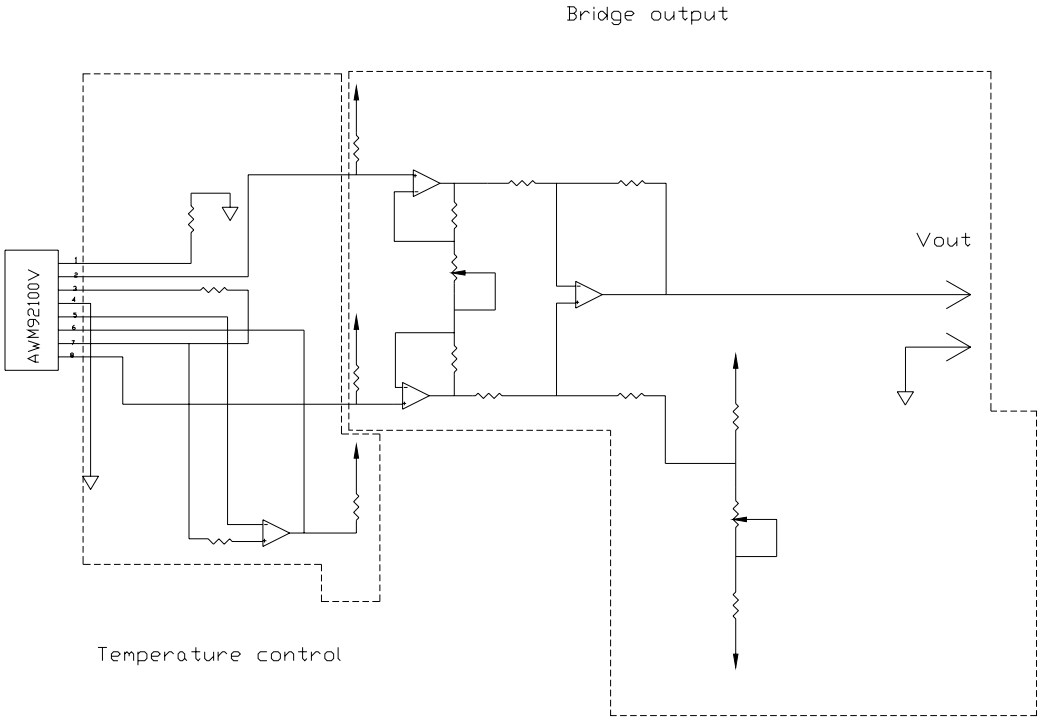

Figure 42: Electric circuit of AWM92100V

4.1.3 Novel C-MOS Compatible Monolithic Silicon Gas Flow Sensor With Porous Silicon Thermal Isolation

Integrated silicon flow sensors are advantageous because they can be mass fabricated and integrated into a circuit on the same ship.

The most obvious application of silicon temperature sensors is the direct measurement of temperature and temperature differences. The use of silicon is appropriate as long as the

temperatures are measured in the range of -50°C to 150°C. The most common method for measuring gas or liquid flow velocity is based on the measurements of temperature difference, ΔT, between the upstream and downstream ends of a heated temperature sensor as shown in figure 40. For small values of the flow velocity, the temperature difference can be expressed as:

$$\Delta T = C(T_S - T_F)v \qquad \text{(Equation 20)}$$

Where C is a constant, T_S is the average temperature of the sensor, T_F is the average temperature of the fluid or gas, and v is the flow velocity. For larger values of the flow velocity, the temperature difference becomes approximately proportional to the square root of the velocity.

$$\Delta T = C(T_S - T_F)\sqrt{v} \qquad \text{(Equation 21)}$$

In CMOS technology the resistive sensor and heater can be located on a bridge consisting of a sandwich of field oxide and CVD oxide and nitride (figure 40). The thermocouple cold contacts are usually located on bulk silicon, while the heater is on the tip of an oxide nitride beam (figure 41).

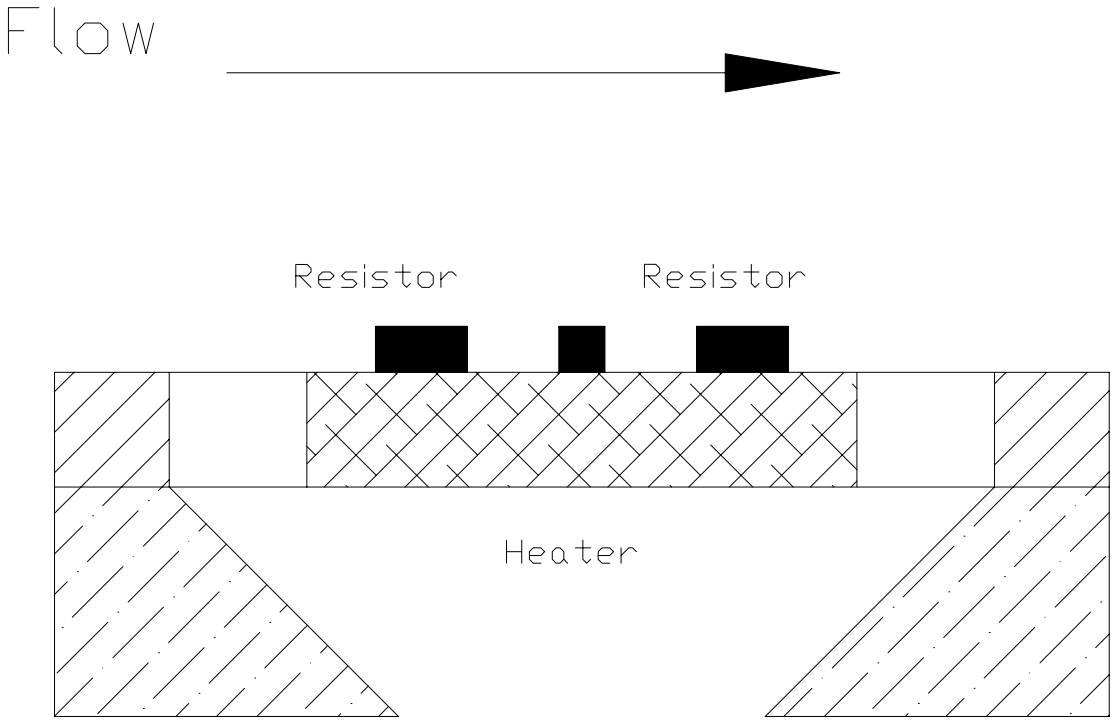

Figure 43: Resistive sensor and heater

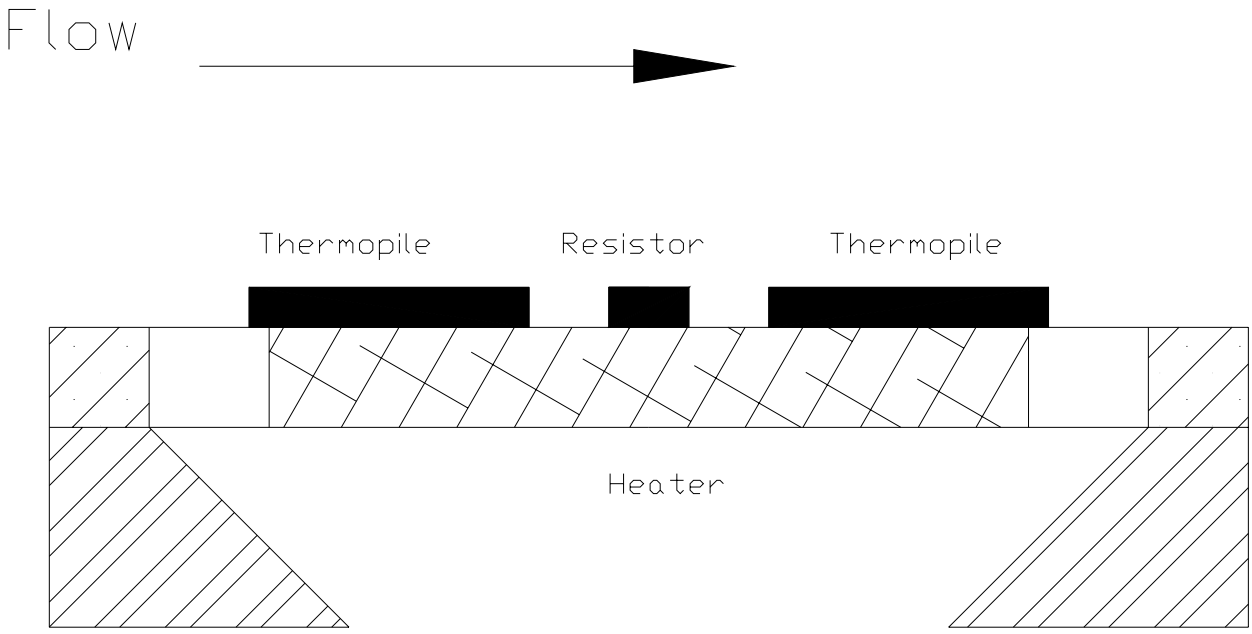

Figure 44: Thermopile sensor and heater

For this sensor they used two thermopiles (one upstream, one downstream) as shown in Figure 42. In this case, where the temperature difference is obtained by constant sensor sensitivity, it is desirable to keep constant power dissipation in the heaters. Special electronic circuits can provide the constant power.

This type of flow sensor is based on a thick porous silicon layer. The two thermopiles are made up of two series of Al/p-type thermocouples, which are placed on both sides of a heater. The heater and thermopiles are placed on a thick porous silicon layer that provides excellent thermal isolation (95, 96) due to the low thermal conductivity of porous silicon (97).

Thermopiles are used as sensing elements because they present many advantages over other sensing elements (98) such as resistors or diodes. Some of the general advantages of thermopiles are their stability, low ohmic value (which implies little pickup of electromagnetic disturbances), good signal-noise ratio and the fact that zero input gives zero output. The high stability of the thermopile is due to the fact that it is modeled as a simple electric circuit consisting of a resistance, R, and a capacitance, C. The disadvantage is that, even though they show a higher sensitivity than resistors and diodes, this sensitivity is still low (i.e. the output is read in mV).

A top view of the sensor is shown in figure 42. The input current is introduced either directly to the heater through the aluminum contact pads 5 and 6, can also be input through a compensation resistor of exactly the same characteristics of the heater, but lying on bulk silicon instead of porous silicon, through aluminum pads 7 and 8. This resistor is used to compensate the resistance change of the heater due to heat exchange with the gas.

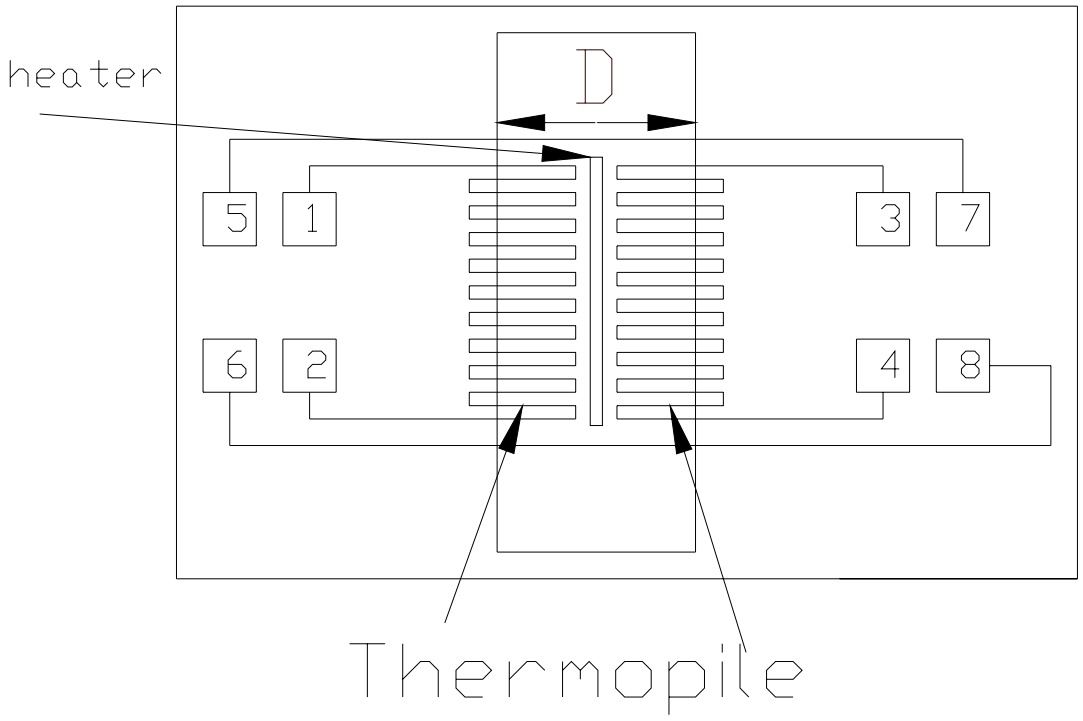

Figure 45: Top view

Table 5: Greek Sensor Specifications

Greek Sensor	
Description of properties	Value
Range of flow	0 to ± 200 standard liter per minute
Length	≤ 4.5 cm
Inner Diameter	2.2 cm
Pressure Drop	0.5 cm H_2O at 200 standard liter per minute

Table 5 (cont'd)	
Ambient operation temperature	0 to 60° Celsius
Humidity	95 % and non-condensing
Measurable gas	Oxygen / Air
Excitation voltage	-16 V To + 16 V
Output voltage	- 5 mV to +5 mV
Output from 0 to 30 SLPM	> 311 mV (8 bit resolution using 12 bit ADC)

4.1.4 Silicon Micro-Structure Differential Pressure Sensor

The SM5652 is a fully calibrated, temperature compensated pressure sensor in dual in-line packages for printed circuit board mounting. Ultra-low pressure ranges are available, resulting in a broad selection of standard pressure ranges.

The SM5652 series pressure sensor is constructed by attaching a highly stable piezoresistive pressure sensor chip to a ceramic substrate. Thick film resistors on the ceramic are laser trimmed to provide zero offset calibration, temperature compensation for zero offset, and temperature compensation for sensitivity. In this sensor, a constant voltage supply can be used and the normalized output span of each sensor can be easily amplified. Those sensors use constant voltage excitation as shown in figure 43.

Table 6: Differential pressure sensor Specifications

SM5652				
Parameter	Min	Typ	Max	Units
Excitation voltage	0	10	20	V
Full scale output span1	24.5	25.0	25.5	MV
Zero pressure output2			2	±mV
Linearity3, 4			0.3	±%FS
Pressure hysteresis4			0.3	±%FS
Input resistance	4		26	KΩ
Output resistance	2.2		6.0	KΩ`

Table 6 (cont'd)				
Temperature coefficient—Span2, 4, 5			0.65	±%FS
Temperature coefficient—Zero2, 4, 5, 6			1.0	±%FS
Thermal hysteresis—Zero5		0.1		±%FS
Response time (10% to 90%)7		1.0		Msec
Pressure overload8			3X	Rated
Operating temperature Range	-40		125	ºC
Compensated temperature Range	0		60	ºC
Storage temperature Range	-55		150	ºC

Notes:

1 Output span of amplified sensor.

2 Compensation resistors are an integral part if the sensor package; no additional external resistors are required. Pins

3 Best fit straight line (BFSL) linearity. For the 0.3 psi range, the linearity is ±0.5% FS. For the 0.15 psi range, the linearity is ± 2.5% FS.

4 FS denotes full-scale output.

5 Peak error measured over compensated temperature range. For 0.3-psi range, TC span is ± 0.75%FS. For the 0.15 psi range, TC span is ± 2.0%FS.

6 For 0.15-psi range, TC-zero is ± 2.5%FS

7 For a zero-to-full scale pressure step change.

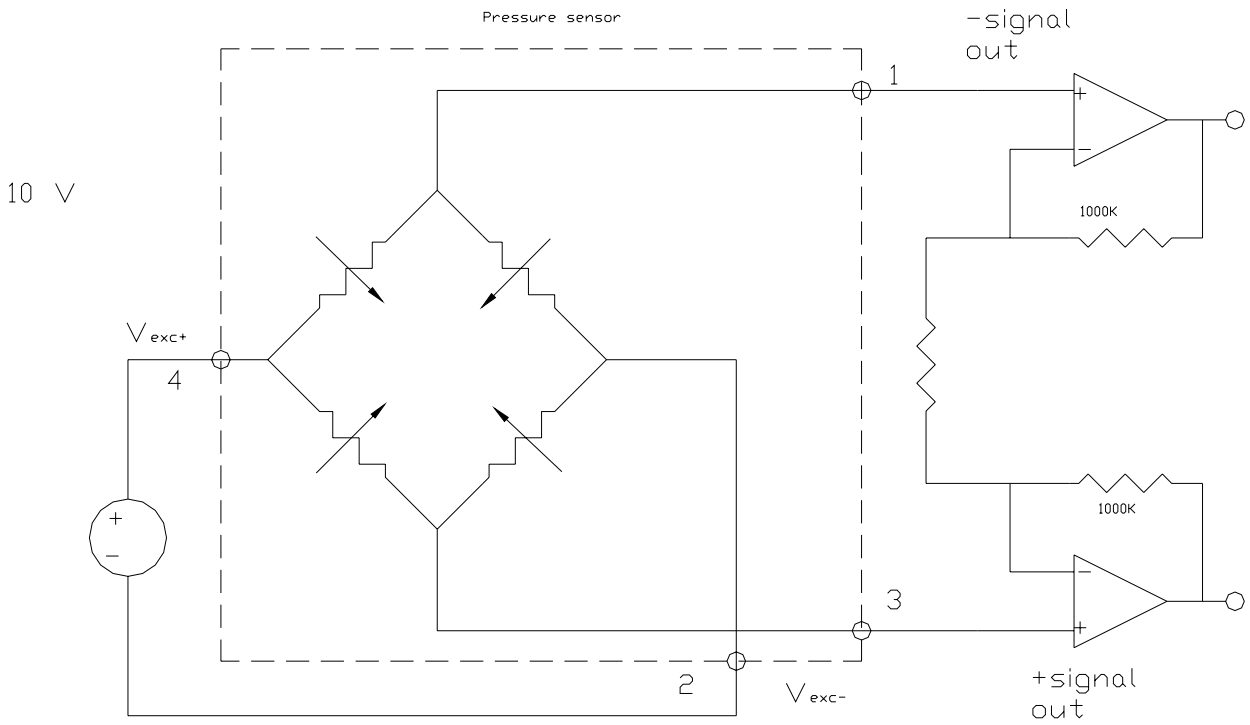

Figure 46: Constant voltage supply and differential output

Piezo-resistors undergo a change in resistance due to the applied pressure. This resistance change is converted into a voltage signal by means of a Wheatstone bridge. Applying known pressures on the diaphragms and recording the output voltages help calibrate the sensor. These pressure sensors can be used for many applications such as (1) measuring absolute pressure in a medium in which case the diaphragm is exposed to vacuum on one side and the unknown pressure on the other side, (2) measuring gauge pressure wherein the diaphragm is exposed to atmospheric pressure on one side and the unknown pressure on the other or (3) for measuring the difference between two pressures which are applied on either side of the diaphragm. This application uses the latter configuration. The sensing element in all the above cases is the piezoresistive element on the diaphragm.

Pressure Measurement Technique:

The Si diaphragm is doped with n-type or p-type elements such as phosphorus or boron at specific locations where the piezoresistor need to be placed. The position and orientation of the resistors is chosen so that the value of the output voltage of the Wheatstone bridge is maximized. In all cases it is preferred to have a linear relationship between the output voltage of the circuit

and the applied pressure. This requires the resistors to meet certain constraints on their dimensions and orientations on the diaphragm.

Using pressure sensors as flow sensors.

The pressure sensor shown in figure 44 is mounted in parallel with the flow element. The pressure output from the pressure sensor in Volts (V) is linked to the flow of the gas in liters per minute (LPM). Then the sensor will be calibrated according to its sensitivity and the experimental data collected during testing.

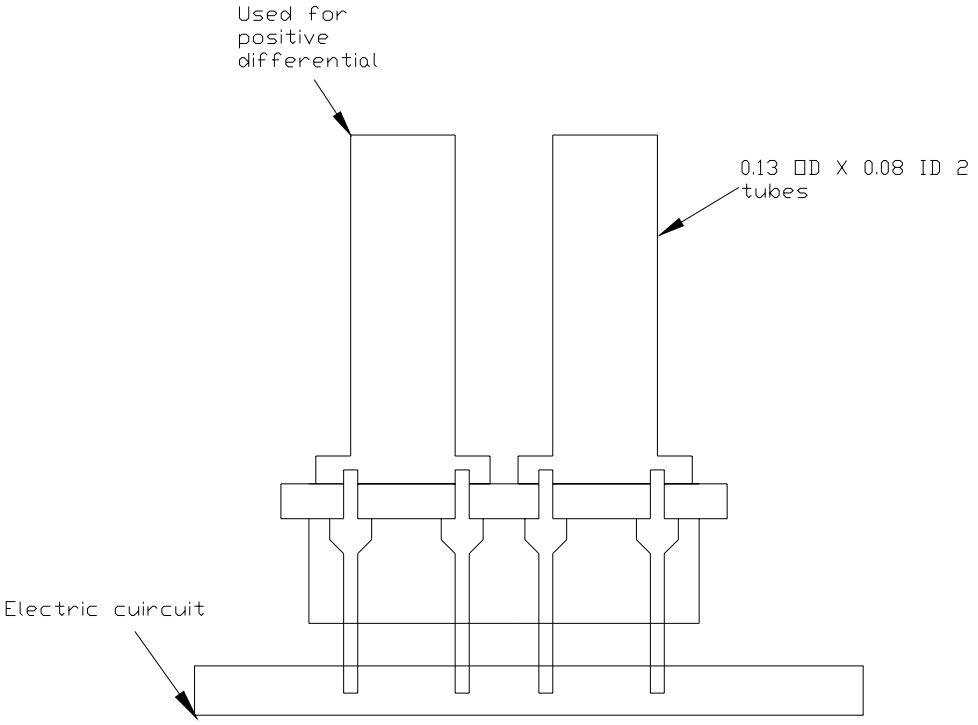

Figure 47: Differential pressure sensor

4.2 Sensor Comparison

Comparing the old AWM2100V Honeywell sensor (currently used) and the new one AWM92100V a lot of common properties are found. When looking at the specifications for both the AWM2100V and the AWM92100V, tables 1 and 2 respectively, one major difference is found. The power consumption for the AWM2100V is 30mW and the AWM92100V is rated at 50mW. This indicates that the AWM2100V uses less energy. This is not a problem because the power supply is able to afford the extra 20mW without affecting anything else. Another

difference is that the AWM2100V uses a gain of 56 where the AWM92100V uses a gain of 14 to produce a similar output. Because less gain is needed, it is easier to suppress the noise output and null drifts on the AWM92100V then it is on the AWM2100V. In other words, shifting the post-amplified output curve to one zero point will be easier to do with the AWM92100V. The output error on the AWM92100 will be much smaller then it is on the AWM2100V.

Looking at the output curve of each sensor will give a better idea on the similarities and differences of both sensors. Eighteen AWM92100V sensors were tested during the experiments. The data from those tests was then compared to the historical data taken before. In addition to this, the testing was performed on an AWM2100V sensor using the procedure described in the experiment section to insure that the historical test results are still valid. The experimental results are shown graphically in figures 45 through 61.

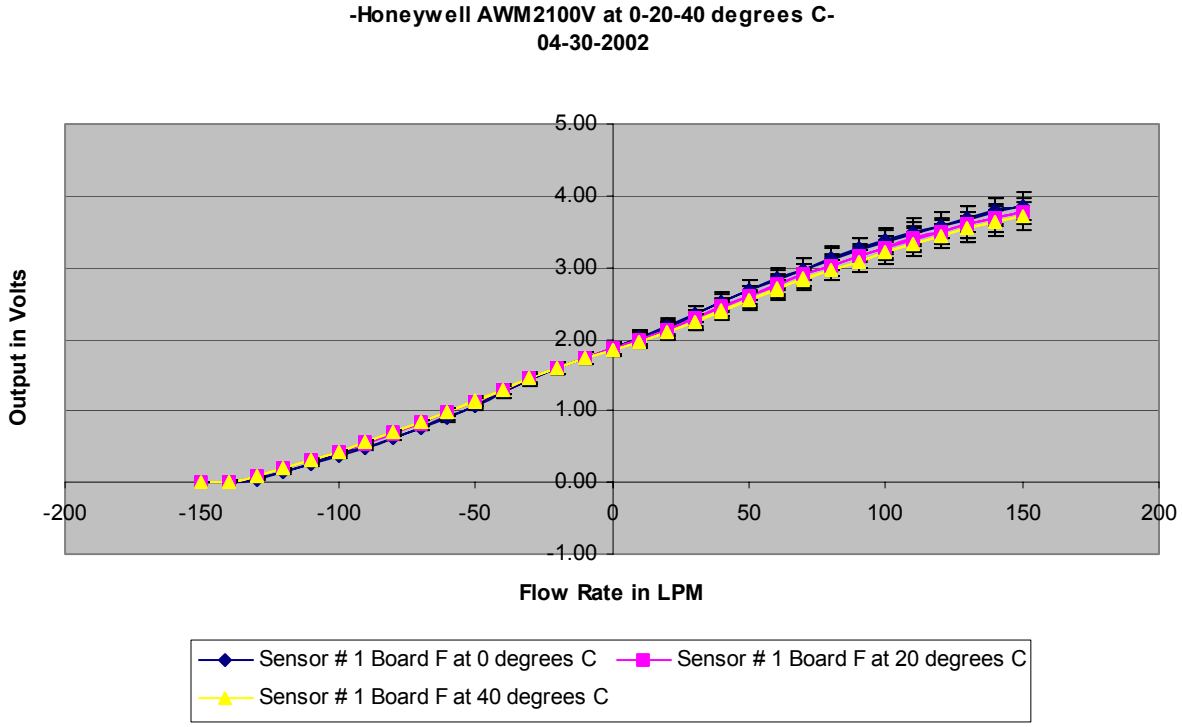

Figure 48: Hysteresis of Honeywell AWM2100V at 0-20 & 40˚C

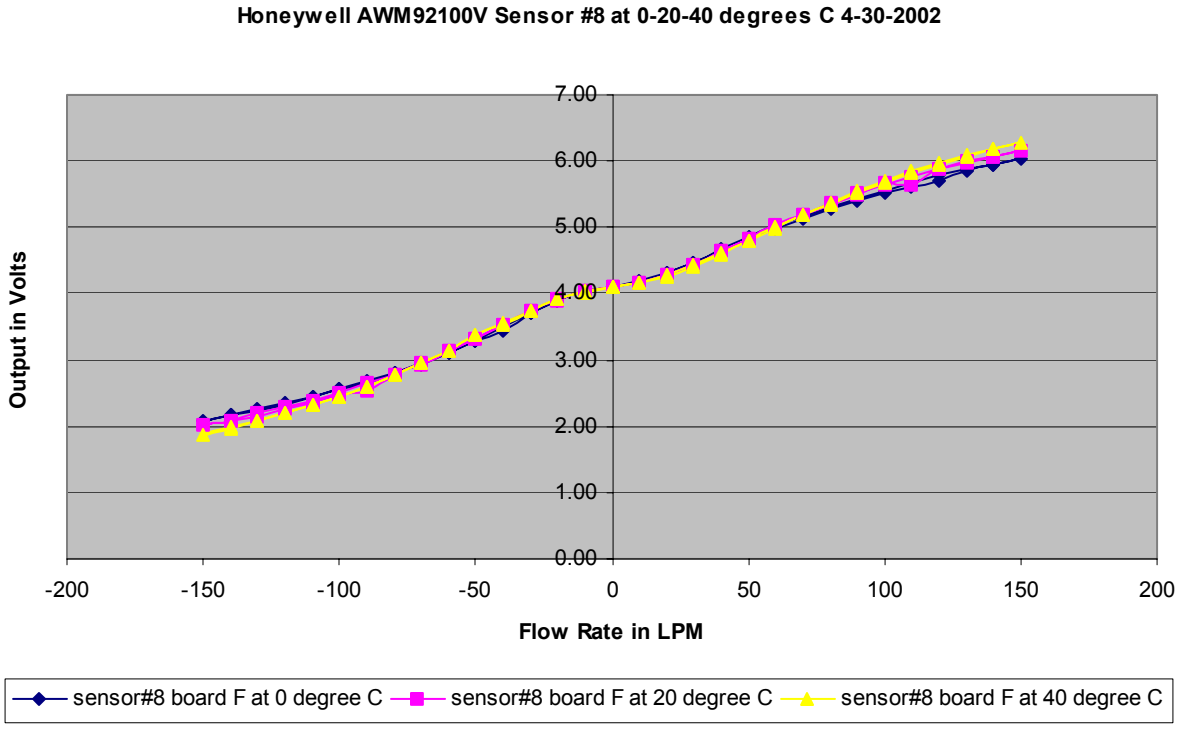

Figure 49: Hysteresis of Honeywell AWM92100V sensor #8 at 0-20 & 40˚C

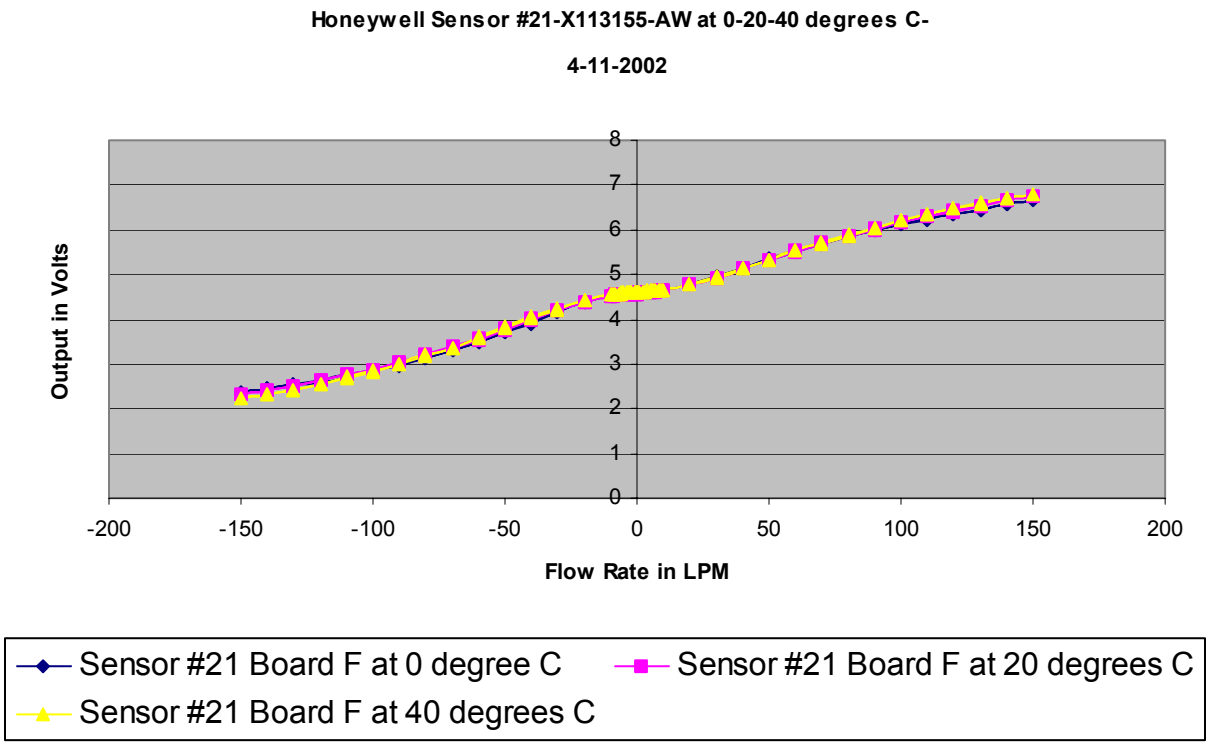

Figure 50: Hysteresis of Honeywell AWM92100V sensor #21 at 0-20 & 40˚C

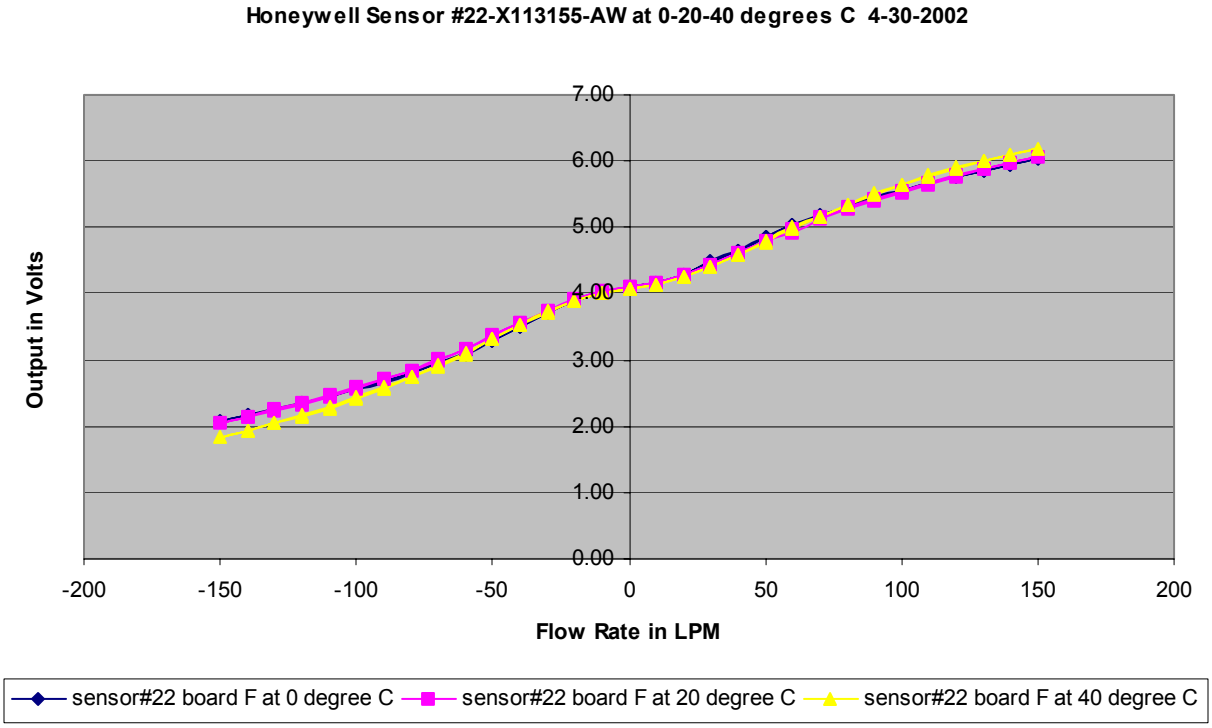

Figure 51: Hysteresis of Honeywell AWM92100V sensor #22 at 0-20 & 40˚C

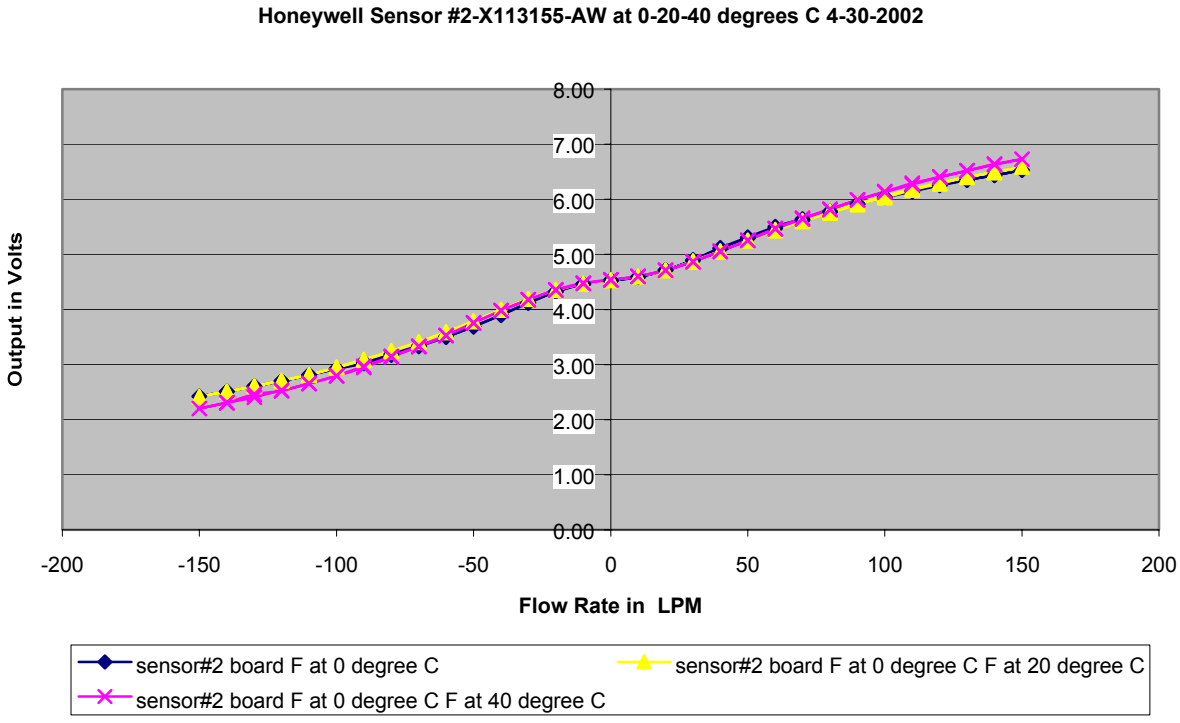

Figure 52: Hysteresis of Honeywell AWM92100V sensor #2 at 0-20 & 40˚C

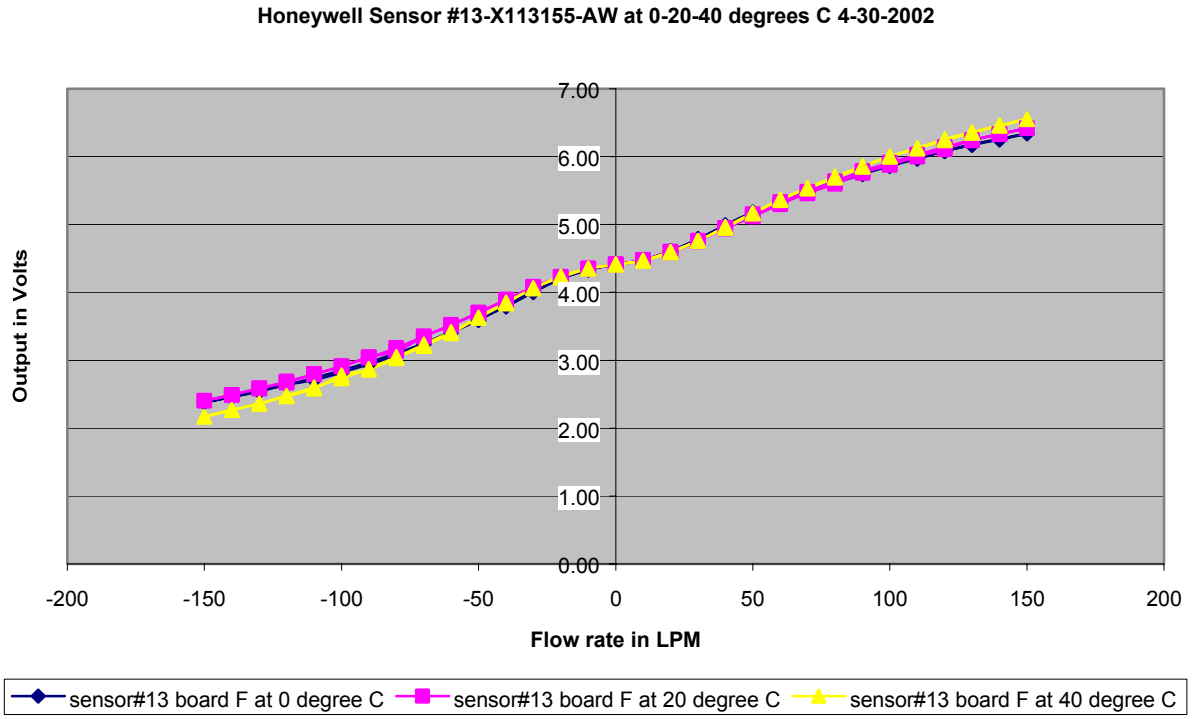

Figure 53: Hysteresis of Honeywell AWM92100V sensor #13 at 0-20 & 40˚C

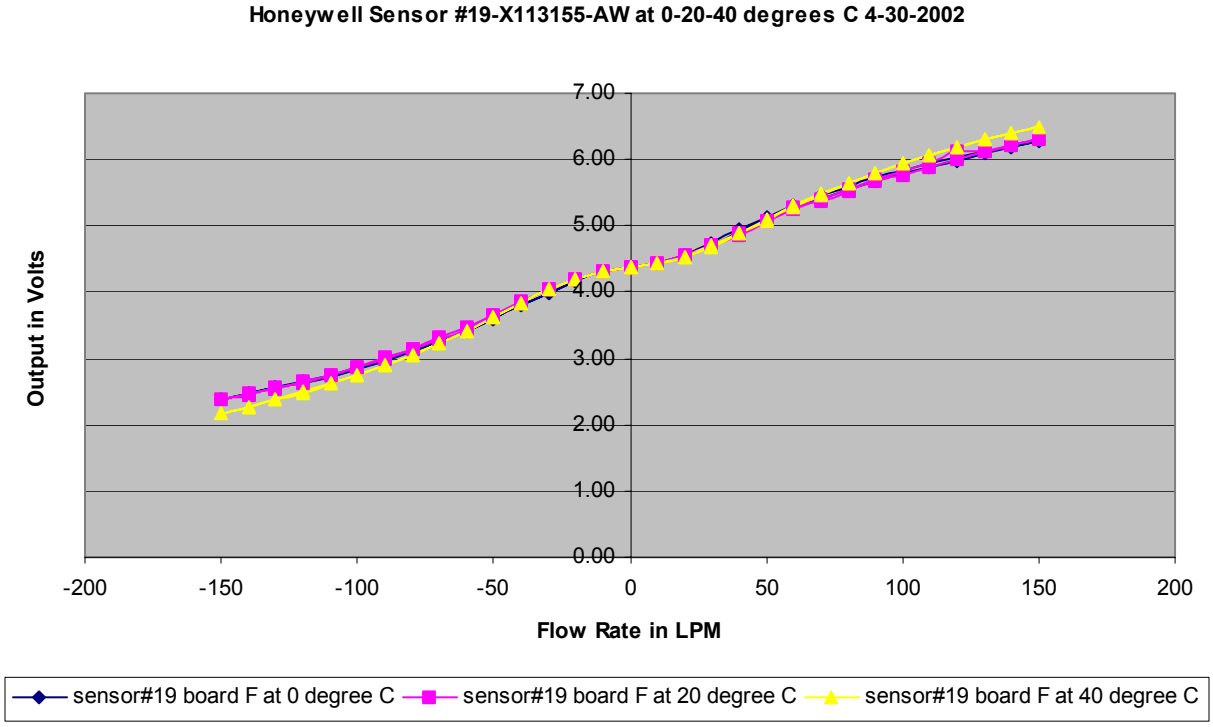

Figure 54: Hysteresis of Honeywell AWM92100V sensor #19 at 0-20 & 40˚C

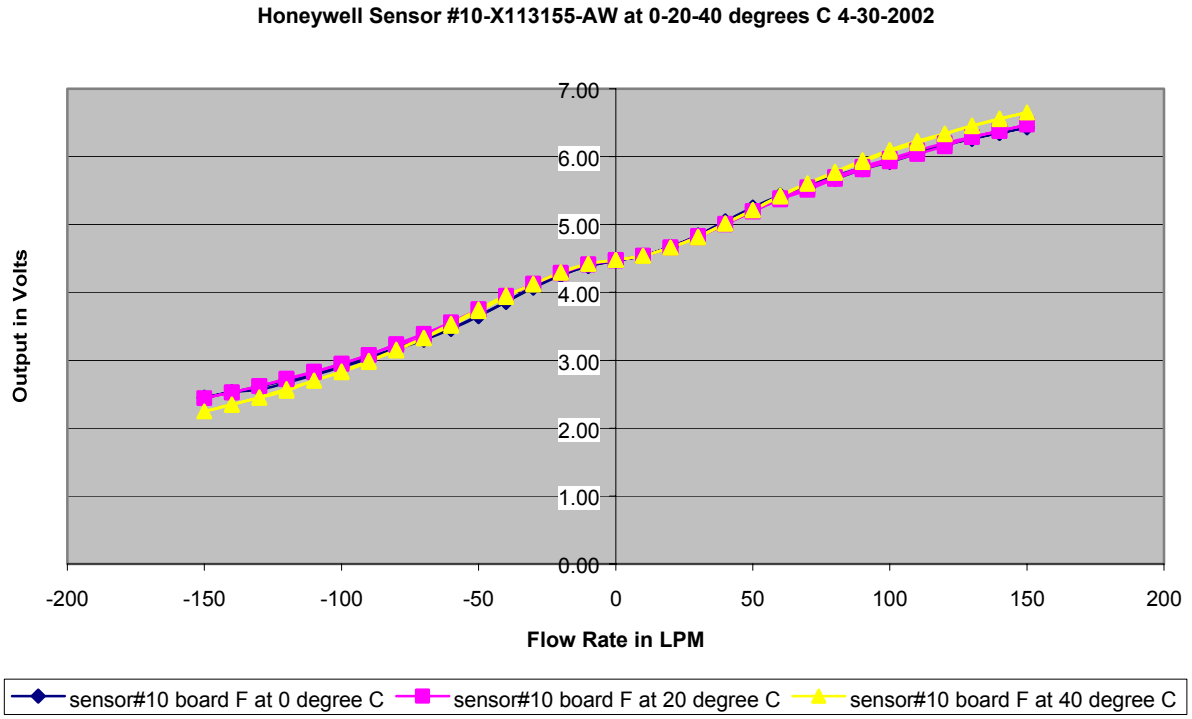

Figure 55: Hysteresis of Honeywell AWM92100V sensor #10 at 0-20 & 40˚C

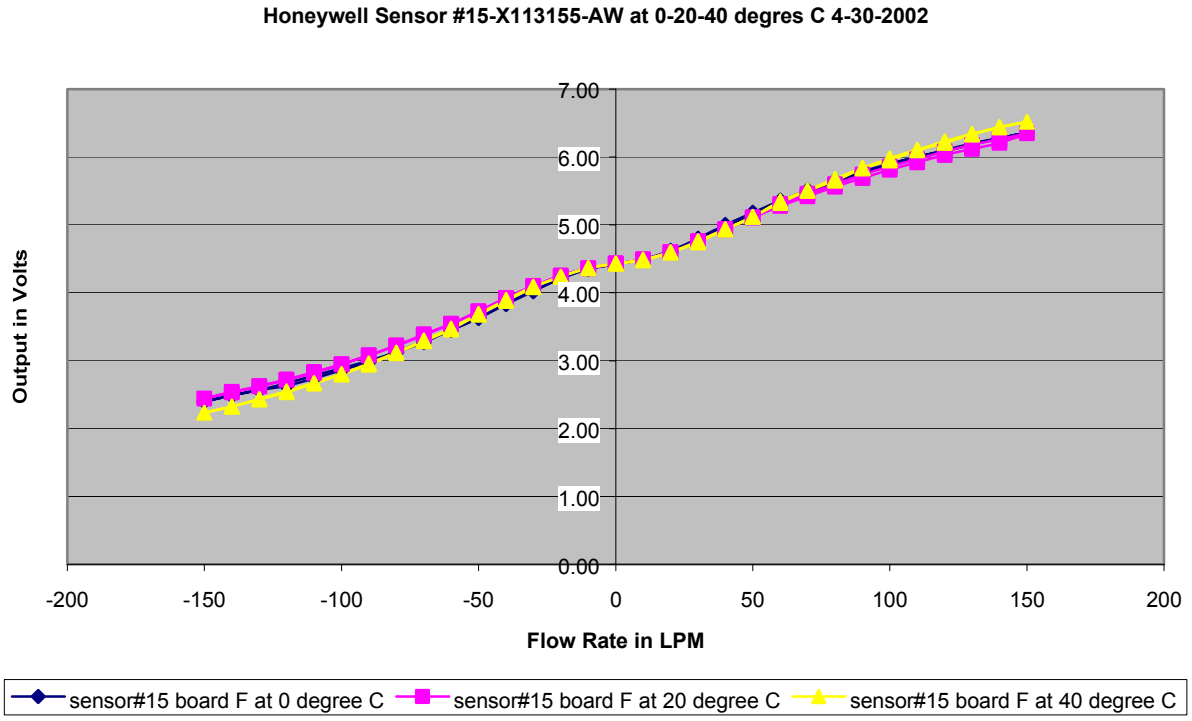

Figure 56: Hysteresis of Honeywell AWM92100V sensor #15 at 0-20 & 40˚C

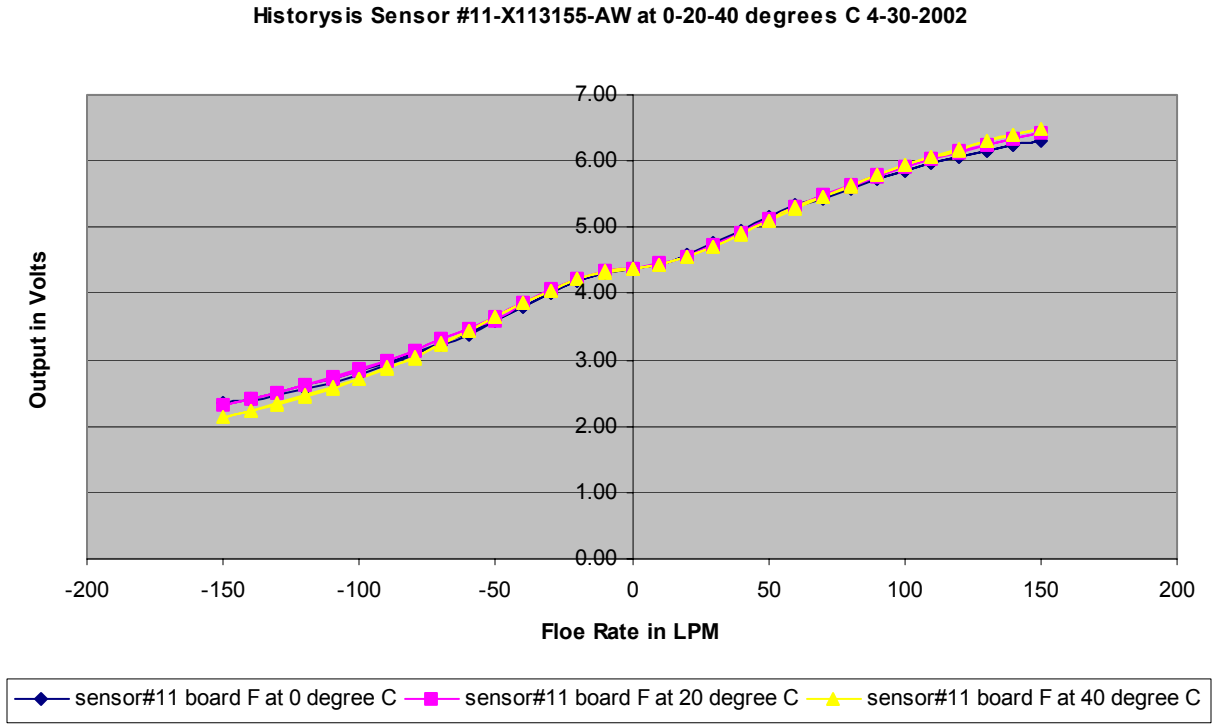

Figure 57: Hysteresis of Honeywell AWM92100V sensor #11 at 0-20 & 40˚C

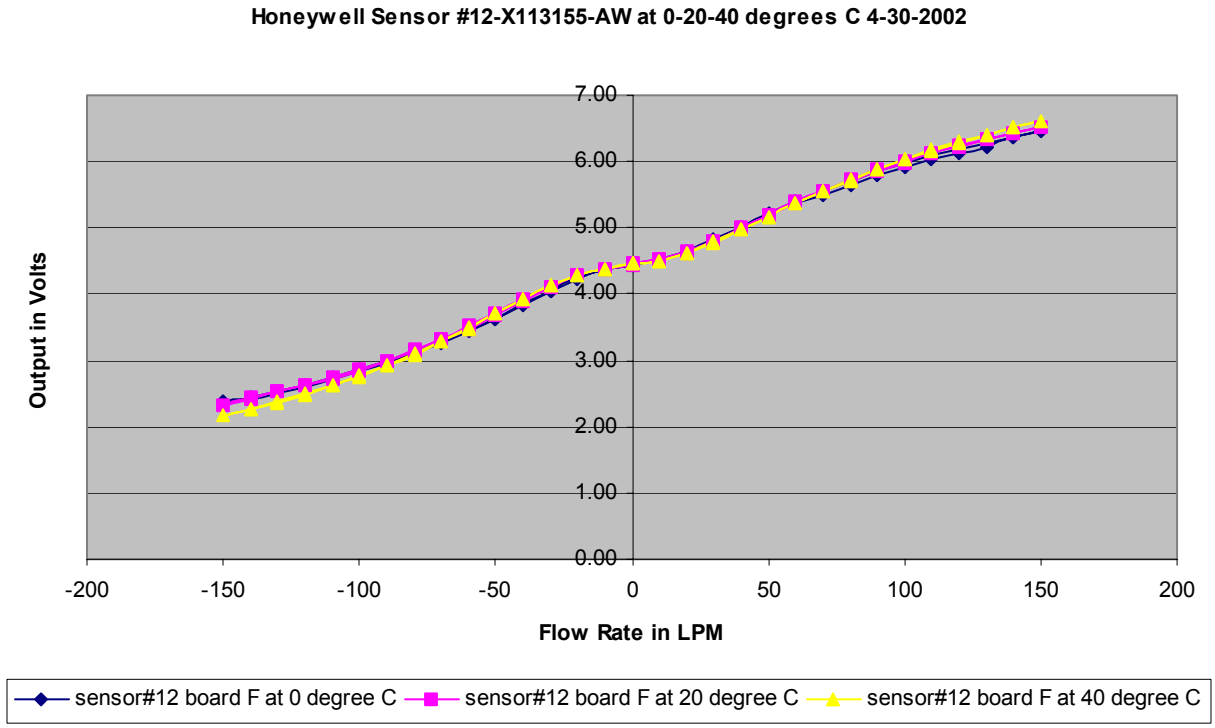

Figure 58: Hysteresis of Honeywell AWM92100V sensor #12 at 0-20 & 40˚C

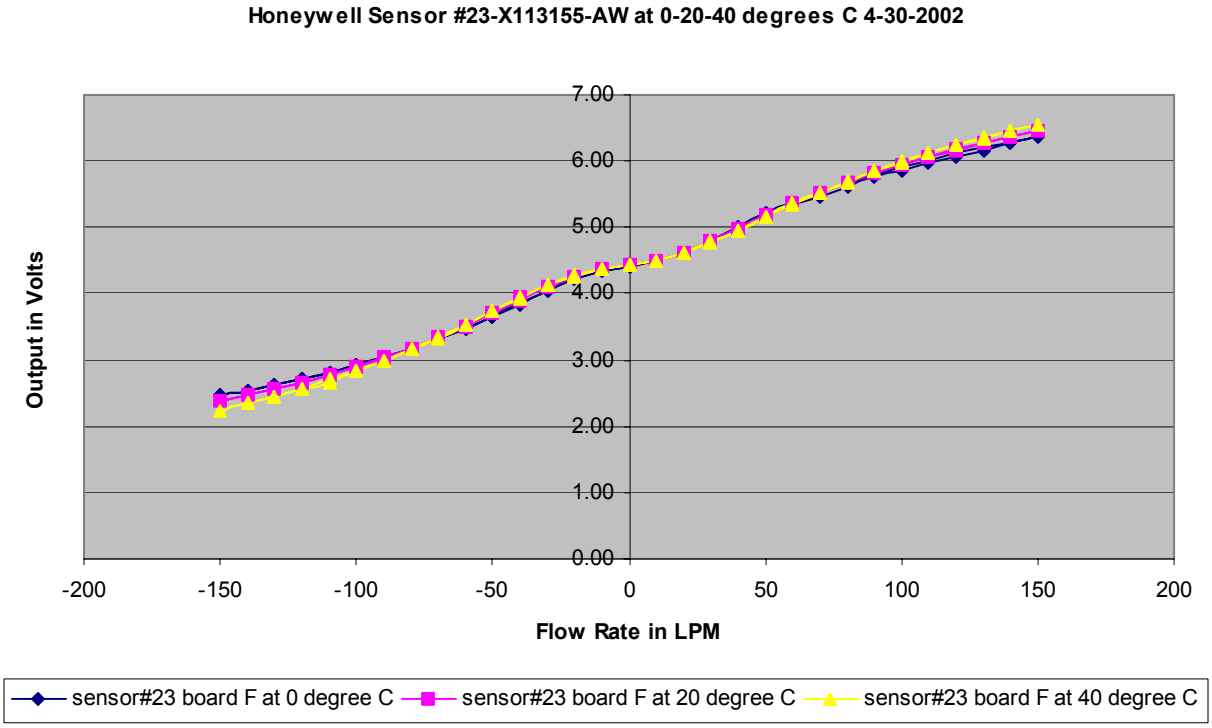

Figure 59: Hysteresis of Honeywell AWM92100V sensor #23 at 0-20 & 40˚C

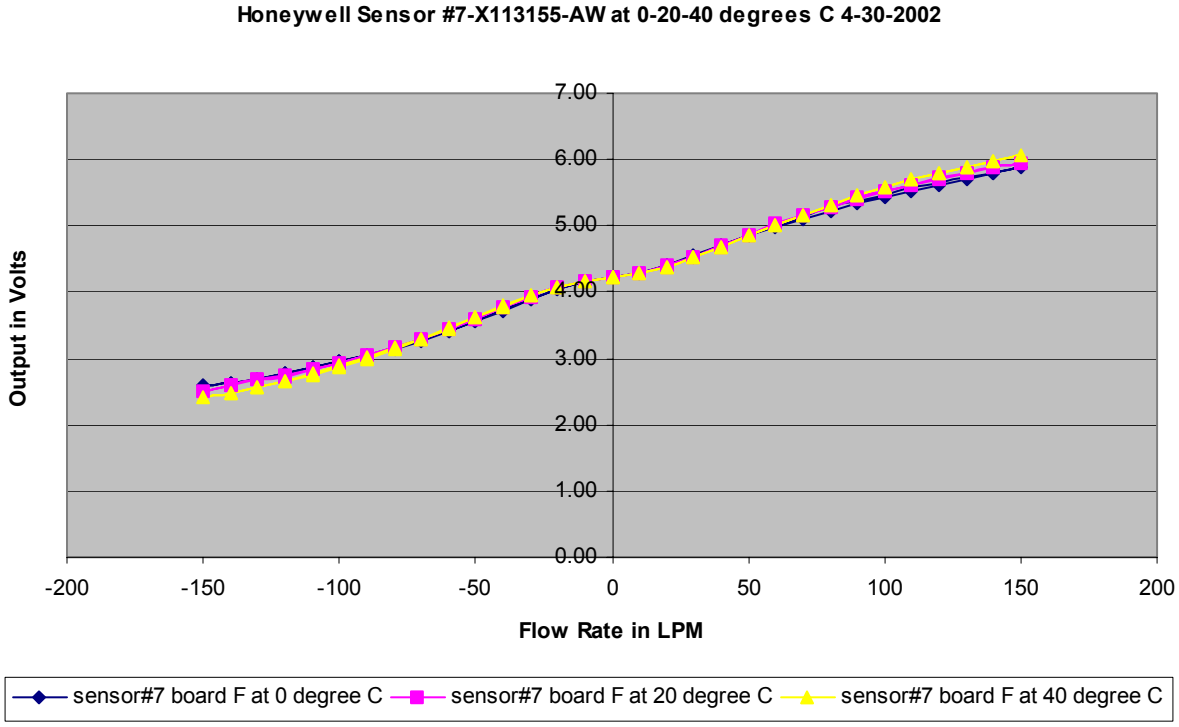

Figure 60: Hysteresis of Honeywell AWM92100V sensor #7 at 0-20 & 40˚C

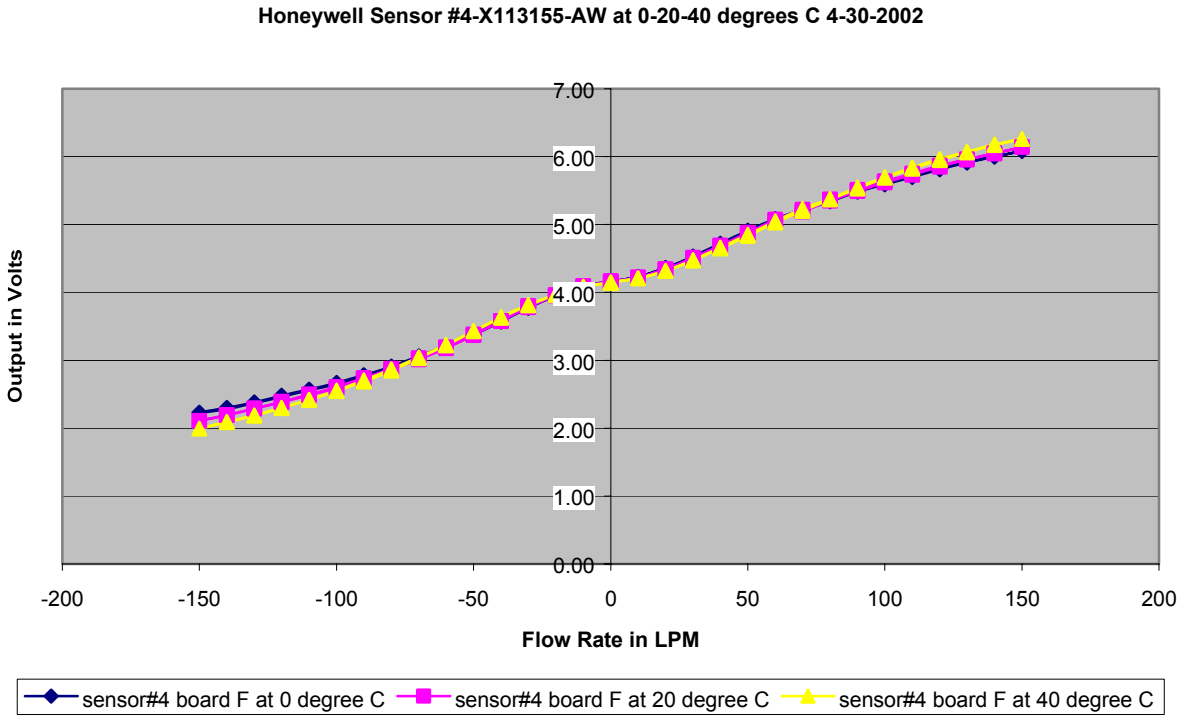

Figure 61: Hysteresis of Honeywell AWM92100V sensor #4 at 0-20 & 40˚C

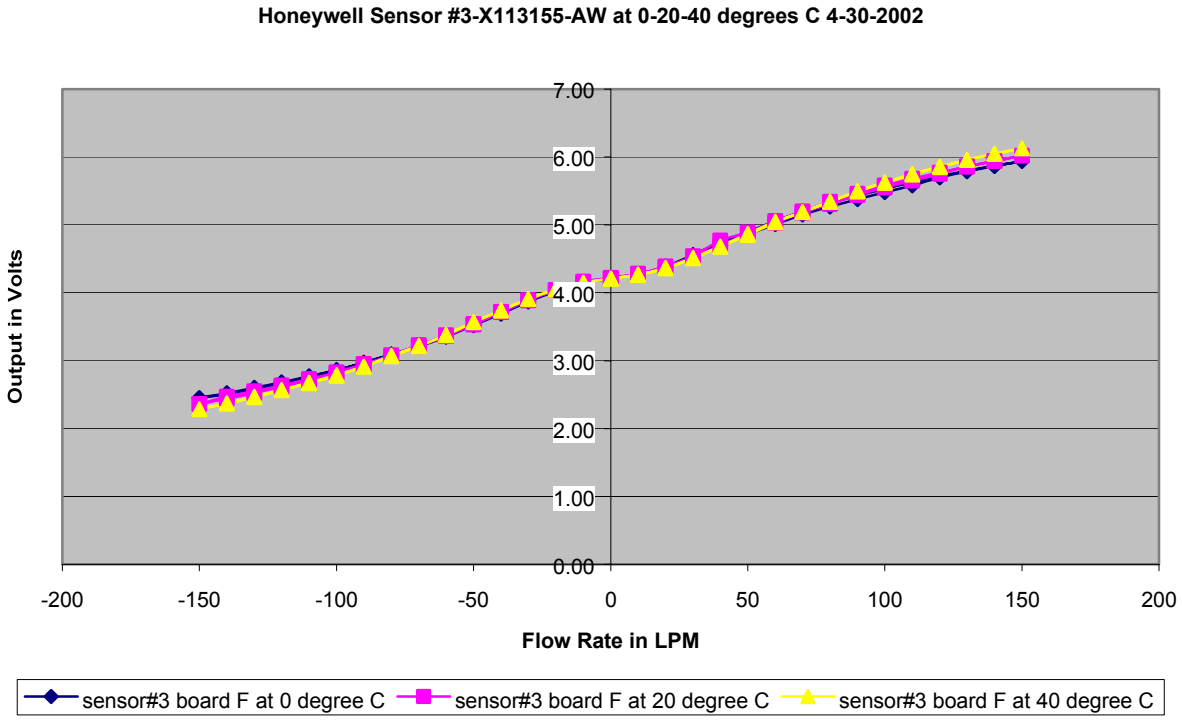

Figure 62: Hysteresis of Honeywell AWM92100V sensor #3 at 0-20 & 40˚C

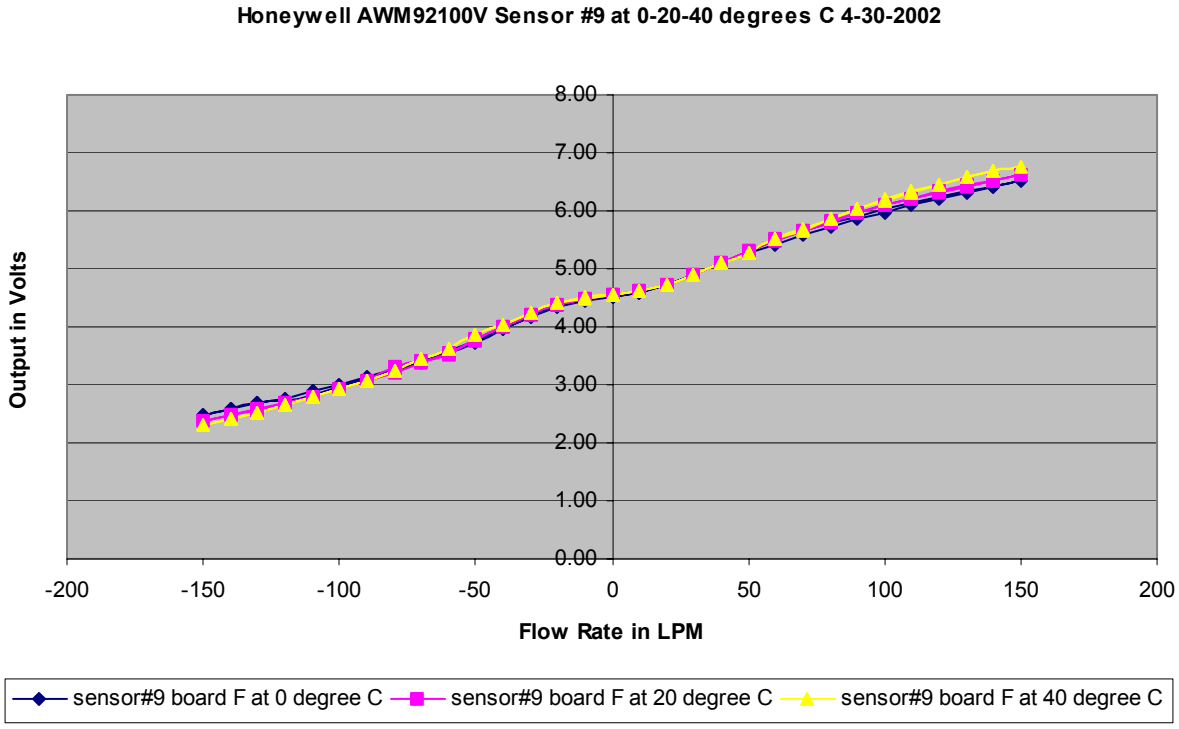

Figure 63: Hysteresis of Honeywell AWM92100V sensor #9 at 0-20 & 40˚C

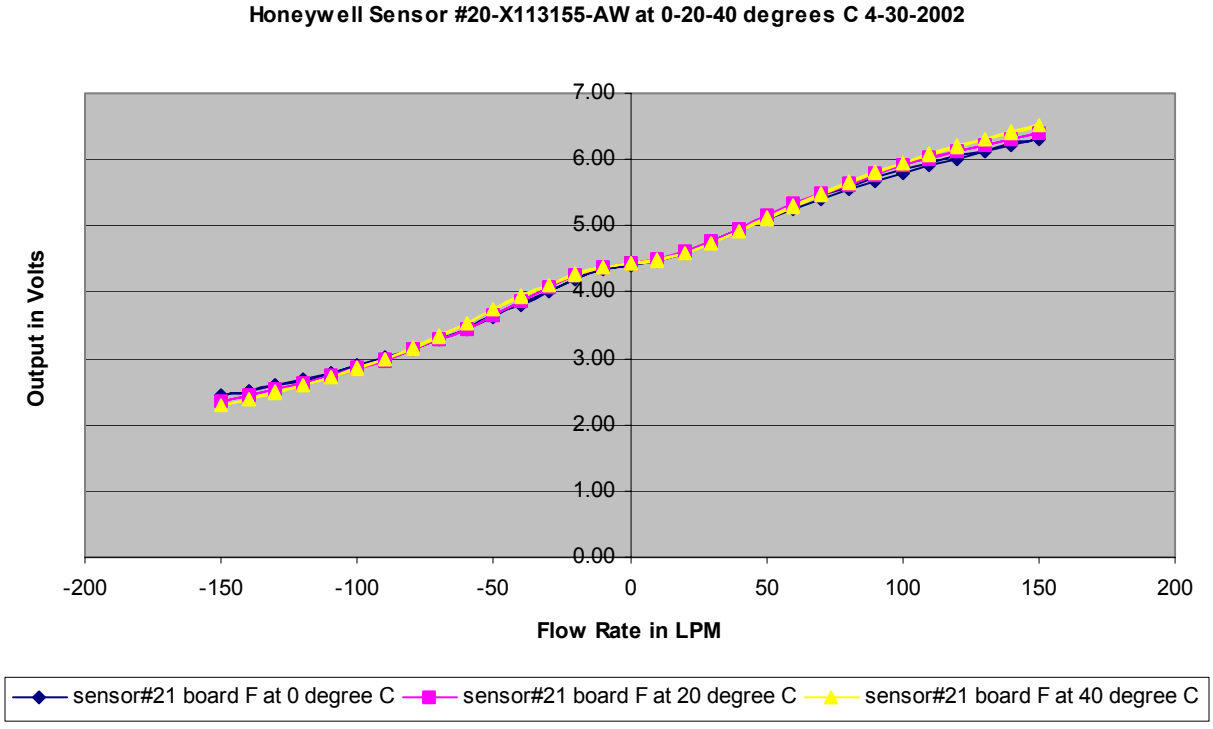

Figure 64: Hysteresis of Honeywell AWM92100V sensor #20 at 0-20 & 40˚C

4.2.1 AWM2100V vs. AWM92100V

It can be easily observed that the output voltages of the AWM92100V sensors are all within 250 mV at zero flow. This level of offset is easily manageable for software correction of the CPAP device. A high level of repeatability with this sensor is also appreciated by those skilled in the art in comparison to that of the more expensive sensor, AWM2100V. Also, the AWM2100V has an offset of 250 mV at zero flow. The range zero flow and 150 LPM flow is translated into approximately 1.93 Volts using the AWM2100V whether the same range using the AWM92100V is translated into approximately 2.2 Volts. Based on these experiments, it is clear that the advantages of the AWM2100V over the AWM92100V are few or none. Because the AWM92100V costs 6 dollars less than the AWM2100V, which will translate into $300,000 assuming the use of 50,000 sensors per year, this data suggests that the old sensor should be replaced. In future comparisons, such as that with the prototypical Thalis Greek sensor or the Silicon Microstructure differential pressure sensor, the AWM92100V should be used as the benchmark.

4.2.2 AWM92100V Vs. Silicon Micro-Structure Differential Pressure Sensor

The Silicon Micro-structure Differential pressure sensor is 3 dollars cheaper than the AWM92100V. The output of the pressure sensor, shown in the following graph, is comparable to the output of the AWM92100V. It is less repeatable but this can be fixed with the CPAP software. Two problems face this pressure sensor. One is the high gain, which is on the order of 1000. The second is the resultant noise associated with high gain systems. It was observed that this signal to noise ratio was unacceptable in our project. And thus this pressure sensor cannot be used in our products.

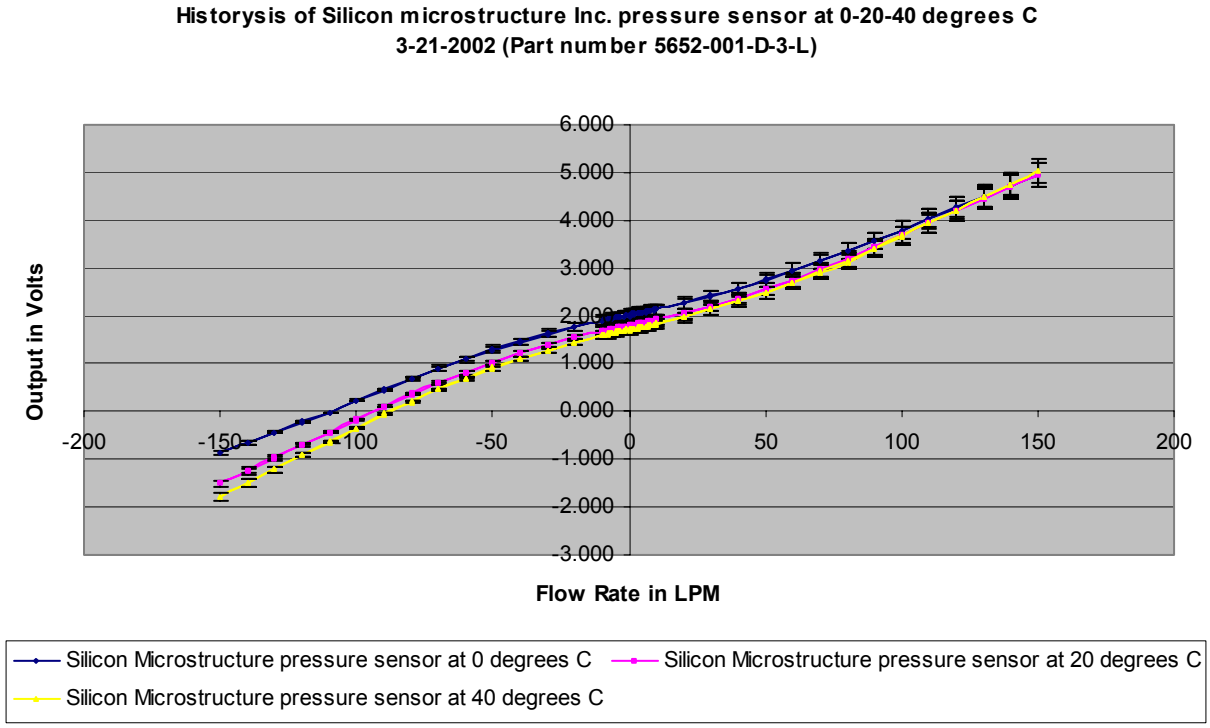

Figure 65: Hysteresis of Silicon Micro-Structure pressure sensor at 0-20 & 40˚C

4.2.3 AWM92100V Vs. Thalis Greek Sensor

The last sensor that can be compared to the AWM92100V is the Thalis Greek sensor. This sensor has a better and more compact design then the AWM92100V because the sensor with all the electronics is attached to the flow element itself as shown in figure 22d. This also eliminates the need to match the performance of the mass flow sensor with the flow element. One prototype of this sensor was available for testing and the other prototypes are expected to be ready in September of 2002. Using the data taken from this prototype shown in figure 62 and comparing it to the AWM92100V will show that both are very comparable in terms of linearity and repeatability.

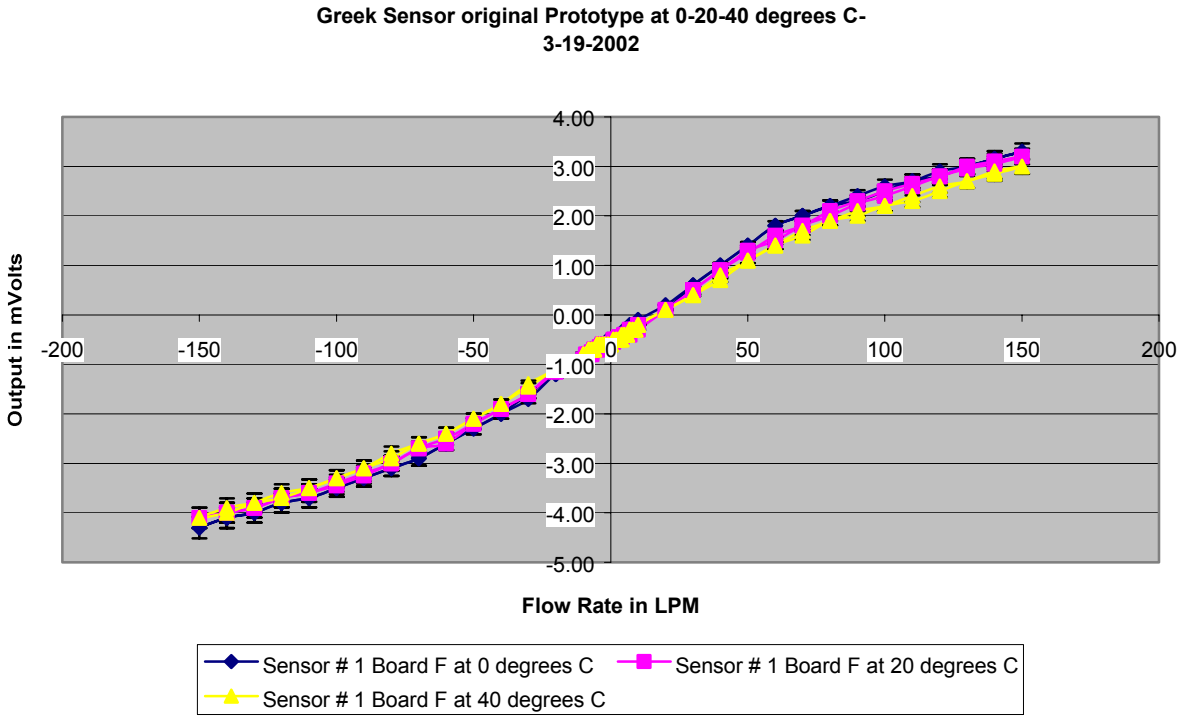

Figure 66: Hysteresis of Thalis Greek sensor at 0-20 & 40˚C

The disadvantage of this sensor is that the excitation voltage is –16 V to +16 V. (higher than what is typically available) The output voltage are –5 mV to +5 mV where the requirements are 0 to +5 V. The taper fitting of the first prototype also fell short of our system requirements. These problems have been discussed and the manufacturer of the sensor promised to fix the product in order to meet the requirements and lower the price. If all the requirements are met and the price of the Greek sensor is X dollars more expensive (accounting for the added electronics necessary for the AWM92100 and not necessary for the Thalis sensor) than the AWM92100V, then this sensor will be desirable. Currently, the price is 6 dollars more than the AWM92100V. An advantage in cost saving then occurs from reducing the assembly time by 38.5 seconds. The difference between the amounts of time needed to assemble the AWM92100V versus the Greek sensor will then save the company $8,500 per year based on a 50,000 parts per year production. This amount does not include the breakage of AWM92100V sensors on the assembly line which will cost the company $30 per sensor.

5.0 CONCLUSION

A standard testing procedure for flow sensors has been then established in the current work for determining the overall performance of different mass flow sensor technologies. Using the standard testing protocol developed in section 3.2, tests were conducted on four different mass flow sensors that could potentially be used in a CPAP device. Examining all the sensors tested in this work, it was found that the qualities and performance of each sensor could be significantly different in the operating range of interest. Table 7 shows all of the sensors studied in this thesis, and lists their advantages and disadvantages determined for our specific application.

Table 7: Advantages and Disadvantages of each sensor

Sensor	Advantages	Disadvantages
AWM2100V	Hysteresis and repeatability ±0.35% reading, 0 to ±200 SLPM flow range; 30 mW power consumption; 1 msec response time; -25 to 85 ºC operating temperature; Null shift typical ±0.2 mV.	Expensive, 45 seconds manual assembly; risk of breakage during assembly; high gain 56.
AWM92100V	Hysteresis and repeatability ±0.35% reading, 0 to ±150 SLPM flow range; Low gain 14; 1 msec response time; -25 to 85 ºC operating temperature; Null shift typical ±0.2 mV. **6 dollars cheaper** then AWM2100V.	50 mW power consumption; 45 seconds manual assembly; Risk of breakage during assembly;
Silicon Micro-Structure	3 dollars cheaper then AWM92100V	High gain 1000; Less repeatability; 45 seconds manual assembly; Risk of breakage during assembly; high noise that affects the performance of the CPAP software.

Table 7 (cont'd)		
Thalis / Greek sensor	0 to ±200 SLPM flow range; 30 mW power consumption; 1 msec response time; 0 to 60 ºC operating temperature; Compact; includes all electronics on board; 3 seconds manual assembly saving money compared to the AWM92100V; no risk of breakage during assembly; same price as AWM92100V with electronics;	Excitation voltage is –16 V to +16 V; output voltage are –5 mV to +5 mV; (**all the disadvantages should be eliminated in the coming prototypes**)

Comparing each sensor in Table 15, it is obvious that the optimum sensor to use right in the existing CPAP unit is the AWM92100V. It should be noted, however, that the Thalis Greek sensor could replace this sensor if it is able to meet all of the performance and cost requirements. The AWM92100V is on the new CPAP circuit boards as of July 2002.

APPENDICES

APPENDIX A

Performance Matching of Mass Flow Sensor and Magwheel.

As a volume flow rate measurement device, the heat transfer based mass flow sensors, Honeywell AWM2100 in particular, are quite insensitive to the fluid temperature and composition variations found in ventilator applications. This was reported in thermal response of AWM2100 mass flow sensor dated February 21, 1994. The design range of flow rates through the sensor is 0 to 0.2 LPM. For this project the maximum flow was set to 150 LPM. The vast majority of the flow must be directed through a path parallel to the AWM2100. The relation ship between the sensor flow, Q_S, and that of the flow element, Q_e, must be known and understood such that the output of the AWM2100 may be used to represent the flow of the unit.

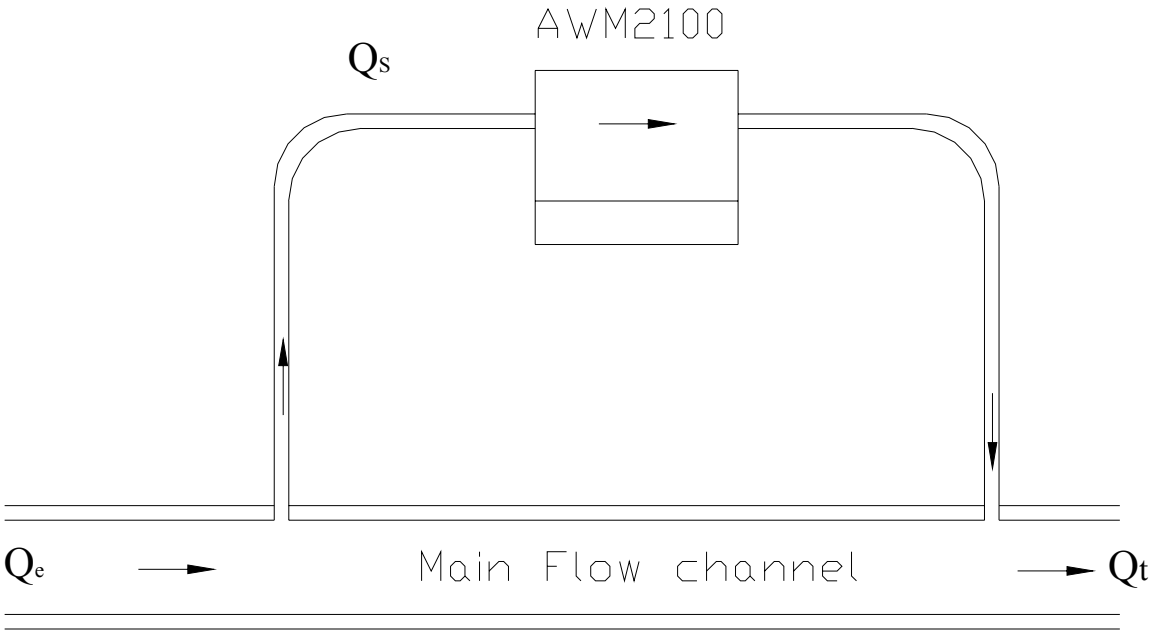

Figure 67: Sensor in parallel with bypass

Where:

Q_t = Volume flow rate, Total

Q_s = Volume flow rate, Sensor

Q_e = Volume flow rate, Element

For order of magnitude comparison, the maximum values for the project are:

$$Q_{t\max} = 280 LPM$$

$$Q_{s\max} = 0.150LPM$$

$$Q_t = Q_s + Q_e$$

$$Q_{e\max} = 279.85LPM \qquad \text{(Equation 22)}$$

For all practical purposes $Q_e = Q_t$

In parallel flow, the head loss, Δh, is the same for both flow path.

$$\Delta h_s = \Delta h_e \qquad \text{(Equation 23)}$$

With negligible differences in elevation in the flow path, the head loss is related to the pressure differential, Δp, as follows

$$\Delta p = \Delta h \rho_f g \qquad \text{(Equation 24)}$$

≈ Δp_s Δh Q_s Q_e Q_t

The relationship between Δp_s and Q_s must be fixed if the AWM2100 is the flow transducer of choice.

The airflow subsystem must relate Q_s to Q_t. The design parameters for the flow element need to be determined such that a stable and reproducible relation between Q_s to Q_t and accurate estimates of Q_t are made. Insensitivity to the variations in temperature, composition and absolute pressure of the working fluid is desired. Determining a controlling function for the ratio of Q_s / Q_t can provide design direction and is the purpose of this analysis.

Analysis

The Darcy-Weisbach equation relates pipe-head loss to the fluid velocity, geometry parameters, and a dimensionless parameter, f, called the Darcy friction factor.

$$\Delta h = f \frac{LV^2}{d2g} \qquad \text{(Equation 25)}$$

This equation is valid for duct flows of any cross section and for laminar and turbulent flow. By continuity,

$$Q = AV \qquad \text{(Equation 26)}$$

Substituting (26) into (25) yields equation (27).

$$\Delta h = f\frac{LQ^2}{dA^2 2g} \qquad \text{(Equation 27)}$$

The Darcy friction factor is a function of the Reynolds number and the relative roughness of the pipe. For laminar flow, the friction factor is related to a geometry-based constant and the Reynolds number as shown in equation (28).

$$f_{lam} = \frac{K_{lam}}{\mathrm{Re}} \qquad \text{(Equation 28)}$$

No exact solutions for turbulent flow are available. The accepted semi-empirical formula representing the Darcy friction factor for turbulent flow in smooth-walled pipe is equation (29)[1].

$$\frac{1}{f_{turb}^{1/2}} = 2.0\log(\mathrm{Re}_d\, f_{turb}^{1/2}) - 0.8 \qquad \text{(Equation 29)}$$

The complexity of evaluating this formula, lead to alternate approximations, such as equation (30)[1].

$$f_{turb} = 0.316\,\mathrm{Re}_d^{-1/4}\ for 4000 \langle \mathrm{Re}_d \langle 10^5 \qquad \text{(Equation 30)}$$

When analyzing flow systems, minor losses are also found. These are entrances, exits, expansions or contractions, fittings, and valves. The flow patterns in these items are very complex and the theory is very weak. Typically, losses are measured experimentally and correlated with the pipe flow parameters in a loss coefficient, K, as in equation (31).

$$K = \frac{h_m}{V^2 \big/ 2g} \qquad \text{(Equation 31)}$$

K is dimensionless, but it is not controlled in the literature with Reynolds number and roughness ratio. K generally behaves consistently with viscous flow theory. It normally decreases as the pipe size and Reynolds number increase and roughness ration decreases[1]. Substitute (26) in (31) and rearrange we get (32).

$$h_m = K\frac{Q^2}{A^2 2g} \qquad \text{(Equation 32)}$$

The total head loss consists of a summation of the component losses, both straight duct flow and minor losses. Equation (32) shows the total head loss as a summation of straight duct flow, Darcy friction, terms plus a summation of minor loss terms.

$$\Delta h = \sum_i \Delta h_i + \sum_j \Delta h_{mj} \qquad \text{(Equation 33)}$$

With equation (27) and (32) substituted into (33), this can be written as equation (34).

$$\Delta h_t = \sum_i f_i \frac{L_i Q^2}{d_i A_i^2 2g} + \sum_j K_j \frac{Q^2}{A_j^2 2g} \qquad \text{(Equation 34)}$$

Both laminar and turbulent Darcy friction terms may exist depending on the geometry of the flow. When the first summation term of equation (34) is separated into laminar and turbulent terms and friction factor relations (28) and (30) are substituted into equation (34, equation (35) results.

$$\Delta h_t = \sum_i \frac{K_{lam} L_i Q^2}{\mathrm{Re}_i\, d_i A_i^2 2g} + \sum_k \frac{0.316 L_k Q^2}{\mathrm{Re}_k^{0.25} d_k A_k^2 2g} + \sum_j K_j \frac{Q^2}{A_j^2 2g} \qquad \text{(Equation 35)}$$

By definition the equation for the Reynolds number is equation (36).

$$\mathrm{Re} = \frac{\rho Q d}{A \mu} \qquad (36)$$

Substituting (36) into (35) and simplifying, yields to (37).

$$\Delta h_t = \sum_i \frac{K_{lam} L_i}{d_i^2 A_i 2g} \frac{\mu}{\rho} Q + \sum_k \frac{0.316 L_k}{d_k^{1.25} A_k^{1.75} 2g} \frac{\mu^{0.25}}{\rho^{0.25}} Q^{1.75} + \sum_j \frac{K_j}{A_j^2 2g} Q^2 \qquad \text{(Equation 37)}$$

Equation (37) represents the total head loss and exists for both the sensor path and the flow element path. The total head loss is equal for both flow paths. Unfortunately we cannot solve for Q immediately because the equation is transcendental. Two simplifying assumptions allow solution and determination of the ratio of the sensor flow to element flow. First, the minor losses can be incorporated into the laminar and turbulent terms. As reported by tanimoto in "theory of operation", in flow transducer, the minor losses are nearly negligible in this system. As discussed earlier, the minor loss coefficient, K, generally follows the Reynolds number dependencies of viscous flow. For these two reasons, error due to incorporating minor loss terms into the other terms may be expected to be small. Second, we can assume that the exponent for turbulent flow on Q is 2 instead of 1.75. At higher-level turbulence, $\mathrm{Re}>10^6$, the exponent is 2. When these two assumptions are made, and a multiplier, C, is included to partially correct for the exponent change on Q, equation 35 reduces to

$$\Delta h_t = \sum_j \frac{K_{lamj} L_j}{d_j^2 A_j 2g} \frac{\mu}{\rho} Q + \sum_k C \frac{0.316 L_k}{d_k^{1.25} A_k^{1.75} 2g} \frac{\mu^{0.25}}{\rho^{0.25}} Q^2 \qquad \text{(Equation 38)}$$

When equation (38) is examined, the coefficients other than viscosity, density and flow are geometry dependent. Each flow path has approximately six to ten individual head losses.

These include entrance into a tube, entrance and exit from fitting and flow through a uniform section. Each head loss component is either laminar or turbulent depending on the value of Reynolds number for that particular term. Fixing the geometry makes the grouping of geometry coefficients constant. For simplification each group of constant coefficient can be represented by a single coefficient, E or B, as shown in (39) and (40).

$$E = \sum_j \frac{K_{lamj} L_j}{d_j^2 A_j 2g} \qquad \text{(Equation 39)}$$

$$B = \sum_k \frac{0.316 L_k}{d_k^{1.25} A_k^{1.75} 2g} \qquad \text{(Equation 40)}$$

When (39) and (40) are substituted into (38), equation (41) results.

$$\Delta h_t = E \frac{\mu}{\rho} Q + B \frac{\mu^{0.25}}{\rho^{0.25}} Q^2 \qquad \text{(Equation 41)}$$

Using the quadratic formula to solve equation (41) for Q, ignoring the trivial solution with negative flow yields to (42).

$$Q = \frac{-E\frac{\mu}{\rho} + \sqrt{\left(E\frac{\mu}{\rho}\right)^2 + 4B\left(\frac{\mu}{\rho}\right)^{0.25} \Delta h_t}}{2B\left(\frac{\mu}{\rho}\right)^{0.25}} \qquad \text{(Equation 42)}$$

Equation (42) exists for both the sensor path and the element path. When they are written, subscripted $_s$ and $_e$ for sensor and flow element, respectively, the ratio of the two equations is shown in (43).

$$\frac{Q_s}{Q_e} = \frac{\left(-E_s\left(\frac{\mu}{\rho}\right)_s + \sqrt{\left(E_s\left(\frac{\mu}{\rho}\right)_s\right)^2 + 4B_s\left(\frac{\mu}{\rho}\right)_s^{0.25} \Delta h_{t_S}}\right) 2B_e\left(\frac{\mu}{\rho}\right)_e^{0.25}}{\left(-E_e\left(\frac{\mu}{\rho}\right)_e + \sqrt{\left(E_e\left(\frac{\mu}{\rho}\right)_e\right)^2 + 4B_e\left(\frac{\mu}{\rho}\right)_e^{0.25} \Delta h_{t_e}}\right) 2B_s\left(\frac{\mu}{\rho}\right)_s^{0.25}} \qquad \text{(Equation 43)}$$

Recognizing that the head loss through both paths is the same and simplifying this equation produces equation (44), which provides a controlling function for the ratio of Q_s/Q_e that is discussed in the following section.

$$\frac{Q_s}{Q_e} = \frac{B_e}{B_s}\frac{E_s}{E_e}\frac{\left(\frac{\mu}{\rho}\right)_s^{0.75}}{\left(\frac{\mu}{\rho}\right)_e^{0.75}}\left(\frac{-1+\sqrt{1+4\Delta h_t \frac{B_s}{E_s^2}\left(\frac{\rho}{\mu}\right)_s^{1.75}}}{-1+\sqrt{1+4\Delta h_t \frac{B_e}{E_e^2}\left(\frac{\rho}{\mu}\right)_e^{1.75}}}\right) \qquad \text{(Equation 44)}$$

Results and conclusions

Examining equation 44 reveals that the ratio of sensor flow to element flow, Q_s/Q_e, can be held constant if two conditions are met. The first condition is that the temperature at the sensor and element must be kept equal so that the ratios of the viscosity, μ, and density ρ, of the fluid for both paths are equal. The second is that a ratio of the geometry coefficients, $\frac{B_s}{E_s^2}$ and $\frac{B_e}{E_e^2}$, be equal to each other. These design conditions can be expressed in equation (45) and (46).

$$\left(\frac{\mu}{\rho}\right)_s = \left(\frac{\mu}{\rho}\right)_e \qquad \text{(Equation 45)}$$

$$\frac{B_s}{E_s^2} = \frac{B_e}{E_e^2} \qquad \text{(Equation 46)}$$

Meeting conditions (45) and (46) minimizes the measurement error introduced by assuming the ratio of flow through the sensor and element remains constant while fluid properties change. Equation (45) and (46) will not directly determine the design geometry. To make (45) true, the fluid temperatures in both the sensor and the flow element must be equal. For (46) to be true, the laminar/turbulent crossover is identical for both flow paths. Utilizing the concept of matching flow impedances of the mass flow sensor and the laminar flow element, the first task was to qualify the flow impedance of the mass flow sensor. The manufacturer has set the geometry characteristics of the mass flow sensor. This part is fixed. The pressure drop versus flow performance from zero to full flow of the Honeywell mass flow sensors was measured at prevailing barometric pressure and at an absolute pressure equivalent to an increase of 7500 feet in elevation above that of the RI laboratory. The data for each sensor and absolute pressure were curve fit to the form of equation (47) with a least squares polynomial regression.

$$\Delta P_t = \left(E\mu Q + B\rho^{0.75}\mu^{0.25}Q^2\right)g \qquad \text{(Equation 47)}$$

The resulting average laminar and turbulent coefficients are:

$$\bar{E}_s = 2.99\times10^4$$

$$\bar{B}_s = 24.6$$

The units are in inchH_2O for pressure drop, LPM for flow, kg/m^3 for density, and Ns/m^2 for viscosity. The resulting ratio of geometry coefficients is

$$\frac{B_s}{E_s^2} = 2.76\times10^{-8}$$

With the sensor flow impedance characterized, the next step is to calculate the flow impedance desired for laminar flow cell. When the laminar flow element is sized such that the ratio of geometry coefficients for both the sensor and the laminar flow element are equal as in equation (46). The flow element is designed such that the temperature of the fluid flowing through the mass flow sensor is equal to that of the fluid flowing through the laminar flow element, equation 23 reduces to

$$\frac{Q_s}{Q_e} = \frac{B_e}{B_s}\frac{E_s}{E_e} \qquad \text{(Equation 48)}$$

By combining equation (46) and (48) the following relationships result defining the pressure/flow coefficients for the laminar flow element.

$$E_e = E_s\frac{Q_s}{Q_e} \qquad \text{(Equation 49)}$$

$$B_e = B_s\frac{Q_s^2}{Q_e^2} \qquad \text{(Equation 50)}$$

To meet the maximum flow of this element and stay comfortably within the range of the Honeywell sensors, the match point has been chosen at

$$Q_e = 280LPM$$

$$Q_s = 0.15LPM$$

Resulting in

$$E_{e_{design}} = 16.01$$

$$B_{e_{design}} = 7.07\times10^{-6}$$

APPENDIX B

Tables of Data For Sensors At 0, 20 and 40˚C

Table 8: Data for all sensors at 0 ˚C

		P1 is Low Side / Temp 0 Degree C														
Flow Reading in LPM		0	10	20	30	40	50	60	70	80	90	100	110	120	130	140
AWM92100V																
Sensor 20	**Output in V**	4.41	4.47	4.59	4.77	4.94	5.10	5.26	5.40	5.55	5.67	5.79	5.91	6.01	6.14	6.24
Sensor 9	**Output in V**	4.53	4.60	4.74	4.89	5.09	5.27	5.43	5.59	5.72	5.86	5.98	6.09	6.19	6.32	6.43
Sensor 3	**Output in V**	4.21	4.27	4.38	4.53	4.70	4.86	5.01	5.15	5.27	5.38	5.48	5.58	5.70	5.79	5.87
Sensor 4	**Output in V**	4.16	4.23	4.36	4.52	4.70	4.85	5.06	5.21	5.34	5.48	5.59	5.70	5.81	5.91	6.00
Sensor 7	**Output in V**	4.23	4.29	4.40	4.54	4.70	4.86	4.99	5.11	5.22	5.33	5.43	5.52	5.60	5.70	5.80
Sensor 23	**Output in V**	4.43	4.50	4.62	4.79	4.99	5.16	5.34	5.47	5.62	5.75	5.86	5.97	6.07	6.15	6.29
Sensor 12	**Output in V**	4.44	4.52	4.63	4.80	4.99	5.18	5.36	5.50	5.65	5.79	5.91	6.03	6.13	6.23	6.37
Sensor 11	**Output in V**	4.39	4.45	4.58	4.75	4.93	5.13	5.30	5.44	5.59	5.72	5.85	5.96	6.05	6.15	6.24
Sensor 15	**Output in V**	4.42	4.49	4.60	4.78	4.97	5.16	5.33	5.48	5.63	5.76	5.89	6.00	6.09	6.18	6.28
Sensor 10	**Output in V**	4.47	4.54	4.67	4.83	5.03	5.22	5.39	5.54	5.67	5.81	5.92	6.05	6.17	6.26	6.35
Sensor 19	**Output in V**	4.37	4.43	4.55	4.72	4.91	5.10	5.27	5.41	5.54	5.66	5.78	5.89	5.98	6.10	6.20
Sensor 13	**Output in V**	4.41	4.47	4.60	4.77	4.96	5.16	5.33	5.47	5.61	5.74	5.86	5.97	6.08	6.17	6.25
Sensor 2	**Output in V**	4.52	4.59	4.71	4.89	5.10	5.29	5.47	5.62	5.77	5.91	6.03	6.14	6.25	6.35	6.44
Sensor 22	**Output in V**	4.09	4.16	4.29	4.47	4.65	4.85	5.03	5.17	5.31	5.44	5.56	5.67	5.76	5.86	5.94
Sensor 21	**Output in V**	4.58	4.65	4.77	4.95	5.14	5.34	5.51	5.67	5.84	5.98	6.11	6.23	6.35	6.45	6.55
Sensor 8	**Output in V**	4.11	4.17	4.30	4.46	4.65	4.83	4.99	5.13	5.27	5.40	5.51	5.62	5.71	5.84	5.95
AWM2100V																
Sensor A	**Output in V**	1.88	2.02	2.18	2.34	2.52	2.69	2.85	2.97	3.13	3.26	3.37	3.50	3.59	3.68	3.79
Silicon Microstructure																
Sensor B	**Output in V**	2	2.14	2.27	2.43	2.58	2.77	2.96	3.15	3.37	3.58	3.8	4.05	4.28	4.5	4.7
Thalis Greek Sensors																
Sensor C	**Output in mV**	-0.5	-0.1	0.2	0.6	1	1.4	1.8	2	2.2	2.4	2.6	2.7	2.9	3	3.15
Flow Reading in LPM		150	140	130	120	110	100	90	80	70	60	50	40	30	20	10
AWM92100V																
Sensor 20	**Output in V**	6.32	6.23	6.14	6.06	5.95	5.85	5.72	5.59	5.45	5.31	5.13	4.95	4.77	4.59	4.47

Table 8 (cont'd)

Sensor 9	**Output in V**	6.52	6.43	6.33	6.24	6.14	6.04	5.91	5.78	5.64	5.47	5.31	5.12	4.91	4.72	4.60
Sensor 3	**Output in V**	5.94	5.87	5.80	5.72	5.63	5.53	5.43	5.32	5.20	5.06	4.90	4.74	4.56	4.39	4.27
Sensor 4	**Output in V**	6.08	6.00	5.92	5.83	5.72	5.61	5.50	5.36	5.22	5.08	4.91	4.72	4.53	4.36	4.23
Sensor 7	**Output in V**	5.87	5.80	5.73	5.65	5.57	5.47	5.38	5.27	5.14	5.02	4.87	4.72	4.56	4.41	4.29
Sensor 23	**Output in V**	6.37	6.29	6.21	6.12	6.01	5.91	5.80	5.66	5.52	5.37	5.21	5.00	4.81	4.63	4.49
Sensor 12	**Output in V**	6.45	6.37	6.29	6.19	6.08	5.97	5.84	5.70	5.56	5.40	5.22	5.02	4.83	4.64	4.52
Sensor 11	**Output in V**	6.32	6.24	6.15	6.07	5.96	5.86	5.74	5.61	5.47	5.33	5.15	4.95	4.77	4.59	4.45
Sensor 15	**Output in V**	6.36	6.28	6.20	6.10	6.00	5.90	5.79	5.65	5.51	5.36	5.18	5.00	4.80	4.62	4.49
Sensor 10	**Output in V**	6.43	6.35	6.27	6.17	6.07	5.96	5.84	5.72	5.57	5.43	5.25	5.05	4.84	4.67	4.54
Sensor 19	**Output in V**	6.28	6.20	6.12	6.03	5.93	5.83	5.72	5.58	5.45	5.31	5.13	4.94	4.74	4.56	4.44
Sensor 13	**Output in V**	6.34	6.26	6.18	6.08	5.98	5.88	5.76	5.63	5.49	5.34	5.18	4.99	4.79	4.61	4.48
Sensor 2	**Output in V**	6.53	6.44	6.35	6.26	6.15	6.04	5.92	5.78	5.64	5.50	5.31	5.12	4.90	4.72	4.59
Sensor 22	**Output in V**	6.02	5.95	5.86	5.77	5.67	5.56	5.45	5.32	5.18	5.05	4.85	4.66	4.49	4.29	4.16
Sensor 21	**Output in V**	6.64	6.56	6.45	6.35	6.24	6.13	5.99	5.86	5.68	5.54	5.36	5.16	4.96	4.78	4.66
Sensor 8	**Output in V**	6.03	5.95	5.87	5.78	5.67	5.56	5.44	5.31	5.17	5.03	4.85	4.67	4.47	4.31	4.18
AWM2100V																
Sensor A	**Output in V**	3.85	3.78	3.67	3.58	3.46	3.36	3.23	3.11	2.97	2.83	2.68	2.51	2.35	2.16	2.02
Sensor B	**Output in V**	4.95	4.7	4.5	4.26	4.02	3.8	3.58	3.35	3.14	2.95	2.74	2.56	2.4	2.26	2.14
Thalis Greek Sensors																
Sensor C	**Output in mV**	3.3	3.15	3	2.8	2.7	2.5	2.3	2.2	2	1.8	1.4	1	0.6	0.1	-0.2
Flow Reading in LPM		0	-10	-20	-30	-40	-50	-60	-70	-80	-90	-100	-110	-120	-130	-140
AWM92100V																
Sensor 20	**Output in V**	4.41	4.34	4.20	4.01	3.82	3.62	3.44	3.28	3.13	2.99	2.90	2.78	2.67	2.60	2.51
Sensor 9	**Output in V**	4.53	4.47	4.33	4.16	3.95	3.74	3.55	3.39	3.23	3.09	2.96	2.84	2.73	2.69	2.59
Sensor 3	**Output in V**	4.21	4.15	4.03	3.88	3.71	3.53	3.37	3.22	3.09	2.97	2.86	2.76	2.67	2.59	2.51
Sensor 4	**Output in V**	4.16	4.09	3.95	3.78	3.59	3.38	3.21	3.06	2.91	2.77	2.65	2.56	2.46	2.37	2.28
Sensor 7	**Output in V**	4.23	4.17	4.04	3.89	3.73	3.56	3.41	3.28	3.17	3.04	2.95	2.86	2.77	2.69	2.62
Sensor 23	**Output in V**	4.42	4.35	4.22	4.05	3.85	3.65	3.48	3.32	3.18	3.04	2.93	2.81	2.71	2.61	2.53
Sensor 12	**Output in V**	4.44	4.37	4.24	4.05	3.84	3.63	3.43	3.25	3.11	2.95	2.83	2.71	2.60	2.49	2.42
Sensor 11	**Output in V**	4.39	4.31	4.19	4.00	3.80	3.59	3.39	3.23	3.07	2.92	2.79	2.67	2.57	2.47	2.37
Sensor 15	**Output in V**	4.42	4.35	4.21	4.03	3.84	3.63	3.45	3.27	3.12	2.98	2.86	2.74	2.63	2.57	2.49
Sensor 10	**Output in V**	4.47	4.39	4.25	4.08	3.86	3.65	3.46	3.30	3.16	3.02	2.90	2.78	2.67	2.57	2.53
Sensor 19	**Output in V**	4.37	4.30	4.16	3.99	3.80	3.59	3.41	3.25	3.11	2.97	2.84	2.73	2.63	2.56	2.48

Table 8 (cont'd)

Sensor 13	**Output in V**	4.41	4.33	4.20	4.01	3.81	3.59	3.41	3.24	3.07	2.94	2.82	2.71	2.64	2.54	2.46	
Sensor 2	**Output in V**	4.53	4.46	4.32	4.12	3.90	3.69	3.50	3.33	3.17	3.02	2.92	2.81	2.70	2.61	2.51	
Sensor 22	**Output in V**	4.09	4.02	3.90	3.71	3.51	3.30	3.12	2.95	2.81	2.67	2.55	2.45	2.34	2.25	2.16	
Sensor 21	**Output in V**	4.58	4.51	4.36	4.15	3.91	3.69	3.48	3.31	3.13	2.97	2.84	2.72	2.6	2.54	2.45	
Sensor 8	**Output in V**	4.11	4.03	3.89	3.71	3.50	3.30	3.11	2.96	2.82	2.68	2.56	2.44	2.34	2.25	2.16	
AWM2100V																	
Sensor A	**Output in V**	1.88	1.75	1.59	1.42	1.25	1.06	0.89	0.77	0.61	0.48	0.37	0.25	0.13	0.05	0.01	
Silicon Microstructure																	
Sensor B	**Output in V**	2.01	1.91	1.78	1.63	1.46	1.28	1.09	0.89	0.69	0.44	0.22	-0.02	-0.22	-0.43	-0.66	
Thalis Greek Sensors																	
Sensor C	**Output in mV**	-0.6	-0.9	-1.2	-1.7	-2	-2.3	-2.6	-2.9	-3.1	-3.3	-3.5	-3.7	-3.8	-4	-4.1	
Flow Reading in LPM		-150	-140	-130	-120	-110	-100	-90	-80	-70	-60	-50	-40	-30	-20	-10	0
AWM92100V																	
Sensor 20	**Output in V**	2.43	2.51	2.59	2.69	2.79	2.90	3.01	3.14	3.29	3.44	3.64	3.81	4.01	4.20	4.34	4.41
Sensor 9	**Output in V**	2.50	2.59	2.68	2.78	2.89	3.01	3.13	3.26	3.43	3.57	3.75	3.97	4.16	4.35	4.46	4.53
Sensor 3	**Output in V**	2.45	2.52	2.60	2.68	2.77	2.86	2.97	3.09	3.21	3.35	3.52	3.69	3.87	4.02	4.15	4.21
Sensor 4	**Output in V**	2.23	2.30	2.38	2.48	2.57	2.67	2.78	2.90	3.05	3.19	3.37	3.57	3.77	3.95	4.09	4.16
Sensor 7	**Output in V**	2.59	2.63	2.70	2.77	2.86	2.95	3.05	3.15	3.27	3.40	3.55	3.72	3.88	4.03	4.16	4.23
Sensor 23	**Output in V**	2.46	2.54	2.62	2.71	2.81	2.92	3.04	3.18	3.32	3.48	3.64	3.84	4.03	4.21	4.35	4.42
Sensor 12	**Output in V**	2.38	2.45	2.54	2.64	2.75	2.87	2.98	3.13	3.30	3.46	3.63	3.85	4.04	4.23	4.37	4.44
Sensor 11	**Output in V**	2.34	2.42	2.51	2.61	2.72	2.83	2.96	3.10	3.26	3.41	3.59	3.81	4.00	4.19	4.31	4.39
Sensor 15	**Output in V**	2.40	2.49	2.57	2.67	2.78	2.89	3.00	3.13	3.29	3.45	3.63	3.83	4.02	4.21	4.35	4.42
Sensor 10	**Output in V**	2.45	2.53	2.61	2.71	2.81	2.93	3.04	3.18	3.33	3.47	3.66	3.86	4.07	4.25	4.39	4.47
Sensor 19	**Output in V**	2.39	2.48	2.56	2.65	2.75	2.86	2.98	3.11	3.26	3.41	3.59	3.80	3.97	4.17	4.30	4.37
Sensor 13	**Output in V**	2.38	2.46	2.55	2.64	2.74	2.85	2.97	3.10	3.25	3.42	3.60	3.79	4.00	4.20	4.34	4.41
Sensor 2	**Output in V**	2.42	2.51	2.60	2.70	2.81	2.92	3.05	3.19	3.34	3.51	3.69	3.90	4.12	4.32	4.46	4.53
Sensor 22	**Output in V**	2.07	2.16	2.24	2.34	2.45	2.55	2.68	2.81	2.96	3.09	3.30	3.50	3.72	3.89	4.02	4.10
Sensor 21	**Output in V**	2.36	2.44	2.54	2.64	2.75	2.87	3	3.15	3.32	3.49	3.7	3.92	4.16	4.36	4.51	4.58
Sensor 8	**Output in V**	2.07	2.16	2.24	2.33	2.44	2.55	2.67	2.80	2.94	3.10	3.29	3.45	3.70	3.89	4.03	4.10
AWM2100V																	
Sensor A	**Output in V**	0.01	0.01	0.06	0.15	0.26	0.39	0.49	0.62	0.76	0.91	1.08	1.25	1.43	1.59	1.73	1.88
Silicon Microstructure																	
Sensor B	**Output in V**	-0.86	-0.66	-0.43	-0.21	-0.02	0.24	0.46	0.7	0.91	1.11	1.33	1.47	1.63	1.78	1.9	2.03
Thalis Greek Sensors																	

Table 8 (cont'd)																
Sensor C	**Output in mV**	-4.3	-4.1	-4	-3.8	-3.7	-3.5	-3.3	-3.1	-2.9	-2.6	-2.3	-2	-1.6	-1.2	-0.85	-0.5

Table 9: Data for all sensors at 20 ˚C

		P1 is Low Side / Temp 20 Degree C														
Flow Reading in LPM		0	10	20	30	40	50	60	70	80	90	100	110	120	130	140
AWM92100V																
Sensor 20	**Output in V**	4.43	4.49	4.60	4.78	4.95	5.13	5.31	5.47	5.62	5.77	5.90	6.01	6.12	6.22	6.31
Sensor 9	**Output in V**	4.56	4.63	4.74	4.90	5.09	5.30	5.50	5.65	5.81	5.96	6.09	6.22	6.32	6.42	6.52
Sensor 3	**Output in V**	4.22	4.28	4.38	4.52	4.70	4.87	5.03	5.18	5.31	5.44	5.55	5.65	5.75	5.86	5.94
Sensor 4	**Output in V**	4.16	4.22	4.34	4.49	4.68	4.86	5.05	5.19	5.35	5.49	5.62	5.73	5.85	5.96	6.05
Sensor 7	**Output in V**	4.23	4.29	4.39	4.53	4.69	4.86	5.01	5.15	5.28	5.40	5.52	5.62	5.71	5.80	5.88
Sensor 23	**Output in V**	4.44	4.50	4.62	4.79	4.97	5.16	5.35	5.51	5.67	5.81	5.93	6.06	6.17	6.27	6.36
Sensor 12	**Output in V**	4.46	4.52	4.63	4.81	4.99	5.19	5.37	5.55	5.70	5.85	5.98	6.11	6.22	6.33	6.43
Sensor 11	**Output in V**	4.39	4.46	4.57	4.72	4.92	5.10	5.30	5.48	5.62	5.77	5.91	6.03	6.14	6.24	6.33
Sensor 15	**Output in V**	4.43	4.49	4.60	4.75	4.93	5.11	5.28	5.42	5.56	5.69	5.81	5.92	6.03	6.12	6.21
Sensor 10	**Output in V**	4.48	4.54	4.66	4.81	5.00	5.19	5.37	5.51	5.67	5.81	5.93	6.04	6.15	6.29	6.38
Sensor 19	**Output in V**	4.37	4.43	4.55	4.70	4.87	5.07	5.28	5.37	5.52	5.66	5.77	5.88	5.99	6.13	6.22
Sensor 13	**Output in V**	4.41	4.48	4.59	4.75	4.94	5.12	5.30	5.46	5.60	5.76	5.88	6.00	6.11	6.24	6.33
Sensor 2	**Output in V**	4.53	4.60	4.71	4.86	5.05	5.25	5.43	5.60	5.75	5.90	6.03	6.17	6.28	6.40	6.49
Sensor 22	**Output in V**	4.09	4.16	4.27	4.43	4.61	4.79	4.91	5.12	5.27	5.41	5.53	5.65	5.76	5.89	5.98
Sensor 21	**Output in V**	4.58	4.65	4.77	4.92	5.12	5.31	5.51	5.68	5.85	6.01	6.15	6.29	6.41	6.53	6.64
Sensor 8	**Output in V**	4.10	4.17	4.28	4.45	4.64	4.83	5.02	5.19	5.34	5.49	5.67	5.65	5.87	5.99	6.07
AWM2100V																
Sensor A	**Output in V**	1.87	2.00	2.13	2.28	2.45	2.61	2.76	2.90	3.02	3.16	3.28	3.40	3.50	3.60	3.69
Silicon Microstructure																
Sensor B	**Output in V**	1.8	1.919	2.049	2.204	2.358	2.549	2.753	2.953	3.181	3.436	3.69	3.95	4.2	4.45	4.71
Thalis Greek Sensors																
Sensor C	**Output in mV**	-0.6	-0.2	0.1	0.5	0.9	1.25	1.6	1.8	2.1	2.3	2.5	2.65	2.8	3	3.1
Flow Reading in LPM		150	140	130	120	110	100	90	80	70	60	50	40	30	20	10
AWM92100V																

Table 9 (cont'd)

Sensor 20	**Output in V**	6.40	6.31	6.23	6.14	6.02	5.91	5.78	5.64	5.49	5.33	5.15	4.96	4.78	4.61	4.49
Sensor 9	**Output in V**	6.62	6.52	6.44	6.33	6.22	6.10	5.97	5.83	5.67	5.51	5.30	5.10	4.91	4.74	4.62
Sensor 3	**Output in V**	6.02	5.94	5.86	5.77	5.68	5.58	5.46	5.34	5.20	5.06	4.89	4.77	4.54	4.39	4.28
Sensor 4	**Output in V**	6.14	6.05	5.96	5.87	5.75	5.64	5.51	5.37	5.22	5.07	4.88	4.69	4.51	4.34	4.22
Sensor 7	**Output in V**	5.95	5.88	5.80	5.72	5.62	5.53	5.42	5.29	5.16	5.03	4.87	4.70	4.54	4.40	4.29
Sensor 23	**Output in V**	6.45	6.36	6.28	6.18	6.07	5.95	5.83	5.68	5.53	5.37	5.18	4.99	4.79	4.62	4.50
Sensor 12	**Output in V**	6.52	6.43	6.34	6.25	6.12	6.01	5.87	5.72	5.56	5.39	5.20	5.00	4.81	4.64	4.52
Sensor 11	**Output in V**	6.43	6.34	6.25	6.15	6.04	5.92	5.79	5.65	5.49	5.32	5.14	4.93	4.73	4.57	4.45
Sensor 15	**Output in V**	6.35	6.26	6.18	6.08	5.97	5.86	5.74	5.60	5.46	5.31	5.11	4.94	4.76	4.60	4.49
Sensor 10	**Output in V**	6.47	6.38	6.29	6.20	6.09	5.97	5.85	5.70	5.55	5.39	5.20	5.01	4.83	4.66	4.54
Sensor 19	**Output in V**	6.31	6.21	6.13	6.14	5.93	5.82	5.69	5.55	5.40	5.26	5.08	4.89	4.71	4.55	4.43
Sensor 13	**Output in V**	6.42	6.33	6.24	6.14	6.03	5.91	5.79	5.64	5.48	5.33	5.15	4.95	4.76	4.60	4.48
Sensor 2	**Output in V**	6.59	6.49	6.40	6.30	6.19	6.06	5.92	5.78	5.61	5.45	5.25	5.06	4.88	4.71	4.60
Sensor 22	**Output in V**	6.07	5.98	5.89	5.79	5.68	5.56	5.44	5.30	5.15	4.99	4.80	4.62	4.43	4.28	4.16
Sensor 21	**Output in V**	6.73	6.64	6.54	6.42	6.31	6.17	6.03	5.86	5.7	5.53	5.33	5.13	4.93	4.77	4.65
Sensor 8	**Output in V**	6.16	6.07	5.97	5.87	5.76	5.64	5.51	5.36	5.19	5.04	4.84	4.64	4.45	4.29	4.17
AWM2100V																
Sensor A	**Output in V**	3.78	3.69	3.59	3.50	3.39	3.27	3.15	3.02	2.90	2.75	2.60	2.43	2.28	2.14	1.99
Silicon Microstructure																
Sensor B	**Output in V**	4.96	4.71	4.45	4.2	3.94	3.68	3.432	3.19	2.969	2.75	2.56	2.37	2.21	2.06	1.93
Thalis Greek Sensors																
Sensor C	**Output in mV**	3.2	3.05	2.95	2.8	2.6	2.4	2.25	2	1.8	1.5	1.3	0.9	0.5	0.1	-0.3
Flow Reading in LPM		0	-10	-20	-30	-40	-50	-60	-70	-80	-90	-100	-110	-120	-130	-140
AWM92100V																
Sensor 20	**Output in V**	4.43	4.36	4.24	4.07	3.86	3.65	3.45	3.29	3.13	2.99	2.85	2.74	2.64	2.53	2.44
Sensor 9	**Output in V**	4.56	4.49	4.37	4.21	3.99	3.80	3.50	3.40	3.33	3.07	2.94	2.80	2.69	2.58	2.48
Sensor 3	**Output in V**	4.22	4.16	4.04	3.89	3.72	3.53	3.36	3.21	3.08	2.94	2.82	2.71	2.62	2.52	2.44
Sensor 4	**Output in V**	4.16	4.09	3.96	3.80	3.58	3.38	3.19	3.03	2.88	2.74	2.61	2.50	2.39	2.29	2.19
Sensor 7	**Output in V**	4.23	4.17	4.06	3.92	3.76	3.59	3.43	3.29	3.16	3.03	2.92	2.82	2.73	2.68	2.59
Sensor 23	**Output in V**	4.44	4.37	4.26	4.09	3.96	3.71	3.51	3.34	3.18	3.04	2.90	2.78	2.67	2.56	2.47
Sensor 12	**Output in V**	4.46	4.39	4.27	4.11	3.91	3.70	3.52	3.33	3.16	3.00	2.85	2.73	2.64	2.53	2.43
Sensor 11	**Output in V**	4.39	4.33	4.21	4.06	3.87	3.60	3.48	3.31	3.15	3.00	2.85	2.74	2.62	2.51	2.42
Sensor 15	**Output in V**	4.43	4.36	4.25	4.10	3.92	3.73	3.55	3.39	3.23	3.08	2.95	2.83	2.72	2.63	2.54
Sensor 10	**Output in V**	4.48	4.41	4.29	4.13	3.95	3.75	3.56	3.39	3.24	3.08	2.95	2.83	2.73	2.62	2.53

Table 9 (cont'd)

Sensor 19	**Output in V**	4.37	4.31	4.19	4.03	3.85	3.65	3.43	3.30	3.15	2.99	2.87	2.76	2.64	2.55	2.46
Sensor 13	**Output in V**	4.41	4.35	4.23	4.08	3.89	3.70	3.52	3.35	3.14	3.05	2.92	2.79	2.69	2.58	2.49
Sensor 2	**Output in V**	4.53	4.47	4.35	4.19	3.99	3.79	3.59	3.41	3.25	3.09	2.95	2.81	2.71	2.61	2.51
Sensor 22	**Output in V**	4.09	4.03	3.91	3.75	3.57	3.38	3.18	3.02	2.85	2.72	2.58	2.46	2.35	2.25	2.15
Sensor 21	**Output in V**	4.58	4.52	4.39	4.22	4.01	3.79	3.58	3.39	3.21	3.04	2.88	2.75	2.64	2.52	2.42
Sensor 8	**Output in V**	4.10	4.04	3.91	3.73	3.53	3.33	3.14	2.94	2.78	2.53	2.49	2.37	2.26	2.16	2.10
AWM2100V																
Sensor A	**Output in V**	1.87	1.74	1.60	1.45	1.29	1.13	0.97	0.83	0.68	0.54	0.42	0.30	0.20	0.10	0.02
Silicon Microstructure																
Sensor B	**Output in V**	1.8	1.675	1.543	1.386	1.216	1.028	0.812	0.591	0.367	0.103	-0.18	-0.44	-0.68	-0.98	-1.24
Thalis Greek Sensors																
Sensor C	**Output in mV**	-0.6	-0.9	-1.15	-1.6	-1.9	-2.2	-2.6	-2.7	-3	-3.25	-3.45	-3.6	-3.7	-3.9	-4
Flow Reading in LPM		-150	-140	-130	-120	-110	-100	-90	-80	-70	-60	-50	-40	-30	-20	-10	0
AWM92100V																
Sensor 20	**Output in V**	2.36	2.44	2.53	2.63	2.73	2.85	2.96	3.12	3.28	3.44	3.64	3.86	4.06	4.24	4.36	4.43
Sensor 9	**Output in V**	2.37	2.47	2.57	2.68	2.80	2.92	3.06	3.22	3.38	3.57	3.77	4.00	4.20	4.37	4.49	4.56
Sensor 3	**Output in V**	2.36	2.47	2.55	2.64	2.73	2.83	2.95	3.08	3.23	3.37	3.54	3.72	3.89	4.04	4.16	4.22
Sensor 4	**Output in V**	2.11	2.19	2.28	2.38	2.48	2.59	2.72	2.87	3.01	3.18	3.37	3.58	3.78	3.96	4.09	4.16
Sensor 7	**Output in V**	2.50	2.59	2.68	2.75	2.84	2.94	3.04	3.16	3.30	3.43	3.59	3.76	3.92	4.07	4.17	4.23
Sensor 23	**Output in V**	2.37	2.47	2.56	2.67	2.77	2.89	3.02	3.17	3.33	3.51	3.70	3.91	4.09	4.25	4.37	4.44
Sensor 12	**Output in V**	2.34	2.42	2.52	2.62	2.73	2.85	2.99	3.14	3.32	3.48	3.70	3.90	4.09	4.27	4.39	4.45
Sensor 11	**Output in V**	2.33	2.42	2.52	2.61	2.73	2.85	2.98	3.14	3.30	3.47	3.66	3.86	4.04	4.21	4.33	4.39
Sensor 15	**Output in V**	2.44	2.53	2.62	2.72	2.82	2.94	3.08	3.22	3.38	3.54	3.73	3.92	4.09	4.25	4.36	4.43
Sensor 10	**Output in V**	2.44	2.53	2.62	2.72	2.82	2.95	3.08	3.23	3.34	3.55	3.75	3.94	4.12	4.28	4.41	4.47
Sensor 19	**Output in V**	2.37	2.46	2.55	2.64	2.75	2.87	3.00	3.15	3.30	3.46	3.65	3.84	4.03	4.19	4.31	4.37
Sensor 13	**Output in V**	2.40	2.49	2.59	2.68	2.80	2.91	3.04	3.18	3.35	3.51	3.70	3.89	4.07	4.23	4.35	4.41
Sensor 2	**Output in V**	2.42	2.51	2.60	2.71	2.81	2.95	3.08	3.24	3.41	3.59	3.79	4.00	4.19	4.35	4.47	4.53
Sensor 22	**Output in V**	2.06	2.15	2.24	2.34	2.45	2.56	2.70	2.85	3.00	3.17	3.35	3.56	3.75	3.91	4.03	4.09
Sensor 21	**Output in V**	2.33	2.42	2.52	2.63	2.75	2.87	3.02	3.19	3.36	3.55	3.77	3.98	4.21	4.39	4.52	4.58
Sensor 8	**Output in V**	2.01	2.09	2.19	2.29	2.39	2.51	2.65	2.79	2.95	3.12	3.33	3.53	3.73	3.91	4.04	4.10
AWM2100V																
Sensor A	**Output in V**	0.01	0.02	0.10	0.20	0.30	0.43	0.55	0.69	0.83	0.98	1.12	1.29	1.45	1.60	1.74	1.86
Silicon Microstructure																
Sensor B	**Output in V**	-1.51	-1.25	-0.96	-0.69	-0.43	-0.14	0.117	0.375	0.598	0.814	1.03	1.22	1.39	1.54	1.68	1.81

Table 9 (cont'd)

Thalis Greek Sensors																
Sensor C	**Output in mV**	-4.1	-4	-3.9	-3.7	-3.6	-3.4	-3.2	-3	-2.7	-2.5	-2.2	-1.9	-1.6	-1.1	-0.9	-0.6

Table 10: Data for all sensors at 40 ˚C

		P1 is Low Side / Temp 40 Degree C														
Flow Reading in LPM		0	10	20	30	40	50	60	70	80	90	100	110	120	130	140
AWM92100V																
Sensor 20	**Output in V**	4.43	4.49	4.59	4.74	4.91	5.10	5.29	5.47	5.63	5.80	5.95	6.07	6.20	6.32	6.41
Sensor 9	**Output in V**	4.56	4.63	4.73	4.89	5.09	5.29	5.51	5.67	5.86	6.02	6.18	6.32	6.45	6.57	6.68
Sensor 3	**Output in V**	4.21	4.26	4.37	4.51	4.68	4.85	5.04	5.19	5.34	5.49	5.62	5.74	5.85	5.96	6.05
Sensor 4	**Output in V**	4.15	4.21	4.32	4.47	4.65	4.83	5.03	5.20	5.37	5.53	5.69	5.82	5.95	6.06	6.17
Sensor 7	**Output in V**	4.22	4.28	4.38	4.52	4.68	4.85	5.01	5.17	5.30	5.45	5.58	5.69	5.79	5.89	5.98
Sensor 23	**Output in V**	4.44	4.50	4.61	4.77	4.95	5.15	5.35	5.51	5.68	5.84	5.98	6.12	6.25	6.35	6.45
Sensor 12	**Output in V**	4.46	4.51	4.63	4.78	4.97	5.16	5.37	5.54	5.71	5.87	6.03	6.16	6.28	6.41	6.51
Sensor 11	**Output in V**	4.39	4.45	4.56	4.71	4.90	5.09	5.29	5.46	5.62	5.78	5.93	6.07	6.17	6.30	6.41
Sensor 15	**Output in V**	4.43	4.48	4.59	4.74	4.93	5.12	5.32	5.50	5.65	5.83	5.95	6.10	6.21	6.33	6.44
Sensor 10	**Output in V**	4.48	4.54	4.66	4.81	5.01	5.21	5.41	5.60	5.76	5.92	6.07	6.20	6.33	6.45	6.55
Sensor 19	**Output in V**	4.37	4.43	4.54	4.69	4.89	5.08	5.29	5.46	5.63	5.79	5.94	6.07	6.19	6.30	6.39
Sensor 13	**Output in V**	4.41	4.47	4.59	4.76	4.95	5.16	5.36	5.53	5.69	5.85	6.00	6.12	6.24	6.35	6.46
Sensor 2	**Output in V**	4.54	4.60	4.71	4.86	5.06	5.25	5.46	5.64	5.81	5.99	6.13	6.27	6.40	6.52	6.63
Sensor 22	**Output in V**	4.08	4.14	4.25	4.41	4.60	4.78	4.99	5.16	5.33	5.49	5.64	5.77	5.89	6.00	6.10
Sensor 21	**Output in V**	4.61	4.67	4.78	4.93	5.12	5.3	5.52	5.68	5.86	6.03	6.19	6.33	6.46	6.57	6.69
Sensor 8	**Output in V**	4.09	4.15	4.26	4.42	4.60	4.80	4.99	5.18	5.35	5.52	5.68	5.83	5.95	6.07	6.18
AWM2100V																
Sensor A	**Output in V**	1.85	1.97	2.10	2.24	2.39	2.54	2.70	2.82	2.97	3.08	3.21	3.32	3.43	3.54	3.63
Silicon Microstructure																
Sensor B	**Output in V**	1.702	1.834	1.97	2.128	2.296	2.488	2.69	2.909	3.132	3.416	3.667	3.95	4.21	4.49	4.76
Thalis Greek Sensors																

Table 10 (cont'd)

Sensor C	Output in mV	-0.6	-0.2	0.1	0.4	0.8	1.1	1.4	1.7	1.9	2.1	2.2	2.4	2.6	2.7	2.9
Flow Reading in LPM		150	140	130	120	110	100	90	80	70	60	50	40	30	20	10
AWM92100V																
Sensor 20	Output in V	6.51	6.42	6.31	6.22	6.08	5.95	5.82	5.66	5.48	5.31	5.12	4.92	4.74	4.59	4.48
Sensor 9	Output in V	6.77	6.68	6.57	6.46	6.33	6.19	6.04	5.87	5.68	5.51	5.28	5.10	4.90	4.74	4.62
Sensor 3	Output in V	6.13	6.05	5.96	5.86	5.75	5.63	5.50	5.34	5.19	5.05	4.87	4.68	4.51	4.36	4.27
Sensor 4	Output in V	6.26	6.18	6.07	5.97	5.84	5.70	5.55	5.38	5.23	5.05	4.85	4.66	4.48	4.32	4.21
Sensor 7	Output in V	6.05	5.97	5.89	5.80	5.70	5.58	5.46	5.32	5.17	5.02	4.86	4.69	4.53	4.38	4.28
Sensor 23	Output in V	6.54	6.46	6.36	6.25	6.13	6.00	5.86	5.70	5.53	5.36	5.17	4.95	4.79	4.62	4.50
Sensor 12	Output in V	6.61	6.51	6.41	6.30	6.18	6.04	5.89	5.72	5.55	5.38	5.17	4.98	4.79	4.63	4.51
Sensor 11	Output in V	6.50	6.40	6.31	6.20	6.07	5.94	5.80	5.64	5.47	5.30	5.10	4.91	4.72	4.56	4.45
Sensor 15	Output in V	6.52	6.44	6.34	6.23	6.11	5.98	5.84	5.68	5.51	5.35	5.12	4.94	4.76	4.60	4.49
Sensor 10	Output in V	6.65	6.56	6.46	6.34	6.23	6.10	5.95	5.78	5.61	5.43	5.22	5.02	4.82	4.66	4.54
Sensor 19	Output in V	6.49	6.39	6.30	6.19	6.07	5.95	5.80	5.65	5.48	5.31	5.10	4.88	4.70	4.54	4.43
Sensor 13	Output in V	6.55	6.46	6.36	6.26	6.13	6.00	5.86	5.71	5.54	5.37	5.17	4.97	4.76	4.60	4.47
Sensor 2	Output in V	6.73	6.64	6.52	6.41	6.29	6.14	5.99	5.82	5.66	5.47	5.26	5.05	4.87	4.71	4.60
Sensor 22	Output in V	6.19	6.10	6.01	5.90	5.78	5.64	5.51	5.34	5.17	5.00	4.79	4.60	4.40	4.25	4.14
Sensor 21	Output in V	6.79	6.69	6.6	6.47	6.34	6.21	6.05	5.88	5.71	5.52	5.31	5.12	4.95	4.79	4.67
Sensor 8	Output in V	6.28	6.18	6.08	5.97	5.84	5.70	5.55	5.36	5.19	5.00	4.81	4.61	4.43	4.27	4.15
AWM2100V																
Sensor A	Output in V	3.72	3.63	3.54	3.43	3.33	3.22	3.09	2.96	2.85	2.69	2.55	2.40	2.25	2.10	1.97
Silicon Microstructure																
Sensor B	Output in V	5.03	4.76	4.49	4.21	3.95	3.7	3.41	3.156	2.93	2.708	2.502	2.314	2.14	1.99	1.851
Thalis Greek Sensors																
Sensor C	Output in mV	3	2.85	2.7	2.5	2.3	2.2	2	1.9	1.6	1.4	1.1	0.7	0.4	0.1	-0.2
Flow Reading in LPM		0	-10	-20	-30	-40	-50	-60	-70	-80	-90	-100	-110	-120	-130	-140
AWM92100V																
Sensor 20	Output in V	4.43	4.36	4.27	4.11	3.94	3.73	3.52	3.34	3.16	2.99	2.85	2.72	2.60	2.50	2.39
Sensor 9	Output in V	4.56	4.50	4.40	4.24	4.04	3.85	3.63	3.44	3.26	3.08	2.93	2.79	2.66	2.53	2.42
Sensor 3	Output in V	4.21	4.15	4.05	3.91	3.74	3.57	3.38	3.22	3.07	2.92	2.78	2.67	2.57	2.47	2.37
Sensor 4	Output in V	4.15	4.08	3.97	3.82	3.64	3.43	3.23	3.05	2.87	2.70	2.55	2.42	2.30	2.19	2.09
Sensor 7	Output in V	4.22	4.17	4.08	3.95	3.80	3.63	3.46	3.30	3.16	3.01	2.89	2.77	2.66	2.57	2.49
Sensor 23	Output in V	4.44	4.37	4.26	4.12	3.95	3.75	3.54	3.34	3.17	3.00	2.84	2.70	2.58	2.46	2.35
Sensor 12	Output in V	4.46	4.39	4.28	4.12	3.92	3.70	3.48	3.28	3.09	2.92	2.76	2.61	2.48	2.35	2.25

Table 10 (cont'd)

Sensor 11	**Output in V**	4.39	4.32	4.22	4.05	3.87	3.66	3.45	3.25	3.03	2.89	2.71	2.58	2.46	2.35	2.24	
Sensor 15	**Output in V**	4.43	4.36	4.24	4.09	3.90	3.69	3.48	3.30	3.12	2.96	2.81	2.68	2.55	2.44	2.33	
Sensor 10	**Output in V**	4.48	4.42	4.30	4.12	3.96	3.75	3.54	3.34	3.16	3.00	2.84	2.70	2.58	2.46	2.35	
Sensor 19	**Output in V**	4.37	4.31	4.19	4.03	3.83	3.62	3.41	3.24	3.06	2.90	2.74	2.61	2.50	2.37	2.28	
Sensor 13	**Output in V**	4.41	4.35	4.24	4.06	3.85	3.63	3.42	3.23	3.05	2.88	2.74	2.60	2.48	2.36	2.27	
Sensor 2	**Output in V**	4.54	4.47	4.35	4.18	3.98	3.76	3.53	3.33	3.15	2.97	2.80	2.66	2.53	2.41	2.31	
Sensor 22	**Output in V**	4.08	4.01	3.89	3.74	3.54	3.31	3.12	2.93	2.75	2.58	2.43	2.29	2.18	2.06	1.95	
Sensor 21	**Output in V**	4.61	4.55	4.43	4.26	4.05	3.83	3.6	3.34	3.2	3.01	2.85	2.71	2.54	2.43	2.32	
Sensor 8	**Output in V**	4.09	4.02	3.91	3.74	3.57	3.37	3.15	2.95	2.78	2.61	2.45	2.32	2.20	2.07	1.97	
AWM2100V																	
Sensor A	**Output in V**	1.85	1.73	1.60	1.45	1.29	1.14	0.98	0.83	0.69	0.56	0.43	0.31	0.20	0.09	0.02	
Silicon Microstructure																	
Sensor B	**Output in V**	1.722	1.593	1.45	1.282	1.098	0.908	0.68	0.458	0.194	-0.05	-0.35	-0.64	-0.91	-1.22	-1.49	
Thalis Greek Sensors																	
Sensor C	**Output in mV**	-0.6	-0.8	-1.1	-1.45	-1.8	-2.1	-2.4	-2.6	-2.9	-3.1	-3.3	-3.5	-3.6	-3.8	-4	
Flow Reading in LPM		-150	-140	-130	-120	-110	-100	-90	-80	-70	-60	-50	-40	-30	-20	-10	0
AWM92100V																	
Sensor 20	**Output in V**	2.30	2.39	2.48	2.59	2.71	2.84	2.99	3.15	3.32	3.52	3.73	3.93	4.11	4.26	4.37	4.43
Sensor 9	**Output in V**	2.32	2.42	2.53	2.64	2.78	2.92	3.08	3.25	3.44	3.63	3.85	4.05	4.24	4.40	4.51	4.56
Sensor 3	**Output in V**	2.29	2.37	2.46	2.56	2.68	2.79	2.91	3.06	3.21	3.39	3.57	3.75	3.91	4.05	4.15	4.21
Sensor 4	**Output in V**	2.00	2.09	2.19	2.30	2.42	2.55	2.69	2.85	3.03	3.22	3.43	3.62	3.81	3.97	4.09	4.14
Sensor 7	**Output in V**	2.41	2.49	2.56	2.65	2.75	2.87	3.00	3.15	3.29	3.45	3.62	3.79	3.94	4.07	4.17	4.22
Sensor 23	**Output in V**	2.25	2.34	2.45	2.57	2.65	2.83	2.99	3.16	3.33	3.52	3.74	3.93	4.12	4.27	4.38	4.44
Sensor 12	**Output in V**	2.16	2.25	2.37	2.49	2.62	2.77	2.93	3.11	3.30	3.49	3.72	3.92	4.13	4.28	4.39	4.46
Sensor 11	**Output in V**	2.14	2.23	2.34	2.45	2.58	2.71	2.88	3.04	3.24	3.44	3.66	3.86	4.05	4.21	4.33	4.39
Sensor 15	**Output in V**	2.24	2.33	2.43	2.54	2.66	2.80	2.94	3.11	3.29	3.46	3.68	3.88	4.08	4.24	4.37	4.43
Sensor 10	**Output in V**	2.25	2.35	2.45	2.55	2.70	2.83	2.98	3.15	3.32	3.51	3.72	3.93	4.13	4.29	4.42	4.48
Sensor 19	**Output in V**	2.18	2.27	2.38	2.48	2.61	2.74	2.89	3.06	3.23	3.42	3.62	3.83	4.03	4.19	4.31	4.37
Sensor 13	**Output in V**	2.17	2.27	2.36	2.47	2.58	2.78	2.86	3.03	3.21	3.40	3.62	3.84	4.06	4.22	4.35	4.41
Sensor 2	**Output in V**	2.20	2.30	2.47	2.52	2.66	2.80	2.95	3.14	3.33	3.53	3.76	3.98	4.18	4.36	4.48	4.54
Sensor 22	**Output in V**	1.86	1.95	2.04	2.15	2.28	2.41	2.56	2.74	2.91	3.09	3.31	3.52	3.72	3.89	4.01	4.08
Sensor 21	**Output in V**	2.22	2.32	2.43	2.55	2.69	2.82	2.99	3.16	3.36	3.56	3.78	4.02	4.22	4.41	4.55	4.61
Sensor 8	**Output in V**	1.88	1.98	2.08	2.19	2.32	2.45	2.59	2.76	2.95	3.12	3.37	3.53	3.76	3.91	4.03	4.09
AWM2100V																	

Table 10 (cont'd)

Sensor A	**Output in V**	0.02	0.02	0.09	0.20	0.32	0.44	0.56	0.70	0.83	0.99	1.13	1.30	1.46	1.59	1.73	1.85
Silicon Microstructure																	
Sensor B	**Output in V**	-1.78	-1.49	-1.21	-0.91	-0.63	-0.35	-0.05	0.221	0.463	0.701	0.914	1.107	1.28	1.45	1.596	1.73
Thalis Greek Sensors																	
Sensor C	**Output in mV**	-4.1	-3.9	-3.8	-3.7	-3.5	-3.3	-3.1	-2.8	-2.6	-2.4	-2.1	-1.8	-1.4	-1.1	-0.8	-0.6

		P1 is Low Side / Temp 0 Degree C																P1 is Low Side / Temp 0 Degree C													
Flow Reading in LPM		0	10	20	30	40	50	60	70	80	90	100	110	120	130	140	150	140	130	120	110	100	90	80	70	60	50	40	30	20	10
AWM92100V																															
Sensor 20	Output in V	4.41	4.47	4.59	4.77	4.94	5.10	5.26	5.40	5.55	5.67	5.79	5.91	6.01	6.14	6.24	6.32	6.23	6.14	6.06	5.95	5.85	5.72	5.59	5.45	5.31	5.13	4.95	4.77	4.59	4.47
Sensor 9	Output in V	4.53	4.60	4.74	4.89	5.09	5.27	5.43	5.59	5.72	5.86	5.98	6.09	6.19	6.32	6.43	6.52	6.43	6.33	6.24	6.14	6.04	5.91	5.78	5.64	5.47	5.31	5.12	4.91	4.72	4.60
Sensor 3	Output in V	4.21	4.27	4.38	4.53	4.70	4.86	5.01	5.15	5.27	5.38	5.48	5.58	5.70	5.79	5.87	5.94	5.87	5.80	5.72	5.63	5.53	5.43	5.32	5.20	5.06	4.90	4.74	4.56	4.39	4.27
Sensor 4	Output in V	4.16	4.23	4.36	4.52	4.70	4.85	5.06	5.21	5.34	5.48	5.59	5.70	5.81	5.91	6.00	6.08	6.00	5.92	5.83	5.72	5.61	5.50	5.36	5.22	5.08	4.91	4.72	4.53	4.36	4.23
Sensor 7	Output in V	4.23	4.29	4.40	4.54	4.70	4.86	4.99	5.11	5.22	5.33	5.43	5.52	5.60	5.70	5.80	5.87	5.80	5.73	5.65	5.57	5.47	5.38	5.27	5.14	5.02	4.87	4.72	4.56	4.41	4.29
Sensor 23	Output in V	4.43	4.50	4.62	4.79	4.99	5.16	5.34	5.47	5.62	5.75	5.86	5.97	6.07	6.15	6.29	6.37	6.29	6.21	6.12	6.01	5.91	5.80	5.66	5.52	5.37	5.21	5.00	4.81	4.63	4.49
Sensor 12	Output in V	4.44	4.52	4.63	4.80	4.99	5.18	5.36	5.50	5.65	5.79	5.91	6.03	6.13	6.23	6.37	6.45	6.37	6.29	6.19	6.08	5.97	5.84	5.70	5.56	5.40	5.22	5.02	4.83	4.64	4.52
Sensor 11	Output in V	4.39	4.45	4.58	4.75	4.93	5.13	5.30	5.44	5.59	5.72	5.85	5.96	6.05	6.15	6.24	6.32	6.24	6.15	6.07	5.96	5.86	5.74	5.61	5.47	5.33	5.15	4.95	4.77	4.59	4.45
Sensor 15	Output in V	4.42	4.49	4.60	4.78	4.97	5.16	5.33	5.48	5.63	5.76	5.89	6.00	6.09	6.18	6.28	6.36	6.28	6.20	6.10	6.00	5.90	5.79	5.65	5.51	5.36	5.18	5.00	4.80	4.62	4.49
Sensor 10	Output in V	4.47	4.54	4.67	4.83	5.03	5.22	5.39	5.54	5.67	5.81	5.92	6.05	6.17	6.26	6.35	6.43	6.35	6.27	6.17	6.07	5.96	5.84	5.72	5.57	5.43	5.25	5.05	4.84	4.67	4.54
Sensor 19	Output in V	4.37	4.43	4.55	4.72	4.91	5.10	5.27	5.41	5.54	5.66	5.78	5.89	5.98	6.10	6.20	6.28	6.20	6.12	6.03	5.93	5.83	5.72	5.58	5.45	5.31	5.13	4.94	4.74	4.56	4.44
Sensor 13	Output in V	4.41	4.47	4.60	4.77	4.96	5.16	5.33	5.47	5.61	5.74	5.86	5.97	6.08	6.17	6.25	6.34	6.26	6.18	6.08	5.98	5.88	5.76	5.63	5.49	5.34	5.18	4.99	4.79	4.61	4.48
Sensor 2	Output in V	4.52	4.59	4.71	4.89	5.10	5.29	5.47	5.62	5.77	5.91	6.03	6.14	6.25	6.35	6.44	6.53	6.44	6.35	6.26	6.15	6.04	5.92	5.78	5.64	5.50	5.31	5.12	4.90	4.72	4.59
Sensor 22	Output in V	4.09	4.16	4.29	4.47	4.65	4.85	5.03	5.17	5.31	5.44	5.56	5.67	5.76	5.86	5.94	6.02	5.95	5.86	5.77	5.67	5.56	5.45	5.32	5.18	5.05	4.85	4.66	4.49	4.29	4.16
Sensor 21	Output in V	4.58	4.65	4.77	4.95	5.14	5.34	5.51	5.67	5.84	5.98	6.11	6.23	6.35	6.45	6.55	6.64	6.56	6.45	6.35	6.24	6.13	5.99	5.86	5.68	5.54	5.36	5.16	4.96	4.78	4.66
Sensor 8	Output in V	4.11	4.17	4.30	4.46	4.65	4.83	4.99	5.13	5.27	5.40	5.51	5.62	5.71	5.84	5.95	6.03	5.95	5.87	5.78	5.67	5.56	5.44	5.31	5.17	5.03	4.85	4.67	4.47	4.31	4.18
Standard Deviation		0.15	0.16	0.16	0.16	0.17	0.18	0.18	0.18	0.19	0.20	0.21	0.21	0.22	0.22	0.22	0.23	0.22	0.22	0.21	0.21	0.21	0.20	0.19	0.19	0.18	0.18	0.17	0.16	0.15	0.15

		P1 is Low Side / Temp 0 Degree C																P1 is Low Side / Temp 0 Degree C													
Flow Reading in LPM		0	-10	-20	-30	-40	-50	-60	-70	-80	-90	-100	-110	-120	-130	-140	-150	-140	-130	-120	-110	-100	-90	-80	-70	-60	-50	-40	-30	-20	-10	0
AWM92100V																															
Sensor 20	Output in V	4.41	4.34	4.20	4.01	3.82	3.62	3.44	3.28	3.13	2.99	2.90	2.78	2.67	2.60	2.51	2.43	2.51	2.59	2.69	2.79	2.90	3.01	3.14	3.29	3.44	3.64	3.81	4.01	4.20	4.34	4.41
Sensor 9	Output in V	4.53	4.47	4.33	4.16	3.95	3.74	3.55	3.39	3.23	3.09	2.96	2.84	2.73	2.69	2.59	2.50	2.59	2.68	2.78	2.89	3.01	3.13	3.26	3.43	3.57	3.75	3.97	4.16	4.35	4.46	4.53
Sensor 3	Output in V	4.21	4.15	4.03	3.88	3.71	3.53	3.37	3.22	3.09	2.97	2.86	2.76	2.67	2.59	2.51	2.45	2.52	2.60	2.68	2.77	2.86	2.97	3.09	3.21	3.35	3.52	3.69	3.87	4.02	4.15	4.21
Sensor 4	Output in V	4.16	4.09	3.95	3.78	3.59	3.38	3.21	3.06	2.91	2.77	2.65	2.56	2.46	2.37	2.28	2.23	2.30	2.38	2.48	2.57	2.67	2.78	2.90	3.05	3.19	3.37	3.57	3.77	3.95	4.09	4.16
Sensor 7	Output in V	4.23	4.17	4.04	3.89	3.73	3.56	3.41	3.28	3.17	3.04	2.95	2.86	2.77	2.69	2.62	2.59	2.63	2.70	2.77	2.86	2.95	3.05	3.15	3.27	3.40	3.55	3.72	3.88	4.03	4.16	4.23
Sensor 23	Output in V	4.42	4.35	4.22	4.05	3.85	3.65	3.48	3.32	3.18	3.04	2.93	2.81	2.71	2.61	2.53	2.46	2.54	2.62	2.71	2.81	2.92	3.04	3.18	3.32	3.48	3.64	3.84	4.03	4.21	4.35	4.42
Sensor 12	Output in V	4.44	4.37	4.24	4.05	3.84	3.63	3.43	3.25	3.11	2.95	2.83	2.71	2.60	2.49	2.42	2.38	2.45	2.54	2.64	2.75	2.87	2.98	3.13	3.30	3.46	3.63	3.85	4.04	4.23	4.37	4.44
Sensor 11	Output in V	4.39	4.31	4.19	4.00	3.80	3.59	3.39	3.23	3.07	2.92	2.79	2.67	2.57	2.47	2.37	2.34	2.42	2.51	2.61	2.72	2.83	2.96	3.10	3.26	3.41	3.59	3.81	4.00	4.19	4.31	4.39
Sensor 15	Output in V	4.42	4.35	4.21	4.03	3.84	3.63	3.45	3.27	3.12	2.98	2.86	2.74	2.63	2.57	2.49	2.40	2.49	2.57	2.67	2.78	2.89	3.00	3.13	3.29	3.45	3.63	3.83	4.02	4.21	4.35	4.42
Sensor 10	Output in V	4.47	4.39	4.25	4.08	3.86	3.65	3.46	3.30	3.16	3.02	2.90	2.78	2.67	2.57	2.53	2.45	2.53	2.61	2.71	2.81	2.93	3.04	3.18	3.33	3.47	3.66	3.86	4.07	4.25	4.39	4.47
Sensor 19	Output in V	4.37	4.30	4.16	3.99	3.80	3.59	3.41	3.25	3.11	2.97	2.84	2.73	2.63	2.56	2.48	2.39	2.48	2.56	2.65	2.75	2.86	2.98	3.11	3.26	3.41	3.59	3.80	3.97	4.17	4.30	4.37
Sensor 13	Output in V	4.41	4.33	4.20	4.01	3.81	3.59	3.41	3.24	3.07	2.94	2.82	2.71	2.64	2.54	2.46	2.38	2.46	2.55	2.64	2.74	2.85	2.97	3.10	3.25	3.42	3.60	3.79	4.00	4.20	4.34	4.41
Sensor 2	Output in V	4.53	4.46	4.32	4.12	3.90	3.69	3.50	3.33	3.17	3.02	2.92	2.81	2.70	2.61	2.51	2.42	2.51	2.60	2.70	2.81	2.92	3.05	3.19	3.34	3.51	3.69	3.90	4.12	4.32	4.46	4.53
Sensor 22	Output in V	4.09	4.02	3.90	3.71	3.51	3.30	3.12	2.95	2.81	2.67	2.55	2.45	2.34	2.25	2.16	2.07	2.16	2.24	2.34	2.45	2.55	2.68	2.81	2.96	3.09	3.30	3.50	3.72	3.89	4.02	4.10
Sensor 21	Output in V	4.58	4.51	4.36	4.15	3.91	3.69	3.48	3.31	3.13	2.97	2.84	2.72	2.6	2.54	2.45	2.36	2.44	2.54	2.64	2.75	2.87	3	3.15	3.32	3.49	3.7	3.92	4.16	4.36	4.51	4.58
Sensor 8	Output in V	4.11	4.03	3.89	3.71	3.50	3.30	3.11	2.96	2.82	2.68	2.56	2.44	2.34	2.25	2.16	2.07	2.16	2.24	2.33	2.44	2.55	2.67	2.80	2.94	3.10	3.29	3.45	3.70	3.89	4.03	4.10
Standard Deviation		0.15	0.15	0.15	0.14	0.14	0.13	0.13	0.13	0.13	0.12	0.13	0.13	0.13	0.13	0.14	0.14	0.13	0.13	0.13	0.13	0.13	0.13	0.13	0.14	0.14	0.14	0.15	0.14	0.15	0.15	0.15

Figure 68: Standard Deviation for AWM92100V Sensor

APPENDIX C

Design For Assembly

Manual assembly

The design for assembly method is intended to classify and code the procedures for the handling and assembly of components such that the subsequent analysis of the design is made easier. The AWM2100V flow sensor-tube assembly is selected for this method. All elements from the original design were categorized according to the standard format, shown as figures 66, 67 & 68, that is provided by Boothroyd, Swift and Redford in their book "Design for Assembly Handbook". Figure69 shows a comparison of size and assembly complexity between the AWM series and the new design.

Considering the Flow sensor-tube assembly in this analysis, manual assembly has been selected as the method of choice for this product. This selection is also based on the size of the parts as well as the precision needed in the functioning of the subassembly. When designing for the efficient manual assembly, consideration must be given to the size data of the average person. In other words, the assembly of the components should be analyzed with consideration to the average person regarding the size, weight and shape of the part. As indicated in table 3 and 4, the amount of alignment needed for placement is critical as well as the number of times the object is handled. A design for assembly was done on both the existing design and the redesign of the subassembly, shown in (figure 21a, 21b) respectively. The elimination of hoses in the design of the flow sensor-tube improved the time efficiency by almost 92% compared to the old design, in other words we needed 42 seconds to finish the old subassembly and we only need 3.5 seconds with the new one. Not to mention the risk of breaking the sensor in the old assembly, costing the company around $30 to fix it.

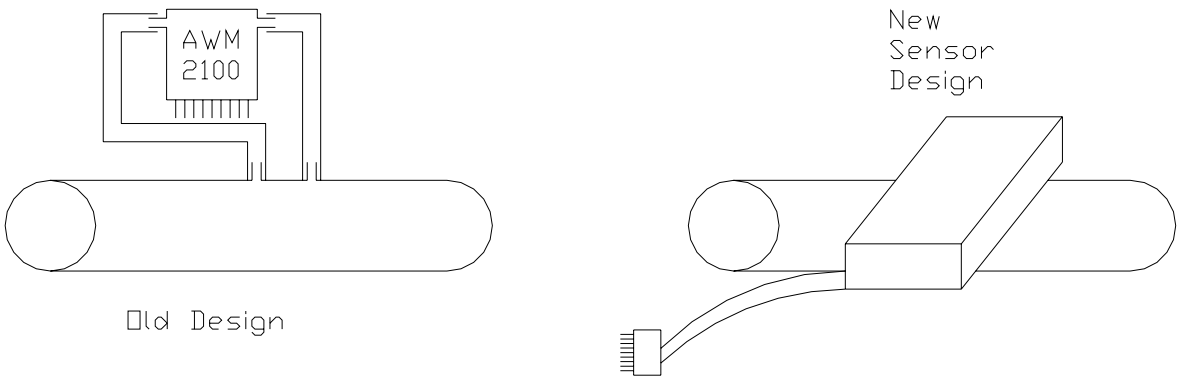

Figure 69: Old design versus new design

Table 11: Manual handling table old subassembly

Manual handling code	Part #	Alpha	Beta	Thickness (mm)	Size (mm)	Comments
1 0	1	360	0	5	180	Tube has to be stretched
1 0	2	360	0	5	180	Tube has to be stretched

Table 12: Manual handling table new subassembly

Manual handling code	Part #	Alpha	Betta	Thickness (mm)	Size (mm)	Comments
1 0	2	360	0	5	180	One way Electronic plug

Table 13: Manual insertion table old subassembly

Part #	Comments	Manual insertion code		Time (s)
1	Plastic deformation immediately after insertion Riveting or similar operation Not easy to align or position during assembly Resistance to insertion Part is being finally secured immediately Part and associated tool (Including hands) can easily reach the desired location easily	7 3	37	9
2	Plastic deformation immediately after insertion Riveting or similar operation Not easy to align or position during assembly Resistance to insertion Part is being finally secured immediately Part and associated tool (Including hands) can easily reach the desired location easily	7 3	37	9

Table 14: Manual insertion table new subassembly

Part #	Comments	Manual insertion code		Time (s)
1	No screwing operation or plastic deformation immediately after insertion Easy to align or position during assembly No Resistance to insertion	0	30	2
	Part is being finally secured immediately Part and associated tool (Including hands) can easily reach the desired location easily	3		

Table 15: design for manual assembly worksheet (old design)

1	2	3	4	5	6	7	8	9	10
Part ID #	Number of times the operation is carried out consecutively	Two digit manual handling code	Manual handling time per part	Two digit manual insertion code	Manual insertion time per part	Operation time in seconds (2)*[(4)+(6)]	Operation cost Cents. 0.4*(7)	estimation of theoretical minimum parts	Money saved in USD based on 250,000 parts
1	2	10	1.5	37	9	21	8.4	0	
2	2	10	1.5	37	9	21	8.4	0	
						42	16.8	0	42000

Table 16: design for manual assembly worksheet (new design)

1	2	3	4	5	6	7	8	9	10
Part ID #	Number of times the operation is carried out consecutively	Two digit manual handling code	Manual handling time per part	Two digit manual insertion code	Manual insertion time per part	Operation time in seconds (2)*[(4)+(6)]	Operation cost Cents. 0.4*(7)	Figures for estimation of theoretical minimum parts	Money saved in USD based on 250,000 parts
1	1	10	1.5	30	2	3.5	1.4	0	
						3.5	1.4	0	3500

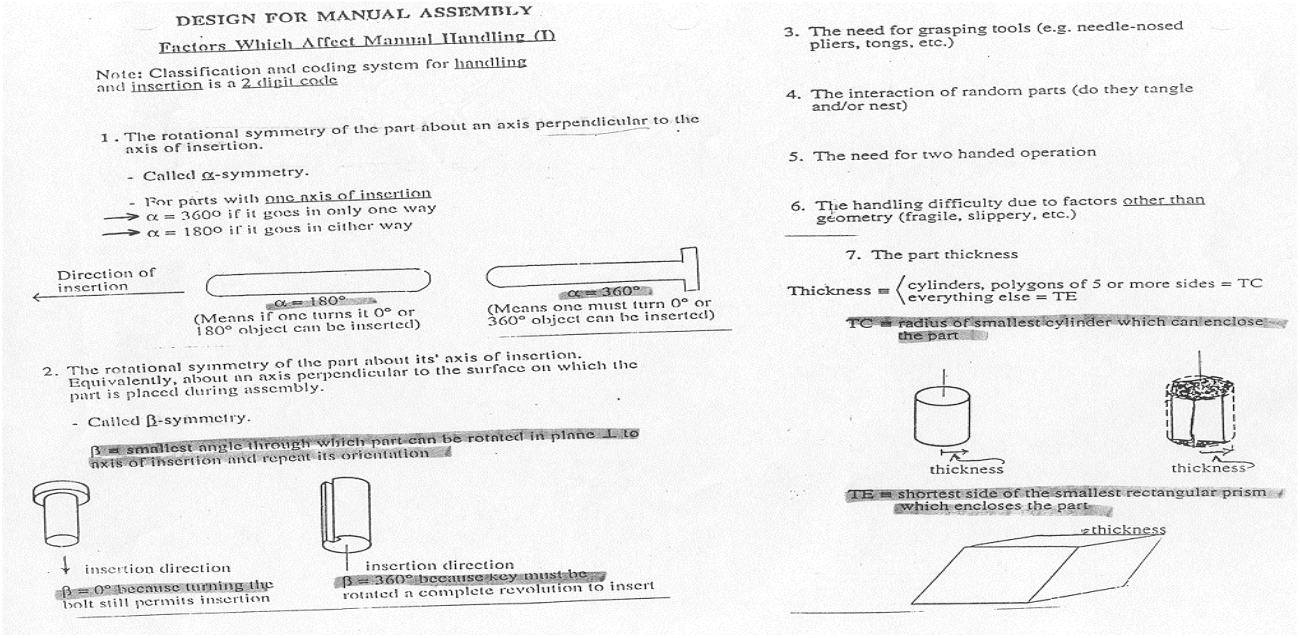

Figure 70: Factors that affects manual handling

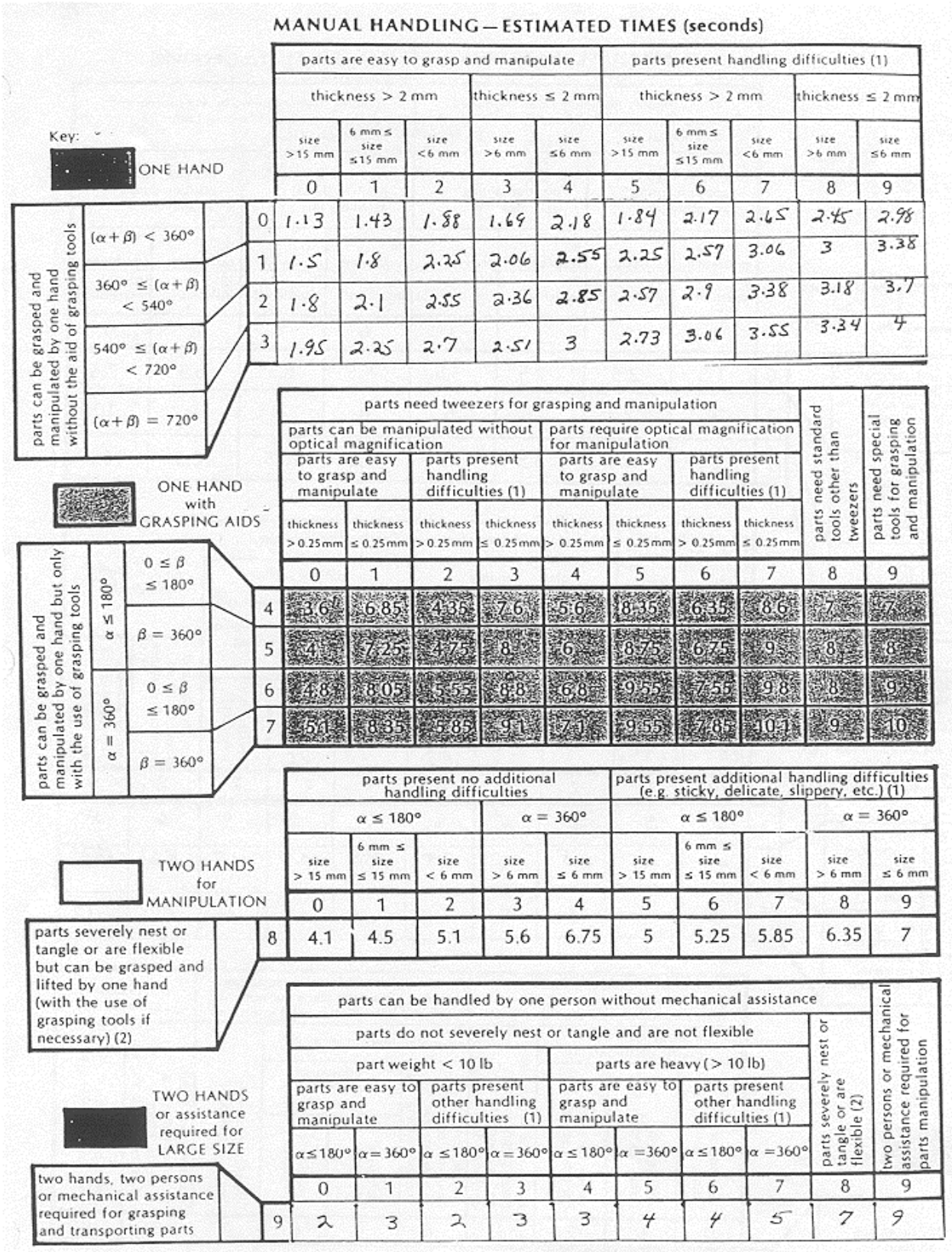

Figure 71: Manual Handling-Estimated times (seconds)

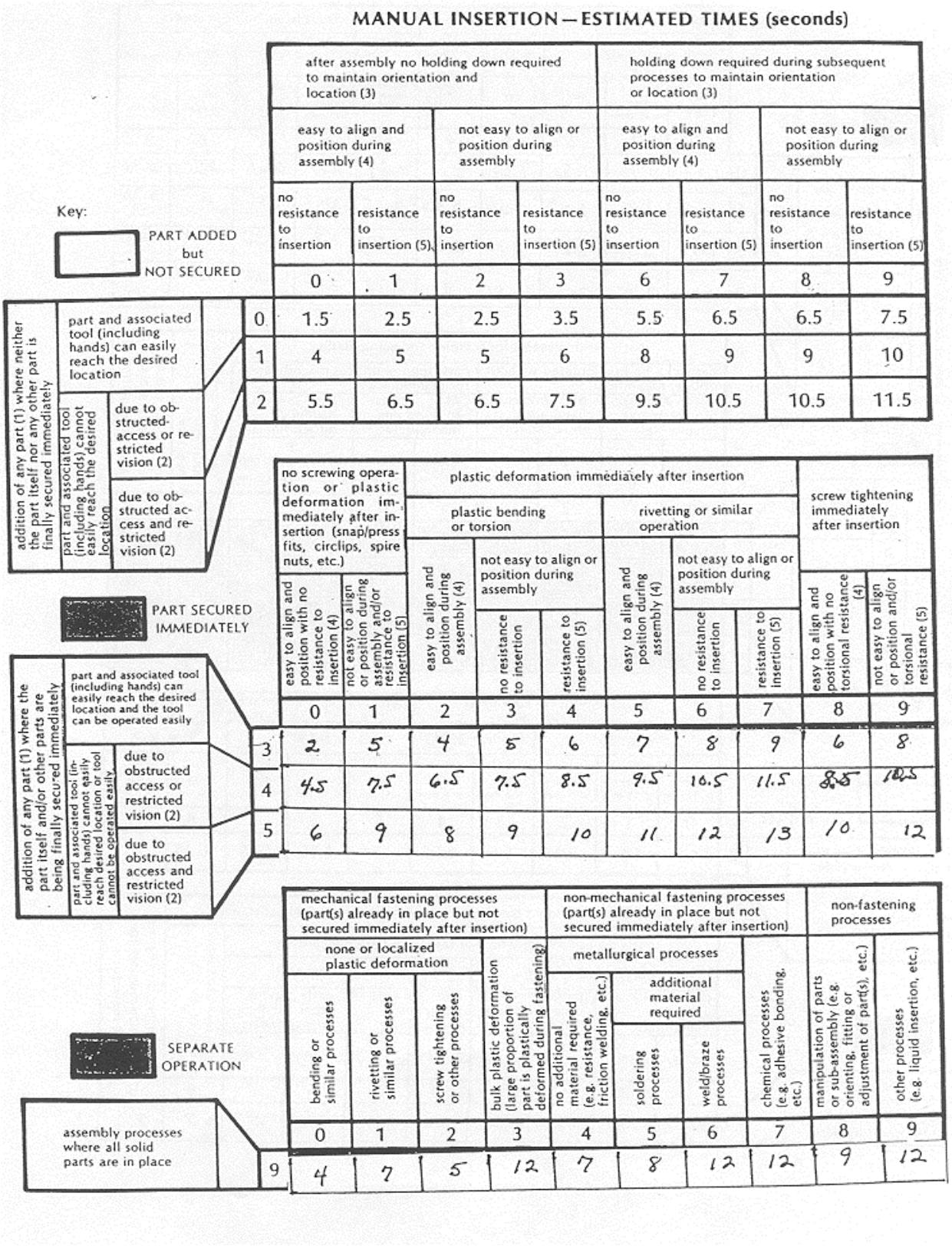

Figure 72: Manual Insertion-Estimated times (seconds)

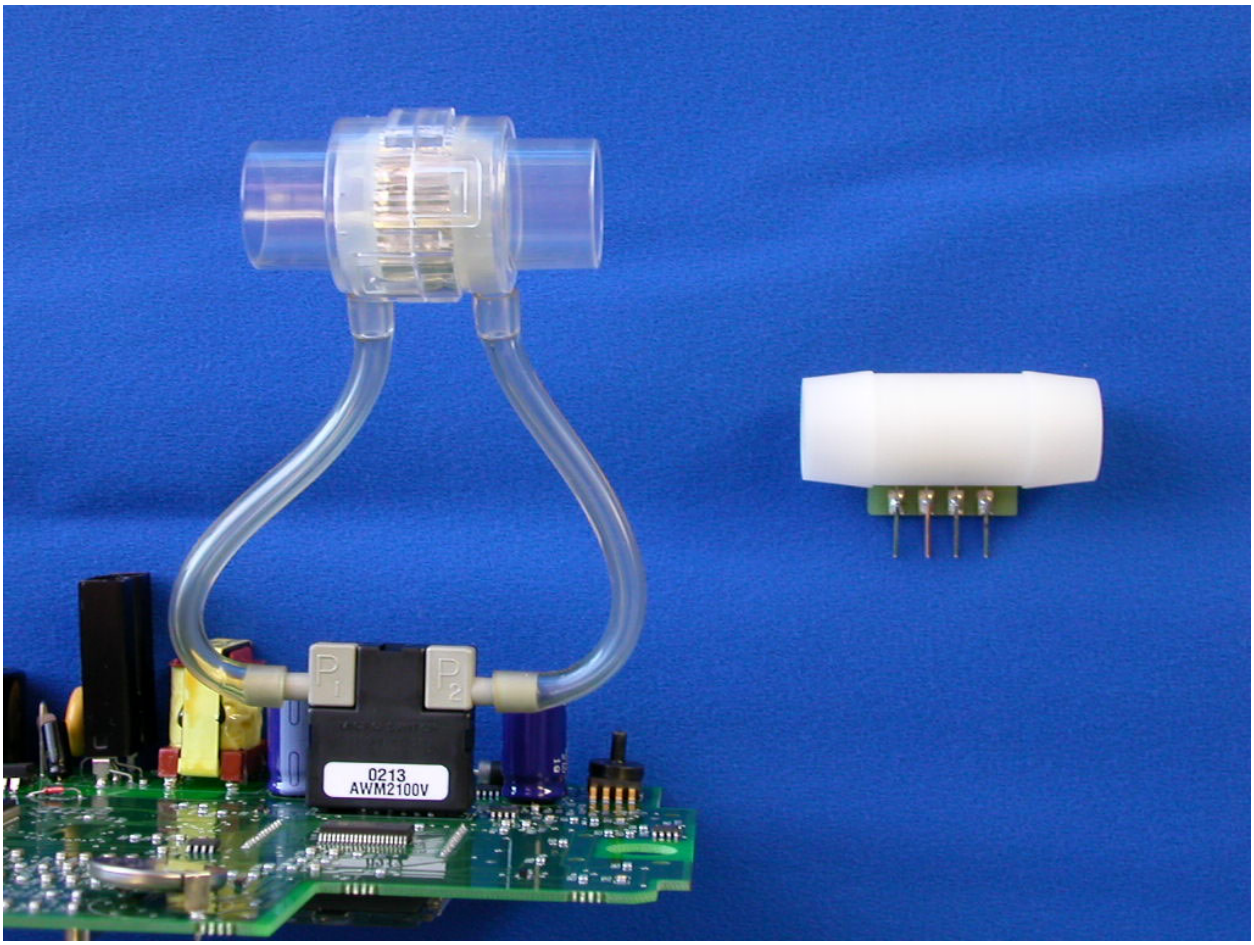

Figure 73: Size comparison between (Honeywell-Magwheel) and Thalis Greek sensor

APPENDIX D

Equipment Description and Specification

B&k-Precision model 1660 triple output DC powers supply

Description:

This power supply is a high quality, general-purpose dc power source. It provides 0-30 volt dc output that is adjustable It is capable of current output of 0-2 Amperes. The two 0-30 volt supplies can be operated independently or in one of two tracking modes, the slave supply tracks the voltage of the master supply. Maximum current setting of the two supplies can still be set independently when in series-tracking operating mode. In the series-tracking mode the master and slave supplies are connected in series, allowing a single output of 0-60 volts at up to 2 Amps. In the parallel tracking mode, the two supplies are connected in parallel, allowing a single 0-30 volt output at up to 4 amps.

Specifications:

Output Voltage Range: 0V (+0/-30 mV) to 30 V +(3% to 7%).

Output Current Limit Range: 0A (+0/-30 mA) to 2 A +(3% to 7%).

Load Regulation (constant voltage): ≤ 0.01% + 3 mV.

Line Regulation 108-132 V (Constant Voltage): ≤0.01% + 3 mV.

Ripple (Constant Voltage): ≤1 mV RMS.

Recovery Time (Constant Voltage): ≤ 100 μS.

Temperature Coefficient (Constant Voltage): ≤300 ppm/°C.

Load Regulation (Constant Current): ≤0.2% + 3 mA.

Line Regulation 108-132 V (Constant Current): ≤0.2% + 3 mA.

Ripple Current (at 108 V for Constant Current): ≤ 3 mA RMS.

Tracking (Series): ± 0.2% + 10 mV.

Panel Meter Accuracy (Volts): ± 0.5% + 2 digits.

Panel Meter Accuracy (Current): ± 0.5% + 2 digits.

Thermal Mass Flow Sensor TSI Model 4040

Description:

The model 4040 Flow meter measures mass flow rate, temperature, and absolute pressure of the gas inside the flow tube. This flow meter can be used for different gases but first it must be calibrated for any particular gas. Flow can be displayed in units of standard liters per minute (Std L/min) or in volumetric units of liters per minute (L/min). This model has an independent temperature transducer, in the flow tube, to measure the gas temperature. The temperature sensor is used for temperature compensation of flow rate. This model also measures absolute pressure near the outlet of the flow meter, in the SI units, of Kilo- Pascal. Temperature and pressure measurements are required for converting flow from standard to volumetric units. Since thermal flow sensors are sensitive to changes in air density and air velocity, all thermal flow meters indicate flow rates with reference to a set of standard conditions. For TSI instruments, standard conditions are defined as 21.1° C (70° F) and 101.4 Kpa (14.7 psia). Standard flow rate is the flow rate the air would be moving if the temperature and pressure were at standard conditions. It is usually the most useful measure of airflow because it defines the heat-carrying capacity of the air.

Volumetric flow rate is the true volume floe of the gas exiting the flow meter. To convert from standard flow rate to volumetric flow rate, we should multiply the standard flow measurement by the following density correction factor:

$$VolumetricFlow = (StdFlow)\left[\frac{273.15 + T_m}{273.15 + 21.11}\right]\frac{101.3}{P_m} \qquad \text{(Equation 51)}$$

Where,

Tm = Gas temperature measured in flow tube in units of degrees Celsius.

Pm = absolute pressure measured in flow tube in units of KPa.

Table 17: Specifications

Flow Measurement	0 to 300 Std L/min.
Measurement Range	2% of reading or 0.05 Std L/min, whichever is greater,
Accuracy	At standard conditions (21.1°C and 101.3 kPa) see notes 1 through 5
Resolution Display	0.01 Std L/min between 0 and 90 Std L/min Std L/min between 90 and 300 Std L/min
Response	Less than 4 msec, 63% of final value at full scale flow
Temperature Measurement	0 to 50°C
Measurement Range	± 1°C, at flows greater than 1 L/min. See note 2 below
Accuracy	0.1°C
Resolution (Display)	Less than 75 msec, 63% of final value for 20°C step change in temperature at full scale flow.
Response	
Static Pressure Measurement	Measured inside flow tube near the exit
Measurement Range	50 to 199 kPa absolute
Accuracy	±1 kPa, see note 6 below
Resolution (Display)	kPa
Response	Less than 4 msec. 63% of final value for 30 kPa step change
Over Pressure	620 kPa

Notes:

Accuracy stated at standard conditions of 21.1°C and 101.3 kPa.

Add an additional 0.075% of reading per 1°C away from standard conditions when operating within the range of 0°C to 50°C.

Add an additional 0.015% of reading per 1 kPa above 101.3 kPa.

Add an additional 0.022% of reading per 1 kPa below 101.3 kPa when operating within the pressure range of 70kPa to 170 kPa.

Accuracy stated with gas temperature and flow body temperature within ±10°C of one another

Accuracy stated measuring dry gas (less than 10% R.H).

Include ±0.5% of reading repeatability

Volumetric flow rate is calculated from the mass flow measurement. Add an additional 0.25% of reading to the flow accuracy to account for the uncertainty in measuring gas temperature and pressure.

Add uncertainty of 0.2 kPa for every 10°C away from 21.1°C.

FLUKE 87 TRUE RMS MULTIMETER

Description:

The meter combines the precision of a digital meter with the speed and versatility of a three-digit resolution analog display. Frequencies between 0.5 Hz and 200 kHz can be measured with up to 0.01 Hz resolution

Specification:

Table 18: Specifications

Function	Range	Resolution	Accuracy			
			50Hz-60Hz	45 Hz-1kHz	1 kHz-5 kHz	5 kHz-20 kHz
	400.0 mV	mV	±(.07% +4)	±(1.0% +4)	±(2.0% +4)	±(2.0% +20)
~	4.000V	0.001V	±(.07% +2)	±(1.0% +4)	±(2.0% +4)	±(2.0% +20)
V	40.00V	0.01V	±(.07% +2)	±(1.0% +4)	±(2.0% +4)	±(2.0% +20)
	400.0V	0.1V	±(.07% +2)	±(1.0% +4)	±(2.0% +4)	±(2.0% +20)
	1000V	1V	±(.07% +2)	±(1.0% +4)	±(2.0% +4)	Unspecified

Accuracy is given as ± ([% of reading] + [number of least significant digits]) at 18°C to 28°C, with relative humidity up to 90%, for a period of one year after calibration. In the 4 ½-digit modes, multiply the number of least significant digits (counts) by 10. AC conversions are ac-coupled, true RMS responding, calibrated to the RMS value of a sine wave input, and valid from 5% to 100% of range. AC crest factor can be up to 3 at full scale, 6 at half scale. For non-sinusoidal waveforms add –(-2% Rdg + 2% Fs) typical, for a crest factor up to 3.

Below 10% of range, add 16 counts.

Below 10% of range, add 6 digits.

BIBLIOGRAPHY

BIBLIOGRAPHY

1- Gislason, T, Almquist, M, Eriksson, G, et al. Prevalence of sleep apnea syndrome among Swedish men. An epidemiological study. J Clin Epideiol 1988; 41:571.

2- Lavie, P. Incidence of sleep apnea in a presumably healthy working population—a significant relationship with excessive daytime sleepiness. Sleep 1983; 6:312.

3- Young, T, Palta, M, Dempsey, J, et al. The occurrence of sleep-disordered breathing among middle-aged adults. N Engl J Med 1993; 328:1230.

4- Block,AJ, Boysen, PG, Wyne, JW, Hunt, LA. Sleep apnea, hypopnea and oxygen desaturation in normal subjects: A strong male predominance. N Engl J Med 1979; 300:513.

5- Gould, GA, Whyte, KF, Rhind, GB, et al. The sleep hypopnea syndrome. Am Rev Respir Dis 1988; 137:895.

6- Remmers, JE, deGroot, WJ, Sauerland, EK, Anch, AM. Pathogenesis of upper airway occlusion during sleep. J Appl Physiol: Respirat Environ Exercise Physiol 1978; 44:931.

7- Yamashiro Y, Kryger MH. Why should sleep apnea be diagnosed and treated? Clin Pulm Med 1994; 1:250-9.

8- Hla KM, Young TB, Bidwell T, Palta M, Skatrud JB, Dempsey J. Sleep apnea and hypertension: a population-based study. Ann Intern Med 1994;120:382-388.

9- Young T, Palta M, Dempsey J, Skatrud J, Weber S, Badr S. The occurrence of sleep-disordered breathing among middle-aged adults. N Engl J Med 1993; 328:1230-1235.

10- Flemons WW, Whitelaw WA, Brant R, Remmers JE. Likelihood ratios for a sleep apnea clinical prediction rule. Am J Respir Crit Care Med 1994; 150:1279-1285.

11- Bearpark, H, Grunstein, R, Touyz, S. Cognitive and psychological dysfunction in sleep apnea before and after treatment with CPAP. Sleep Res 1987; 16:303.

12- Frith, RW, Cant, BR. Severe obstructive sleep apnea treated with long term nasal continuous positive airway pressure Thorax 1985; 40:45.

13- Rajagopai, KR, Bennett, LL, Dillard, TA. Overnight nasal CPAP improves hypersomnolence in sleep apnea. Chest 1986; 90:172.

14- Kribbs, NB, Pack, AI, Kline, LR, et al. Effects of one night without nasal CPAP treatment on sleep and sleepiness in patients with obstructive sleep apnea. Am Rev Respir Dis 1993; 147:1162.

15- McEnvoy, RD, Thornton, AT. Treatment of obstructive sleep apnea syndrome with nasal continuous positive airway pressure. Sleep 1984; 7:313.

16- Berthon-Jones, M. Sullivan, CE. Time course of change of ventilatory response to CO2 with long term CPAP therapy for obstructive sleep apnea. Am Rev Respir Dis 1987; 135:144.

17- Marrone, O, Ferrara, G, Macaluso, C. Sleep-related disorders and internal diseases. Springer, Berlin 1987; 375-9.

18- Kneger, J, Storza, E, Barthelmebs, M, et al. Overnight decrease in hematocrit after nasal CPAP treatment in patients with OSA. Chest 1990; 97:729.

19- Storza, E, Krieger, J, Weitzenblum, E, et al. Long-term effects of treatment with nasal continuous positive airway pressure on daytime lung function and pulmonary hemodynamics in patients with obstructive sleep apnea. Am Rev Respir Dis 1992; 141:866.

20- Krieger, J, Grucker, D, Sforza, E, et al. Left ventricular ejection fraction in obstructive sleep apnea. Chest 1991; 100:917.

21- Berry, RB, Block, AJ. Positive nasal airway pressure eliminates snoring as well as obstructive sleep apnea. Chest 1984; 85:15.

22- Guilleminault, C, Stoohs, R, Duncan, S. Daytime sleepiness in regular heavy snorers. Chest 1991; 99:40.

23- Hoftstein, V, Slutsky, AS. Central sleep apnea reversed by continuous positive airway pressure. Am Rev Respir Dis 1987; 135:1210.

24- Issa, FG, Sullivan, CE. Reversal of central sleep apnea using nasal CPAP. Chest 1986; 90:165.

25- Takasaki, Y, Orr, D, Popkin, J, et al. Effect of nasal continuous positive airway pressure on sleep apnea in congestive heart failure. Am Rev Respir Dis 1989; 140:1578.

26- Bradley, TD, Holloway, RM, McLaughlin, PR, et al. Cardiac output response to continuous positive airway pressure in congestive heart failure. Am Rev Respir Dis 1992; 145:377.

27- Davies, RJO, Harrington, KJ, Ormerod, OJM, Stradling, JR. Nasal continuous positive airway pressure in chronic heart failure with sleep-disordered breathing. Am Rev Respir Dis 1993; 147:630.

28- Sullivan CE, Issa FG. Obstructive sleep apnea. Clin Chest Med 1985; 6:633-650.

29- Davies RJO, Stradling JR. The relationship between neck circumference, radiographic pharyngeal anatomy, and the obstructive sleep apnea syndrome. Eur Respir J 1990; 3:509-514.

30- Woodson BT, Garancis JC, Toohill RJ. Histopathologic changes in snoring and obstructive sleep apnea syndrome. Laryngoscope 1991; 101:1318-1322.

31- Smith PL, Gold AR, Meyers DA, Haponik EF, Bleecker ER. Weight loss in mildly to moderately obese patients with obstructive sleep apnea. Ann Intern Med 1985; 103: 850-855.

32- Indications and standards for use of nasal continuous positive airway pressure in sleep apnea syndromes. Am J Respir Crit Care Med 1994; 150: 1738-1745.

33- Prosise GL, Berry RB. Oral-nasal continuous positive airway pressure as a treatment for obstructive sleep apnea. Chest 1994; 106: 180-186.

34- Sanders MH, Kern NB, Stiller RA, Strollo PJ Jr, Martin TJ, Atwood CW Jr. CPAP therapy via oronasal mask for obstructive sleep apnea. Chest 1994; 106: 774-779.

35- Derderian SS, Bridenbaugh RH, Rajagopal KR. Neuropsychologic symptoms in obstructive sleep apnea improve after treatment with nasal continuous positive airway pressure. Chest 1988; 94: 1023-1027.

36- Lamphere J, Roehrs T, Wittig R, Zorick F, Conway WA, Roth T. Recovery of alertness after CPAP in apnea. Chest 1989; 96: 1364-1367.

37- Levinson PD, Millman RP. Causes and consequences of blood pressure alterations in obstructive sleep apnea. Arch Intern Med 1991; 151: 455-462.

38- Hanzel DA, Proia NG, Hudgel DW. Response of obstructive sleep apnea to fluoxetine and protriptyline. Chest 1991; 100: 416-421.

39- Javaheri, S, Parker, TJ, Wexler, L, et al. Effect of theophylline on sleep-disordered breathing in heart failure. N Engl J Med 1996; 335:562.

40- Cistulli, PA, Barnes, DJ, Grunstein, RR, Sullivan, CE. Effect of short-term hormone replacement in the treatment of obstructive sleep apnea in postmenopausal women. Thorax 1994; 49-699.

41- Suratt, PM, Wilhoit, SC, Brown, ED, Findley, LJ. Effect of doxapram on obstructive sleep apnea. Bull Eur Physiopathol Respir 1986; 22:127.

42- Atkinson, RL, Suratt, PM, Wilhoit, SC, Recant, L. Naloxone improves sleep apnea in obese humans. Int J Obes 1985; 9:233.

43- Gothe, B, Strohl, KP, Levin, S, Cherniack, NS. Nicotine: a different approach to treatment of obstructive sleep apnea. Chest 1985; 87:11.

44- Davila, DG, Hurt, RD, Offord, KP, et al. Acute effects of transdermal nicotine on sleep architecture, snoring, and sleep-disordered breathing in nonsmokers. Am J Respir Crit Care Med 1994; 150:469.

45- Skjodt, NM, Atkar, R, Easton, PA. Screening for hypothyroidism in sleep apnea. Am J Respir Crit Care Med 1999; 160:732.

46- Rajagopal, KR, Abbrecht, PH, Derderian, SS, et al. Obstructive sleep apnea in hypothyroidism. Ann Intern Med 1984; 101:491.

47- Grunstein, RR, Sullivan, CE. Sleep apnea and hypothyroidism. Mechanisms and management. Am J Med 1988; 85:775.

48- Whyte, KF, Gould, GA, Airlie, MA, et al. Role of protriptyline and acetazolamide in the sleep apnea/hypopnea syndrome. Sleep 1988; 11:463.

49- Berry, RB, Yamaura, EM, Gill, K, Reist, C. Acute effects of paroxetine on genioglossus activity in obstructive sleep apnea. Sleep 1999; 22:1087.

50- Grote, L, Heitmann, J, Kohler, U, et al. Effect of angiotensin converting enzyme inhibition [Cilazapril] on blood pressure recording in hypertensive obstructive sleep apneic patients. Blood Press 1997; 6:235.

51- Riley RW, Powell NB, Guilleminault C. Obstructive sleep apnea syndrome: a review of 306 consecutively treated surgical patients. Otolaryngol Head Neck Surg 1993; 108: 117:125.

52- Johnson NT, Chinn J. Uvulopalatopharyngoplasty and inferior sagittal mandibular osteotomy with genioglossus advancement for treatment of obstructive sleep apnea. Chest 1994; 105:278-283.

53- Demirozu, MC, Chediak, AD, Nay, KN, Cohn, MA. A comparison of nine nasal continuous positive airway pressure machines in maintaining mask pressure during simulated inspiration. Sleep 1991; 14:259.

54- Sanders, MH, Kern, N. Obstructive sleep apnea treated by independently adjusted inspiratory and expiratory positive airway pressures via nasal mask. Physiologic and clinical implications. Chest 1992; 98:317.

55- Guilleminault, C, Nino-Murcia, G, Heldt, G, et al. Alternative treatment to tracheostomy in obstructive sleep apnea syndrome: Nasal continuous positive airway pressure in young children. Pediatrics 1986; 78:797.

56- Frith, RW, Cant, BR. Severe obstructive sleep apnea treated with long term nasal continuous positive airway pressure. Thorax 1985; 40:45.

57- McEwy, RD, Thomton, AT. Treatment of obstructive sleep apnea syndrome with continuous positive airway pressure. Sleep 1984; 7:313.

58- Marrone, O, Fenara, G, Macaluso, C. Sleep-related disorders and internal diseases. Benin: Springer, 1987376-g.

59- Krieger, J, Sforza, E, Bartelemew, M, et al. Overnight decrease in hematocrit after nasal CPAP treatment in patients with OSA. Chest 1990; 97:729.

60- Sforza, E, Krieger, J, Weitzenblum, E, et al Long-term effects of treatment with nasal continuous positive airway pressure on daytie lung function and pulmonary hemodynamica in patients with obstructive sleep apnea. Am Rev Respir Dis 1990; 141:866.

61- Krieger, J, Grucker, D, Sforza, E, et al. Left ventricular ejection fraction in obstructive sleep apnea. Chest 1991; 100:917.

62- B.W. van Oudheusden, Silicon thermal flow sensors, Sensors and Actuators, A30 (1992), p.5-26.

63- L.V. King, On the convection of heat from small cylinders in a stream of fluid: determination of the convection constants of small platinum wires, with applications to hot-wire anemometry, Proc. R. Soc. London vol. 90, 1914, p. 563-570.

64- R.G. Johnson and R.E. Higashi, a highly sensitive silicon chip microtransducer for air flow and differential pressure sensing applications, sensors and Actuators, 11 (1987), p. 63-72.

65- R.G. Johnson and R.E. Higashi, Semiconductor device, US patent 4651564.

66- T.S.J. Lammerink, N.R. Tas, M.Elwenspoek and J.H.J. Fluitman, Micro liquid flow sensor, Sensors and Actuators, 37-38 (1993) p. 45-50.

67- H.E. De Bree, H.V. Jansen, T.S.J. Lammerink, G.J.M. Krijnen and M. Elwenspoek, Bi-directional fast flow sensor with large dynamic range, Proc. MME '98, Ulvic June 3-5, 1998, p. 194-197.

68- L.M. Fingerson and P. Freymuth, Thermal Anemometers, in: Fluid mechanics measurements, ed. R.J. Goldstein, Taylor & Francis, Bristol (1996), p. 115-173.

69- Boillat, A.J. van der Wiel, A.C. Hoogerwerf, N.F. de Rooij, A differential pressure liquid flow sensor for flow regulation and dosing systems, IEEE Micro Electrical Mechanical Systems, p. 350-352, 1995.

70- R.E. Oosterbroek, T.S.J. Lammerink, J.W. Berenschot, A. van den Berg, M.C. Elwenspoek, Designing, realization and characterization of a novel capacitive pressure/flow sensor, Transducer '97, International Conference on Solid-State Sensors and Actuators, Chicago, June 16-19, 1997.

71- K. Hermansson, U. Lindberg, B. Hok, G. Palmskog, Wetting properties of silicon surfaces, Transducers 91, Digest of Technical Papers, International Conference on Solid State Sensors and Actuators, S. 193-196, 1991.

72- A.J. Van der Wiel, C. Lindner, N.F. de Rooij and A. Bezinge: Sensors and Actuators A 37-38 (1993) 693-697.

73- Baltes and D. Moser: Transducers, Yokohama (1993), 736-741.

74- Il Hyun Choi and K.D. Wise: IEEE Transactions on electron devices, Vol ED-33, No. 1, Jan, 1986.

75- W. Lang, K. Kuhl and E. Obermeier: Sensors and Actuators, A 21-23, (1990) 473-477.

76- A. Klumpp, K. Kuhl, W. Lang, H. Sandmaier and U. Schaber: Microsystems, Berlin 1994, Tech. Proceedings 289-298.

77- J. Schieferdecker, R. Quad, E. Holzenkampfer, and M. Schulze: Sensors and Actuators A 46-47 (1995) 422-427.

78- F. Volklein, A. Wiegand and V. Baier: Sensors and Actuators A29 (1991) 87-91.

79- K. Kuhl and W. Lang: Sensors and Materials, 2, 5 (1991) 247-251.

80- H.J. Verhoeven, J.H. Huijsing: An integrated gas flow sensor with high sensitivity, low response time and a pulse rate output, Sensors and Actuators, A41 and 42, p. 217-220.

81- F. Mayer, O. Paul, and H. Baltes: Influence of design geometry and packaging on the response of thermal CMOS flow sensors, Transducers 95, Eurosensors IX, Stockholm, 1995, V1 p 528-531.

82- B.W. van Odheusden: Silicon thermal flow sensors, Sensors and Actuators A30, (1992) p.5-26.

83- H. Moller, G. Krotz, W. Legner, Ch. Wagner, G. Muller, L. Smith, B. Leese, A. Jones, and S. Rushworth: In situ p- and n-type doping of low-temperature grown B-SiC epitaxial layers on silicon, Int. Conf. On silicon carbide and related materials Kyoto, Japan, 1995; Inst. Phys. Conf. Ser. No 142, Ch 3, p. 497-500, (1996) IOP Publishing Ltd.

84- C. Wagner and G. Krotz: Thermal properties of B-SiC epitaxial layers between 150 degrees C and 500 degrees C measured by using microstructures, Diamond and Related Materials 6, (1997), p. 1338-1341.

85- E.O. Doebelin, Measurement Systems-Application and Design, McGraw-Hill, Singapore, 4th ed., 1990, p 542-555.

86- E. Yoon, K. Wise, An integrated mass flow sensor with on-chip CMOS interface circuitry, IEEE Transactions on Electron Devices, Vol. 39, No6, June 1992, p. 1376-1386.

87- S. Nakagawa, S. Shoji, M. Esashi, A micro chemical analyzing system integrated on a silicon wafer, proc. IEEE MEMS workshop, Napa Valley, CA, Feb. 1990, p. 89-94.

88- B. H. van der Schoot, S. Jeanneret, A. van den Berg & N.F. de Rooij, A silicon integrated miniature chemical analysis system, sensors and actuators B6 (1992), p. 57-60.

89- O. Tabata, H. Inagaki & I. Igarashi, Monolithic pressure-flow sensor, IEEE Trans. On Electron Devices, Vol. ED-34, No. 12 (1987) 2456-2462.

90- A. Richter, K.A. Hofmann, A. Plettner & H. Sandmaier, The electrohydrodynamic micro flow sensor, IEEE Transducers '91, Chemical Sensors II, catalogue number 91CH2817-5 p. 935-938.

91- J. Branebjerg, O.S. Jensen, N.G. Laursen & O. Leistiko, A micro machined flow sensor for measuring small liquid flows, IEEE Transducers '91, flow sensors, catalogue number 91CH2817-5, p. 41-44.

92- K. Giek, Formulaire Technique, Sixieme edition francaise, 1979, Giek-Verlag, D- 7100 Heilbron, p. N1-N7.

93- Prof. J. Buttet, Cours de Pysique Generale, Ecole Polytechnique Federale de Lausanne, Departement de Pysique, Ecublens 1981, p. 120-124.

94- B. Kloek, Design, Fabrication and Characterization of Piezoresistive Pressure sensors, including the study of electrochemical etch-stop, dissertation, University of Neuchatel, Switzerland, November 1989, p. 32-48.

95- E. Yoon, K.D. Wise, An integrated mass flow sensor with on-chip CMOS interface circuitry, IEEE Trans. Electron Devices ED 39 (6) (1992) 1376-1385.96.

96- O. Tabata, Fast-response silicon flow sensor with and on-chip fluid temperature sensing element, IEEE Trans. Electron Devices ED 33 (3) (1986) 361-365.

97- W. Lang, Thermal conductivity of porous silicon, in: L. Canham (Ed.), Porous Silicon, London, UK, 1988, pp. 138-141.

98- B.W. van Oudheusden, Silicon thermal flow sensors, Sensors and Actuators A 30 (1992) 5-26.